Neurophysiological Properties of Cortico-Cortical Evoked Potentials in Humans

by

Britni Crocker

B.S. Biomedical Engineering
Johns Hopkins University, 2009

M.S. Neural and Behavioral Sciences
Max Planck Institute of Biological Cybernetics, 2011

Submitted to the Harvard-MIT Program in Health Sciences and Technology
in partial fulfillment of the requirements for the degree of

DOCTOR OF PHILOSOPHY IN MEDICAL ENGINEERING AND MEDICAL PHYSICS

AT THE

MASSACHUSETTS INSTITUTE OF TECHNOLOGY

SEPTEMBER 2018

Signature redacted

Signature of Author .....
Department of Health Sciences and Technology
August 31, 2018

Signature redacted

Certified by .....
Sydney Cash, MD, PhD
Associate Professor of Neurology, Harvard Medical School
Thesis Supervisor

Signature redacted

Accepted by .....
Emery N. Brown, MD, PhD
Director, Harvard-MIT Program in Health Sciences and Technology
Professor of Computational Neuroscience and Health Sciences and Technology

Neurophysiological Properties of Cortico-Cortical Evoked Potentials in Humans

by

Britni Crocker

Submitted to the Harvard-MIT Program in Health Sciences and Technology
on August 31, 2018 in partial fulfillment of the requirements for the degree of
Doctor of Philosophy in Medical Engineering and Medical Physics

ABSTRACT

Invasive electrical brain stimulation has been increasingly used to treat an ever wide range of neuropsychiatric disorders from Parkinson's disease to epilepsy and depression. In addition, single pulse electrical stimulation (SPES) is increasingly used to map connections between cortical areas using cortico-cortical evoked potentials (CCEPs). However, the properties and mechanisms underlying brain stimulation remain mostly unknown, hindering the application of stimulation to new neurological disorders and the development of adaptive stimulation technologies that could improve clinical outcome.

To improve understanding of SPES, we systematically explored the effects of cortical electrical stimulation in human epilepsy patients. These patients have intracranial electrodes implanted for intractable epilepsy as part of their clinical course, creating a unique opportunity to simultaneously stimulate and record the human brain in multiple locations. Single pulses of electrical current were delivered across pairs of electrodes in the human cortex, and the neurophysiological responses are recorded.

Examining some fundamental properties of CCEPs, we show that the brain's response to less than a millisecond pulse of stimulation can be detected up to one second post-stimulus. This response has two peaks with distinct properties; compared to the second peak, the first is less variable, and its timing is less delayed by distance, while its magnitude is more diminished by distance. Looking at the spatial distribution of CCEPs, we show that stimulation-derived networks are more closely related to structural connectivity than functional connectivity. However, correcting for distance eliminates this difference. Monitoring CCEPs across different brain states, we show that the second peak of the CCEP is significantly diminished during anesthesia.

Taken together, these results provide important insight into the basic neurophysiological properties of CCEPs, their spatial distribution, and how they are modulated by the state of the brain itself. These characteristics can inform experimental design, provide input parameters for modeling studies, and be applied towards the development of adaptive closed-loop stimulation paradigms.

Thesis Supervisor: Sydney Cash
Title: Associate Professor of Neurology

Acknowledgements

A great number of people contributed to the completion of this work, either by professional advice or personal support.

First, I would like to thank my research advisor, Professor Sydney Cash, for his exceptional mentorship over the last six years, for his patience, even when I was getting up to trouble, and for his incredible kindness – the kind of kindness that permeates throughout the lab and fosters a genuine spirit of friendship in everyone.

I would like to thank my committee members, Professor Matthew Frosch and Professor Patrick Purdon, for challenging me throughout graduate school and for years of insightful advice.

I would like to thank Yangling Chou, who over the past six years has wrestled with slow-moving bureaucracies on my behalf for countless hours, who never once showed me any irritation for being interrupted and asked questions and who frequently went way beyond necessity in helping me seek answers to those questions.

I am grateful for all my past and former labmates and collaborators in both the Cashlab group and the broader MGH community: to Giovanni Piantoni for teaching me about proper repository control for scientific code, to JB Eichenlaub, Alex Hadjinicolaou, and Pariya Salami for answering (always with a smile) any number of MATLAB questions and problems, including silly bugs, to Brian Coughlin for being my first true friend in the lab and an endless source of conversation about music and cartoons, to Angelique Paulk, Rina Zelmann, Kara Farnes, and Ishita Basu for enduring many long days of experiments and for lessening the misery by sharing, to Jason Naftulin for teaching me how to 3D print, to Kyle Pellerin for brightening up so many gloomy winter days with amusing banter, to Lynde Folsom for introducing me to so many amazing ideas and cultural references, to Daniel Song and Lauren Ostrowski, for being very patient in teaching me DTI analysis methods, to Noam Peled for helping me find that DTI data in the first place.

I would like to thank the Senior House community at large for giving me a place to call home at MIT and an occasional outlet for internet flame. Especially, I'd like to thank my fellow GRTs: to Matt Getz for teaching me how to let go of the little things, to Maggie Delano, for teaching me the way through grad school and how to be a better person by example, to Angela Kilby for advice about graduate school and MIT and to Josiah Seale for advice about life, and to all the GRTs for the late nights together – whether spent in revelry or misery.

I am grateful to the graduate students in the HST who mentored me and helped me navigate the department. I would especially like to thank Anik Debnath, Jaeseung Hahn, Susie Mayas, and Rida Mourtada for making graduate school bearable and being amazing friends.

I am deeply grateful to my entire family for their support over the years. To my brother for his selfless help and for all the fun we've had together, to my sister for teaching me so much about computer science and always answering my stupid programming questions, to Maureen for her incredible kindness and generosity and for never flinching when she encounters our family's special brand of weirdness. To the Antonaccio family, who welcomed me with open hearts and supported me over the past 15 years, and especially to the late Mrs. Katie Antonaccio for her unfailing

generosity and attention – even as her health failed her. To my mother, who didn't live to see me enter graduate school, but who instilled in me some of my most cherished values – a respect for my cultural heritage, a deep desire to see justice in the world, and an unabashed anti-authoritarian attitude (the latter of which my mother may have sorely regretted at times). And to my father, who has guided me with excellent advice throughout my life and raised me to independent and intellectually curious.

Finally, I owe enormous gratitude to my life-partner Dan Antonaccio, who has made incredible sacrifices to stay by my side and support me while I pursued my own professional goals, and who has been my closest and deepest friend for over 14 years. He is not only the sole reason I ate any home-cooked meals in the past couple of months, but he also is currently responsible for organizing the move of our entire apartment while I finish up this thesis. I am so grateful for his amazing kindness, for tolerating me and my miserable stress way more than was deserved, and for making all these adventures worth their while by sharing in them. Here's to the next one!

Table of Contents

Table of Figures

1 Background and Significance

Millions of Americans suffer from neurological disorders, including debilitating conditions such as Parkinson's disease and epilepsy (Zack and Kobau, 2017; Marras *et al.*, 2018). Medications are often the first line of treatment, but they sometimes cause unwanted side-effects and are not equally effective for all patients (Jankovic and Poewe, 2012; Smith *et al.*, 2012; Sprenger and Poewe, 2013). In recent years, invasive electrical brain stimulation has been used to successfully treat an increasing number of neurological disorders (mostly movement disorders) in patients who do not respond well to medication; such stimulation has markedly improved their quality of life. For example, deep brain stimulation has been an effective treatment for over a hundred thousand patients with movement disorders such as Parkinson's disease and essential tremor (Larson, 2014); other forms of brain stimulation are effective in treating pain and mood disorders (Boccard, Pereira and Aziz, 2015; Fitzgerald and Segrave, 2015). Brain stimulation is now a commonplace approach to the treatment of refractory epilepsy, including the responsive neurostimulator from Neuropace Inc. – the first closed-loop system approved by the FDA (Morrell and Halpern, 2016).

Despite the enormous potential of this therapeutic method, progress in the field is hampered by the fact that relatively little is known about the physiological mechanisms that underlie the benefits of brain stimulation (Modolo *et al.*, 2011). Stimulation parameters are primarily chosen by trial-and-error (Kuncel and Grill, 2004; Wagle Shukla *et al.*, 2017), and despite the existing consensus that dynamic, adaptive stimulation could improve the efficacy and safety of stimulation devices (Widge, Malone and Dougherty, 2018), development of these devices requires a fairly comprehensive understanding of the effects of different types of stimulation on the local and distant neuronal circuits (Modolo *et al.*, 2011). Advances in recording techniques for human patients and increases in computational power have opened up potential for a new depth of study of cortical and subcortical

circuits, but these techniques have not yet been applied to the comprehensive understanding of brain stimulation.

As a result, surprisingly little is known about how the brain responds to electrical stimulation. Even some of the most basic questions, such as how the response varies to increasing stimulus amplitude, remain unanswered. In order to uncover some of these answers, we have undertaken a study of the human brain's response to a single pulse of electrical stimulation. Brain stimulation has a highly-dimensional set of potential parameters, including amplitude, pulse width, polarity, number of pulses, and pulse frequency. Choosing to focus on single pulse electrical stimulation (SPES) allows us to narrow down the list of possible parameters to a more manageable subset while still exploring the basic properties of the brain's response to electrical stimuli. Single pulse experiments have been a mainstay of electrophysiology for decades, especially in other contexts such as transcranial magnetic stimulation and microstimulation.

1.1 Bioelectricity of the Nervous System

1.1.1 Voltage-gated ion channels

The nervous system and its central organ, the brain, are partially comprised of billions of electrically active cells called neurons (López-Muñoz, Boya and Alamo, 2006). Like many other cells, neurons actively create an ionic and chemical gradient across their membranes at rest: maintaining a relatively high concentration of potassium ions and a relatively low concentration of sodium ions in the cell, and keeping a net negative charge between the intracellular and extracellular space (Hodgkin and Katz, 1985). Uniquely, neurons exploit such gradients to transmit signals by briefly reversing those electrochemical potentials in a wave-like impulse (action potential) that travels along the membrane. Central to the transmission of these action potentials, voltage-gated ion channels open in response to a particular electric field and then allow ionic currents to diffuse across

the membrane according to their electrochemical gradient (Hodgkin and Huxley, 1952). These voltage-gated ion channels can respond to the electrical environment of neighboring areas of the membrane, allowing a cascade of depolarization to propagate over the entire neuron. Biological action potentials are elicited chemically, as receptors on the cell surface respond to chemical signals from sensory receptors or other neurons, but the activity of a neuron can be artificially controlled by exposing it to an external electric field, causing voltage-gated ion channels to open in the absence of a true potential across the membrane. This artificial control of neural activity is the basis for the current brain stimulation therapies.

1.1.2 Stimulation excites primarily axons

Voltage-gated ion channels can be found distributed across the neuron in the axon hillock, nodes of Ranvier, and presynaptic terminals (Lai and Jan, 2006), so any of these neural components could be responsible for the brain's response to stimulation. Biophysical measurements such as the chronaxie of the neural tissue indicate that the biophysical thresholds of intracranial stimulation are very similar to the biophysical thresholds of axons, compared to other neural elements such as cell bodies. Modeling experiments use simulations of neural tissue and electric fields to examine how different neural components respond to stimulation. Finally, two-photon imaging can record the activation of neurons and neural elements simultaneously with electrical stimulation experiments. Taken together, these three forms of evidence indicate that axons are the primary neural component activated during electrical stimulation of the cortex.

In measurements of excitable tissue, the chronaxie is the duration required to elicit a response when stimulating at an amplitude of twice the minimum amplitude to generate a response. Early measurements indicate that the chronaxies of large, myelinated axons are considerably shorter than the chronaxies of small axons and cell bodies (Ranck, 1975; Brocker and Grill, 2013). In extracellular

microstimulation experiments, measurements of both cell body activation and axonal activation show that the chronaxie for microstimulation is very similar to the chronaxie for axons, while being 40 times larger than cell body activation (Nowak and Bullier, 1998). These experiments have since been repeated with the macrostimulation used in clinical settings. Measurements of chronically implanted electrodes on the motor cortex yield a small chronaxie – indicative of axonal activation (Hanajima *et al.*, 2002). Similarly, subcortical measurements with chronically-implanted deep brain stimulation also indicate a chronaxie that corresponds to large myelinated axons (Holsheimer *et al.*, 2000). Chronaxie measurements suggest that axons are the primary targets of electrical stimulation in the human brain.

However, modeling and simulation studies paint a slightly more complex picture. Given that the stimulation electrode creates an electric field that varies in strength by distance, which neuronal elements are activated may be dependent on the particular geometry, orientation, and distance of the neuron to the stimulation electrode (Ranck, 1975). While simple models with point source approximations of stimulation produce reliable activation at the axon at the axon, more complicated stimulation paradigms may change the results (McIntyre and Grill, 1999, 2002). Symmetric, charged-balanced stimuli – the kind used in this thesis – may preferentially activate axons, while asymmetric stimuli may activate a larger portion of cell bodies; still, the threshold for activation of axons is consistently lower than the threshold for cell bodies (McIntyre and Grill, 2002). Ultimately, the activation of axons may explain some otherwise confusing experimental results – that the output of stimulated areas increases while the firing of neurons within stimulated areas decreases; if cell bodies and axons are differentially activated, their activity could be decoupled (McIntyre *et al.*, 2004). Together, these modeling studies confirm that axons have a lower threshold of activation, while allowing for more complicated effects.

Further evidence for the disparate involvement of axons and cells bodies in stimulation comes from calcium imaging experiments. Two-photon calcium imaging is an optical imaging technique to monitor the activity of neurons using fluorescent, calcium-sensitive dye (Göppert-Mayer, 1931; Stosiek *et al.*, 2003). This method has the advantage of not being affected by the electrical stimulus itself, allowing for a simultaneous monitoring of neuronal activity during stimulation. Two-photon imaging during microstimulation of the cortex revealed that a small, sparse number of neurons were activated during stimulation, and that small changes in the position of the stimulating electrode yielded large changes in the population of activated neurons (Histed, Bonin and Reid, 2009). These results indicate that axons are the primary targets of activation during stimulation (Histed, Bonin and Reid, 2009). While the degree of sparsity of activation has been called into question, the fact that axons are primarily activated has not (Tehovnik and Slocum, 2013). Taken together, these three modes of study provide strong evidence that axons are the primary target of electrical stimulation in the cortex.

1.1.3 Models of stimulation mechanisms

Outside of the experimental evidence, mathematical models of stimulation can help predict the effects of stimulation. Broadly speaking, there are two components to these models: a model of the stimulation itself, and a model of the neuronal response to the stimulation. The simplest model of the stimulation itself is a point source of voltage, which can be used to determine appropriate electric fields for the rest of the model (McIntyre and Grill, 1999). More complex representations of the stimulation use finite element modelling to numerically solve differential equations across complex geometric boundaries. These geometric elements can be derived from structural imaging of the brain obtained by MRI or histology, as well as the physical dimensions of the electrode itself (Nathan *et al.*, 1993; McIntyre and Grill, 2002; McIntyre *et al.*, 2004).

Once you have the model of the stimulation and the electric field it induces, you need a model of how the brain will respond. In the seminal paper by Hodgkin and Huxley, the first models of the electrical activity of neurons were developed alongside the discovery of voltage-gated ion channels, as the authors sought to describe the results of their electrical manipulations by analogy to electrical components (Hodgkin and Huxley, 1952). In these first models, voltage-gated ion channels are described by their nonlinear conductance for a specific ion, driven by an electrochemical gradient (represented as a battery), and the membrane itself has some capacitance. Strung together, these components describe a compartment model of nonlinear ordinary differential equations that can be numerically (and sometimes analytically) solved. Because of this model's relative simplicity and strong predictive power, it has been the primary method of describing current flow along a neuron's compartment since its conception (Catterall *et al.*, 2012).

Since the nonlinear conductances of voltage-gated ion channels are represented as a function of voltage and time, the effects of electrical stimulation can already be determined on a neuronal compartment scale by determining the electric field induced by a particular stimulation sequence over time(McIntyre and Grill, 1999). Here, the primary compartment of interest is the neuron's axon – the branch of the cell responsible for transmitting signals to other neurons, and the long-presumed target of electrical stimulation (see section 1.1.1). Such models have had a substantial early success. For example, these models accurately predicted that anodal stimulation would require a lower threshold of stimulation amplitude to elicit a motor response (Manola *et al.*, 2007) and that high-frequency stimulation could paradoxically reduce the neural activity of the proximal brain region and simultaneously increase its output to downstream areas (McIntyre *et al.*, 2004). These compartment models have even been used to make predictions about the optimal electrical stimulus for activating sodium ion channels (Clay, Forger and Paydarfar, 2012).

Hodgkin-Huxley compartment models are a mainstay in the field of stimulation modeling. However, understanding the effects of brain stimulation at a clinically useful scale requires modeling not just individual neurons but neuronal circuits and networks. More recent models of electrical stimulation in the brain take network activity and connectivity into account. In the simplest cases, structural connectivity patterns of different brain regions are determined using imaging techniques such as diffusion tensor imaging (McIntyre and Hahn, 2010; Latteri, Arena and Mazzone, 2011). Other models include rudimentary relationships between stimulation effect and LFP (Hahn and McIntyre, 2010) or using artificial neural networks to predict the response to stimulation (Chaturvedi, Luján and McIntyre, 2013). As computational capabilities increase, our ability to model stimulation for clinical understanding also improves.

1.2 Therapeutic Brain Stimulation

1.2.1 Clinical applications

Brain stimulation is an important tool in a number of areas. Stimulation is used in the clinical mapping of brain areas (Mueller and Morris, 1993; Trébuchon and Chauvel, 2016), in the treatment of movement disorders (Larson, 2014; Mahlknecht, Limousin and Foltynie, 2015), pain disorders (Tsubokawa *et al.*, 1991, 1993), and many other neurological and psychiatric illnesses (Oluigbo, Salma and Rezai, 2012; Laxton, Lipsman and Lozano, 2013; Barrett, 2017). Though there are theoretically an infinite number of possible time-varying electrical fields that could be applied as stimulation to the brain, current clinical stimulation protocols are conventionally limited to rectangular pulses and a few parameters: number of electrodes (typically one or two), polarity (which electrode serves as the anode or cathode), frequency (how many times per second to stimulate), amplitude (the amount of voltage to apply), pulse width (the duration of the stimulus pulse), and location (electrode placement within the brain).

A number of different methods have been employed or proposed for determining clinically useful stimulation parameters within this space. Often, effective targets have been discovered by chance or by accident, as for example the placement of electrodes over the motor cortex for chronic pain (Tsubokawa *et al.*, 1991). Sometimes many different stimulation options are tested, and the best of those is used; the high frequency of stimulation chosen for deep brain stimulation was chosen by testing many different frequencies, and noting that symptoms tend to get worse at lower frequencies (such as 50 Hz) and tend to improve at higher frequencies (>90 Hz) (Birdno and Grill, 2008). Other times, factors other than patient outcome are taken into account, such as energy consumption (Wongsarnpigoon and Grill, 2010). Often, the physician will adjust the parameters slightly for each individual patient.

These arbitrarily chosen stimulation parameters have still been shown to be clinically effective, even having a possible neuroprotective effect (Spieles-Engemann *et al.*, 2010). Therapeutic brain stimulation is poised to treat a number of neurological disorders and even mental illnesses, but as the number and complexity of these diseases increases, the effectiveness of fortuitous discovery or trial-and-error strategies is diminished.

1.2.2 Mechanism hypotheses

Stimulation primarily activates axons, and there are a number of hypotheses to explain how this initial activation mediates the clinical effects seen in patients. Recordings from individual neurons in the brain during stimulation have often led to contradictory results suggesting that neural activity is either increased or suppressed by stimulation; these contradictory results have led to speculation that stimulation simultaneously suppresses somatic activation and increases efferent output in an area by bypassing cell bodies and directly activating axons orthodromically (McIntyre *et al.*, 2004). One prevailing hypothesis is that stimulation overrides the pathological activity of brain disorders,

such as bursts, low frequency oscillations, synchronization, or disrupted firing patterns (Birdno and Grill, 2008). Another hypothesis is that brain stimulation disrupts competing neurological processes between pathological brain areas, and this model of brain stimulation has been used to successfully predict stimulation parameters for patients with essential tremor (Cooper *et al.*, 2008). The competing processes model is a subset of general network theories of brain stimulation: the idea that stimulation primarily achieves therapeutic results by acting on brain networks (Hahn and McIntyre, 2010; McIntyre and Hahn, 2010; Walker *et al.*, 2011). Ultimately, the mechanisms behind the therapeutic effects of brain stimulation are unknown.

1.2.3 Closed-loop brain stimulation

Even in the case of well-managed diseases like Parkinson's disease, most patients must still take some form of medication to compliment the stimulation therapy. As the patient's drug metabolism or energy levels fluctuate throughout the day, the severity of his symptoms will also fluctuate, indicating potential gains for an adaptive stimulation system. Other diseases treated by brain stimulation, such as epilepsy, have intermittent rather than constant symptoms, requiring a responsive brain stimulation paradigm. Consensus exists in the scientific community that dynamic, adaptive stimulation could improve the efficacy and safety of stimulation devices. Indeed, some attempts have been made to develop brain stimulation devices that adaptively respond to symptoms as they arise (Graupe *et al.*, 2010). However, the development of this technology is hindered by a lack of biophysical models of brain stimulation itself (Modolo *et al.*, 2011). Brain-computer interfaces have been developed to include microstimulation as a real-time feedback mechanism (O'Doherty *et al.*, 2009), and insights from this kind of technology may be needed to develop the next generation of brain-stimulation therapies (Widge, Malone and Dougherty, 2018).

1.3 Historical Perspective on Single Pulse Electrical Stimulation

The first recordings of evoked potentials in response to electrical stimulation of the cortex were performed by Edgar Adrian in 1936 (Adrian, 1936). In these studies, the evoked potentials were labeled "direct cortical response" and recorded in anesthetized animals (Adrian, 1936). While the experiments primarily focused on trains of stimulation, some of the frequencies used were low enough to elicit evoked potentials from single pulses (Adrian, 1936). This early work noted two separate phases to the evoked potential: an early response, called a "superficial" response, and a late response, called a "deep" response – the latter only appearing if the electrical stimulus was strong enough (Adrian, 1936). It was hypothesized that the superficial response was generated by the excitation of neurons in the superficial layers of cortex, while the deep response was characterized by the recruitment of neurons in the deeper cortical layers (Eccles, 1951). Soon after, single pulse stimulation was used to provide evidence that the corpus callosum mediates interhemispheric connections in both cats and non-human primates, in one of the first examples of using single pulse electrical stimulation to measure connectivity (Curtis, 1940b, 1940a).

Many subsequent attempts were made to study the properties of the direct cortical response and its two phases. In non-human primates, the direct cortical response to single pulse electrical stimulation was shown to decrease in amplitude as the distance from the stimulation site increases, while the latency, time to peak, and duration increase with distance (Rosenblueth and Cannon, 1941). These responses appeared to be the same even when the cortex was isolated by incision from other areas of the brain (Burns, 1950). While many of these experiments occurred under anesthesia, experiments without anesthetic agents revealed an additional high-frequency component to the response which could last 2 to 4 seconds (Burns, 1951). Paired pulse experiments showed an attenuation of the second evoked potential when the second stimulus was delivered during the late, deep phase of the evoked response (Burns, 1951; Chang, 1951a).

Early discussion of the response to single pulse electrical stimulation provides differing accounts of the relationship between the stimulus amplitude and the evoked response. It was noted that the evoked potential became increasingly polyphasic with increasing stimulus amplitude (Rosenblueth and Cannon, 1941). In isolated cat cortex, the early response is said to have a linear relationship with stimulus amplitude, while the late response is said to be all-or-nothing (Burns, 1950). However, other accounts suggest nearly the opposite, with the early response being linear in only a short range and quickly plateauing, while the late response increased linearly with stimulus amplitude (Chang, 1951b). These varying results could be explained by both the differences in methodology – referencing, stimulation paradigms, and cortex preparation – as well as the possibility of undersampling due to a very small number of recording and stimulation electrodes.

Alongside work understanding the evoked potential itself, individual neurons have been recorded during stimulation. One study in cats found an inconsistent increase in firing of neurons during the superficial response, and a very consistent decrease in firing during the deep response, followed by another wave of activation and inhibition (Creutzfeldt, Ba and Schoen, 1956). In total, they measured changes in firing patterns up to 1 second after stimulation (Creutzfeldt, Ba and Schoen, 1956). Similarly, another study in cats found that stimulating the thalamus lead to inhibition of downstream cortical neurons, and that this inhibition increased in duration with stimulus amplitude (Li and Chou, 1962).

Single pulse studies in humans appear somewhat later in the field literature. One of the first studies to look at the response of the human brain to single pulse electrical stimulation makes qualitative observations that the evoked potential increases in magnitude but not in latency with increasing stimulation amplitude (Delgado, Hamlin and Koskoff, 1955). Similarly, evoked potentials in the medial temporal lobe of epilepsy patients were first recorded using depth electrodes in response to single pulse electrical stimulation (Brazier, 1964). This move to studying human patients was not

without controversy. Many scientists like Brazier followed exemplary ethical standards, even by modern sensibilities; they carried out studies in informed, volunteer patients who were already receiving electrode implantation for other clinical purposes such as preparation for epilepsy surgery. Others conducted experiments involving radical new treatments of unclear benefit in vulnerable patient populations[1] and advocated the use of brain stimulation to control marginalized communities. These experiments and the scientific vision being promoted, as well as increasing awareness of government experiments such as MK Ultra, led to public outrage and, ultimately, congressional hearings. The ultimate results seems to have been a significant reduction in the funding and study of brain stimulation for several decades.

1.4 Overview of Thesis Work

Today, electrical stimulation is used in a number of clinical settings. The most visible application of electrical stimulation is therapeutic brain stimulation, such as deep brain stimulation, in which patients receive electrical pulses through implanted electrical devices for the alleviation of symptoms related to neurological disease. Clinicians also use electrical stimulation of the brain to map the cortex before brain surgery, for patients who have either a malignant or an epileptogenic region of brain tissue. This electrical stimulation can be used to inform neurosurgeons of which areas of the cortex are responsible for essential motor and language tasks. This latter form of electrical stimulation is usually done in conjunction with neurophysiological recordings and provides a unique opportunity to study the mechanisms of electrical stimulation in the brain.

From predictions of the Hodgkin-Huxley-type models, the general consensus within the neuroscience community is that electrical stimulation primarily activates axons. This microscopic

[1] For moral and ethical considerations, I have chosen not to cite this research here. However, curious readers can read "The Forgotten Era of Brain Chips", published in Scientific American in 2005 by John Horgan, for an overview of this research in historical context. Readers should be forewarned that this content includes homophobia and racism.

understanding of stimulation has not translated easily into clinical utility, as neurologists primarily diagnose and treat neurological phenomena that occur on a much greater scale. The higher-level effects of electrical stimulation have yet to be thoroughly studied in humans. The major goal of this thesis was to study the effects of electrical pulses applied to the human brain and develop an empirical model of such effects that is clinically useful. Therefore, this study required four main areas of focus:

1. **Development of a stimulation API for programming stimulation experiments.** In order to enable stimulation studies in this work and other studies, an application programming interface (API) was developed that interfaces with the intracortical stimulation device and that generates and executes sophisticated stimulation experiments. This API has been successfully used in a wide variety of stimulation experiments, not just the ones outlined below.
2. **The local neurophysiological response to single electrical pulse.** In particular, we monitored responses in clinically-relevant local field potentials and show that the two phases of the evoked potential have different properties.
3. **The relationship between functional and structural connectivity with the spatial spread of electrical stimulation effects.** The spread of the response to electrical stimulation across the brain was compared to other common measures of functional connectivity, such as cross-correlation and Granger causality, and structural connectivity as derived from diffusion tensor imaging. We show that stimulation networks are similar to structural networks.
4. **An examination of how the states of local and distant cortical circuits contribute variations in electrical stimulation response.** This examination involved determining to what extent the power and phase of cortical rhythms and brain states such as sleep and anesthesia

affect the response to electrical stimulation. We show that anesthesia induces a decrease in the magnitude of the second phase of the evoked potential.

2 Prior Work

The work in this thesis is built on a strong foundation of previous study into the neurophysiological response to single pulse stimulation in the human brain. Here we describe the related work previously done in the field by others.

2.1 The Development of Cortico-Cortical Evoked Potentials

In 1980s and early 1990s, a set of safety protocols for electrical stimulation in humans began to develop (Babb *et al.*, 1980; Gordon *et al.*, 1990; McCreery and Agnew, 1990; Shannon, 1992). The evoked responses of the human brain were soon used to establish estimates of connectivity between areas – first in resected tissue (Rutecki *et al.*, 1989) and then in human patients (Wilson *et al.*, 1990). The term cortico-cortical evoked potential (CCEP) was coined in 2004 by Riki Matsumoto (Matsumoto, Nair, Lapresto, *et al.*, 2004). Though single pulse electrical stimulation and the subsequent evoked potential had been previously studied and used in a wide variety of contexts, this paper described the evoked response in greater detail, renamed the first and second peaks of the response as "N1" and "N2" respectively, and proposed a standardized – albeit somewhat complex – method for determining the magnitude of the response (Matsumoto, Nair, Lapresto, *et al.*, 2004).

2.2 Basic Properties of Cortico-Cortical Evoked Potentials

As explained previously, the 'direct cortical response' to SPES has been primarily characterized by a CCEP with two peaks, labelled historically as the "superficial" and "deep" responses and most recently as "N1" and "N2" (Adrian, 1936; Purpura *et al.*, 1957; Matsumoto, Nair, Lapresto, *et al.*, 2004). The timing of N1 - the first peak - has been measured from 6 to 40 milliseconds, and N2 - the second peak - from 40 to 200 milliseconds (Wilson *et al.*, 1990; Matsuzaki, Juhász and Asano, 2013). However, the shape of the CCCEP can also be polyphasic, particularly with increasing stimulus

strength(Rosenblueth and Cannon, 1941). In total, the duration of the CCEP has been recorded as lasting about 500 ms (Pigorini *et al.*, 2015), though early measurements of neuronal firing rates after single pulse electrical stimulation showed differences up to 1 second (Creutzfeldt, Ba and Schoen, 1956).

Other differences have been noted between the two peaks of the CCEP. Laminar and single-unit recordings suggest that N1 is characterized by an increase in firing, whereas N2 is characterized by a volley of inhibition (Creutzfeldt, Watanabe and Lux, 1966; Alarcón *et al.*, 2012; Keller, Honey, Mégevand, *et al.*, 2014). In one patient, a laminar electrode captured data from multiple levels of cortex during the CCEP; this recording revealed that, at least in this one case, N1 was characterized by an increase in firing in layers 4-6, followed by an inhibition of firing in those layers, then N2 was characterized by an increase in firing in layers 1-4 (Keller, Honey, Mégevand, *et al.*, 2014).

Historically, the relationship of N1 and N2 to stimulus amplitude varied wildly across studies. In one study of isolated cat cortex, N1 is said to have a linear relationship with stimulus amplitude, while N2 is said to be all-or-nothing (Burns, 1950). However, another study suggested N1 has a linear relationship with stimulus amplitude in only a short range and quickly plateauing, with N2 increasing linearly with stimulus amplitude (Chang, 1951b). More recently, a few studies have shown generally increasing CCEP in response to increasing stimulus strength, but the results are largely qualitative or with very poor resolution in stimulus strength (Entz *et al.*, 2014). In addition to the evoked response, it has been shown that SPES increases high frequency activity (> 80 Hz) during N1 and decreases it during N2 (Kobayashi *et al.*, 2015).

The exploration of CCEP properties has been haphazard and incomplete, often producing contradictory results. Some of these properties were discovered decades ago in animal studies but

were never confirmed in humans with contemporary techniques. In Chapter 4 of this work, we take a more systematic approach to the study of CCEPs.

2.3 Cortico-Cortical Evoked Potential Networks

The bulk of study regarding single pulse electrical stimulation, particularly in humans, has been using CCEPS to map out connections between cortical areas. While the use of stimulation as a "gold standard" for determining physiological connections has been disputed (Borchers *et al.*, 2011), it is still a common tool for clinical and scientific determination of connectivity and function (Ritaccio, Brunner and Schalk, 2018). The use of CCEPs to determine connectivity has been compared to a couple of other common techniques for estimating connectivity – most notably imaging techniques such as resting state functional magnetic resonance imaging and diffusion tensor imaging. CCEPs have been an invaluable tool for studying connectivity in humans, where more drastic techniques like dissection and histochemical tracing are rare.

The properties of CCEP networks have been explored in a number of studies. CCEP networks exhibit a strong dependence on distance, with most evoked responses occurring locally to the stimulation site (Keller *et al.*, 2011; Entz *et al.*, 2014; Keller, Honey, Entz, *et al.*, 2014). The qualitative pattern of frequent local connections and rarer distant connections, combined with the quantitative analysis of cluster coefficients and path lengths, indicate that CCEP networks in the brain have a small-world network topology (Keller, Honey, Entz, *et al.*, 2014). Reciprocity of evoked potentials between brain areas is low, estimated to be somewhere between 5 and 10% for all connections and up to 25% for local connections (Matsuzaki, Juhász and Asano, 2013; Entz *et al.*, 2014; Keller, Honey, Entz, *et al.*, 2014; Araki *et al.*, 2015; Jiménez-Jiménez *et al.*, 2015). This asymmetry is structured, with CCEPs in higher-order areas being evoked from stimulation in lower-order areas such as sensory areas (Matsuzaki, Juhász and Asano, 2013; Keller, Honey, Entz, *et al.*, 2014). These properties, combined

with the causal nature of stimulation, have led many scientists to classify CCEP networks as measuring effective connectivity (Entz *et al.*, 2014; Keller, Honey, Entz, *et al.*, 2014).

CCEP networks have been compared to a handful of other techniques for estimating neural connectivity between brain areas. In Broca's area specifically, both the amplitude and the latency of CCEPs were found to correlate with the number of DTI pathways between the stimulation and recording sites (Conner *et al.*, 2011). Similarly, DTI and CCEPs were shown to have qualitatively similar results in one patient in the pre-supplementary motor area (Swann *et al.*, 2012). CCEPs correlate with networks derived from resting state functional magnetic resonance imaging, both in terms of spatial distribution and magnitude (Keller *et al.*, 2011). High gamma power correlations between ECoG channels, as well as raw voltage correlations, correspond to CCEP networks derived from both N1 and N2, and high gamma power degree correlates negatively with CCEP out-degree, degree, and net flow (Keller, Honey, Entz, *et al.*, 2014). However, N2 has a wider spatial distribution than N1 (Matsumoto, Nair, LaPresto, *et al.*, 2004; Entz *et al.*, 2014), indicating that stimulation-derived networks may vary depending on the estimating methodology. Still, CCEP networks show some similarity, overall, to some common measures of structural and functional connectivity.

Given the utility of CCEPs to estimate connectivity, CCEPs have been used in both scientific and clinical contexts as a tool to estimate connections in a large number of functional areas. These areas include the limbic system (Wilson *et al.*, 1990; Kubota *et al.*, 2013), auditory system(Brugge *et al.*, 2003), visual system(Matsuzaki, Juhász and Asano, 2013), language system(Matsumoto, Nair, LaPresto, *et al.*, 2004; Conner *et al.*, 2011; Entz *et al.*, 2014; Araki *et al.*, 2015; Kunieda *et al.*, 2015), and sensorimotor cortex(Matsumoto *et al.*, 2007; Enatsu *et al.*, 2013). In addition to confirming known connectivity patterns and exploring new ones, these networks have potential for clinical use. CCEPs can be recorded during anesthesia, which allows their use during intraoperative mapping, particularly in cases where awake mapping is not feasible (Yamao *et al.*, 2014, 2017; Matsumoto,

Kunieda and Nair, 2017). When language networks have reorganized in patients with temporal lobe epilepsy, CCEPs can reveal nonstandard network configurations in conjunction with standard clinical mapping of the cortex (Enatsu *et al.*, 2013).

In summary, CCEP networks have demonstrated great utility in mapping connectivity in the brain for both scientific and clinical purposes. These networks correlate with a few other methods of estimating connectivity, such as resting state fMRI, high gamma power, and – in a small number of areas – DTI, and they seem to correspond to known properties of effective brain networks, such as asymmetry, local clustering, and network 'small-worldness'. Building off this knowledge, the degree of similarity between CCEP networks and other common network measures, as well as the relative strength of each similarity, is explored in Chapter 5 of this work.

2.4 State-based Modulation of Cortico-Cortical Evoked Potentials

The large majority of studies involving CCEPs assume that the response to CCEPs is static and independent of brain state. There is some limited evidence, however, that CCEPs may in fact be modulated by dynamic changes in cortical activity and, of course, the brain is anything but static as it shifts through various states over both short and long time scales. For example, CCEPs can be recorded during large, broad changes in brain state such as sleep and sometimes show marked differences in their properties. CCEPs during sleep show marked changes compared to rest. During non-rapid-eye-movement (NREM) sleep, the high gamma activity, defined as power in the 100-200Hz frequency range, increases during N1, as does N1 size (Usami *et al.*, 2015). This increase is followed by a decrease in HGA between N1 and N2 (Usami *et al.*, 2015). Similarly, the power above 20 Hz was found to show a similar pattern, with a short increase during N1 followed by suppression during NREM sleep (Pigorini *et al.*, 2015). Other spectral changes during sleep include an increase in slow wave activity, defined as the rectified amplitude of the signal below 4 Hz, and a decrease in

the phase locking across trials (Pigorini *et al.*, 2015). Interestingly, these changes from wakefulness to NREM seem to be graded, with the responses to single pulse electrical stimulation during rapid eye movement (REM) sleep showing a qualitatively similar response to NREM sleep, but to a lesser degree (Usami *et al.*, 2015, 2017). These results show changes in connectivity and excitability during sleep, which are reflected in the CCEPs.

Sleep represents a very large change in brain state, but more subtle state changes can be monitored using the amplitude and phase of oscillatory activity. The power in the alpha and beta frequency bands (8-13 Hz and 13-20 Hz respectively) has been shown in one study to modulate the effect of single pulse electrical stimulation, with higher power immediately preceding the stimulus yielding a larger response (Usami *et al.*, 2018). A similar result has been found with single pulse transcranial magnetic stimulation, where prestimulus phase in the beta or alpha frequency bands was shown to modulate motor evoked potentials or visual evoked stimuli (phosphenes) respectively (van Elswijk *et al.*, 2010; Dugue, Marque and VanRullen, 2011). These studies suggest that CCEPs could be modulated by changes in brain state during wakefulness.

Together, these studies suggest that CCEPs may not be as static of a phenomenon as is assumed. We explore this possibility further with studies conducted on CCEPs during sleep, anesthesia, and changes in oscillatory activity in Chapter 6.

3 CereLAB: a MATLAB API for CereStim Stimulation

3.1 Introduction

Performing stimulation experiments requires the ability to deliver electrical stimuli to the patient's brain. In the previous decades, stimulation by hand-controlled electrodes was the norm; as technology advances, programmable stimulation has increasingly been used. Programmable stimulation allows more consistent timing and location of stimulus delivery, in addition to more sophisticated experimental protocols such as random interstimulus intervals. The programmable stimulation device used for all stimulation experiments presented in this thesis is the BlackRock CereStim 96 (BlackRock Microsystems Inc., Salt Lake City, Utah).

The CereStim is a programmable neurostimulator that can stimulate 96 different electrodes – including up to 16 at once. In addition to a graphical user interface for simple manual stimuli and basic programs, the CereStim includes a C++ API for more complex development of stimulation routines. However, C++ is not a common programming language among scientists, who often prefer to use higher level languages such as MATLAB and Python. To bridge this gap and enable a broad audience of scientists to use the CereStim device for their own stimulation experiments, I developed a MATLAB API for the CereStim called CereLAB. This MATLAB API wraps the C++ API methods and classes through a MATLAB executable (MEX) interface, provides additional warnings and errors for common use cases, includes high-level stimulation programs for oft-repeated stimulation tasks, and is fully documented within the MATLAB environment.

The CereStim device was acquired by the laboratory in 2014; an official BlackRock MATLAB API for the device was released in early 2016. However, the custom-built CereLAB API continued to be used both for the work of this thesis and for experiments by others due to increased internal consistency, convenient higher-order programs for common shared stimulation routines such as

safety testing, and the difficulty of overhauling code to implement a new system. Since the initial development of the CereLAB API, the code has been used for a number of experiments, including the exploration of the parameter space of stimulation trains in both frequency and amplitude and task-dependent stimulation to different regions of the brain based on real-time analysis of cognitive task performance, and the API is being developed for real-time neurophysiological applications.

3.2 Wrapping C++ Classes into MATLAB Classes

The BlackRock CereStim C++ API is structured such that each stimulation device is an object with callable functions from the BStimulator class. MATLAB itself can be used as an object-oriented programming language, with support for class creation including properties and methods (MATLAB, 2016b). Since both C++ and MATLAB support classes, the most straightforward method for creating a MATLAB wrapper of a C++ class is to create a MATLAB shell class with methods that each individually call their C++ counterparts. This strategy has the benefit of allowing very easy transition between C++ and MATLAB APIs for users of either or both languages and of maintaining consistency of code that is simple and easy to debug. However, using this method also requires some kind of reference of the BStimulator object to be passed between the C++ and MATLAB APIs. In a C++ environment, this reference would be implemented with pointers, but pointers are not natively available in MATLAB. Instead, MATLAB refers to objects with object handles, and it has a class type called Handle class for passing references to underlying data rather than the data itself (MATLAB, 2016a).

In order to create a MATLAB wrapper for a C++ class, a method of converting pointers into handles, and handles into pointers, is required. This process is carried out in a MEX intermediary interface between the MATLAB and C++ APIs. Since MATLAB allows for objects of the Handle class to have an arbitrary handle set upon construction, instantiation of the BStimulator class is a four-step process

outlined in Figure 3-1. First, the MATLAB constructor for BStimulator is called in user code. This constructor seeks to define the MATLAB object handle of this particular instance, so next, the MATLAB API calls the underlying mex constructor from the MEX interface. The MEX constructor calls the C++ API, which creates a new BStimulator object in memory, along with a corresponding C++ pointer reference. Finally, this pointer is converted first into a mex Array within the MEX interface, which is then passed to the initial MATLAB API and set as the MATLAB object handle.

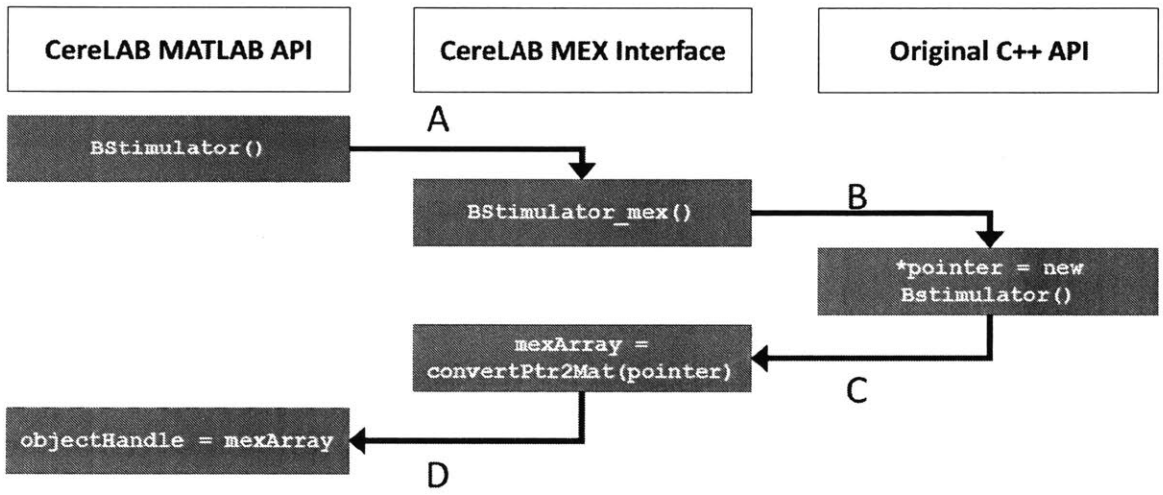

Figure 3-1: an overview of the CereLAB API constructor and its communication with the original BlackRock C++ CereStim API via the CereLAB MEX interface. **A**: MATLAB constructor calls MEX constructor. **B**: MEX constructor calls C++ constructor, which creates new object with pointer reference. **C**: The pointer is returned to the MEX interface and converted to a MEX array. **D**: The MATLAB constructor receives the converted pointer as an object handle.

Fortunately, conversion of pointers into mex arrays has been implemented in community code through a class_handle template header, enabling C++ code to convert any pointers into MATLAB-friendly handles (Woodford, 2018). The class_handle methods in this software allow for converting from pointers to object handles by casting pointers as an unsigned 64-bit integer, and then storing this data directly into a mex Array using mxGetData (Woodford, 2018). Similarly, the header recasts the object handle from a 64-bit unsigned integer back to a pointer (Woodford, 2018). These two

functions together enable seamless communication between the MATLAB wrapper and the C++ API for any method that has been implemented in both APIs.

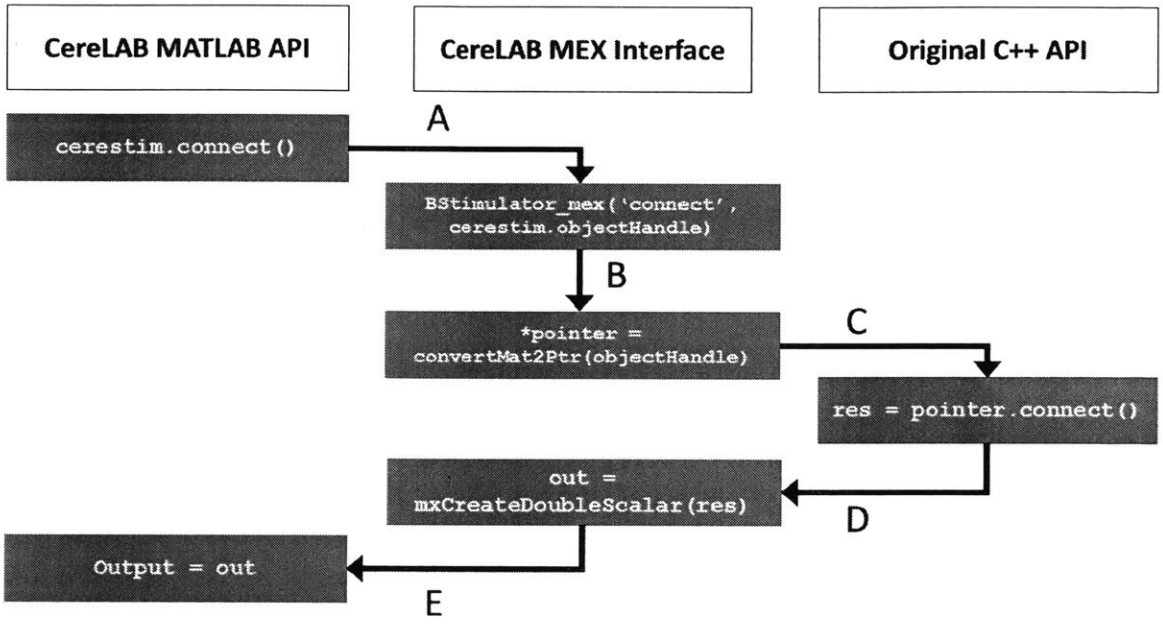

Figure 3-2: an example of a CereLAB function call and its communication with the original C++ API via the MEX interface. A: MATLAB API calls MEX interface with BStimulator object cerestim. B: MEX interface converts object handle to C++ pointer. C: MEX interface calls C++ API with any input arguments. D: C++ output from function call is converted into the corresponding MEX datatype. E: MATLAB method receives converted result as output.

Just as C++ pointers need to be converted to MATLAB object handles to create a BStimulator object, function calls from the CereLAB API must perform the reverse conversion to call the underlying C++ methods. Any method call from the CereLAB API requires a five-step process to complete outlined in Figure 3-2. First the CereLAB function is called from user code using the previously created BStimulator object. This object passes the name of the function call, along with any accompanying arguments, to the MEX C++ API, which first converts the handle back into a C++ pointer, and then calls the appropriate C++ method with any provided input arguments. When the C++ method call has completed and output arguments have been returned, the MEX C++ API may convert these

output arguments into the appropriate MATLAB format before returning the output to the MATLAB API for the user.

3.3 Warnings and Errors for Intuitive Use Cases

The bulk of the CereLAB API is comprised of the MATLAB BStimulator handle class with its associated MEX interface for converting data structures between the two regimes. Most of the functions recreated in the MATLAB API are direct pipelines to the C++ API, with no additional functionality added. However, there are a few differences in some of the key methods where the original C++ API did not lend itself well to translation into a MATLAB environment. These changes allow for more intuitive and familiar use within the MATLAB framework.

The native C++ API for the CereStim has a function for connecting to the CereStim device. This function attempts connection one time and returns an error if a connection has not been established. Due to timeouts and potential cable mistakes, this function often fails on the first try, leaving the user to manually and repeatedly call the connect method until a connection has finally been achieved. The CereLAB API circumvents some of this user frustration by automating the repeated connection process. If a connection has not been established on the first method call, the API will automatically reattempt the connection process for up to 100 tries. In addition, the API provides helpful status messages within the MATLAB environment to indicate when the CereLAB API will first attempt to connect, when it fails to connect but will reattempt connection, when it has successfully connected, and/or when it has repeatedly failed to connect and will no longer attempt to do so.

Another area of expansion has been the method for configuring the stimulation parameters on the device. According to the C++ API of the CereStim device, the API will accept stimulation frequencies from 4 Hz to 1000 Hz. However, the CereStim device is unable to maintain a wait period longer than

65,535 microseconds (the largest number that can be defined with a 16-bit integer). This limitation means that the CereStim is not capable of producing stimulation at frequencies lower than 16 Hz, since the period between pulses is longer than the CereStim can handle. The C++ API will still allow you to attempt stimulation at these lower frequencies, producing erratic and undefined results which depend on the degree of integer overflow. The CereLAB API, however, checks the intended stimulation frequency and produces an error if the frequency is below 16 Hz. Stimulation at frequencies below 16 Hz is still possible in both APIs, but it requires delivering each pulse individually with a sequence of pulses and wait periods.

Finally, when querying the CereStim status, the CereLAB API has included an option to display the status in text in the MATLAB environment. The original C++ API returns an integer value between 0 and 5 inclusive to indicate the real-time status of the CereStim when queried. These values indicate whether the CereStim is currently delivering stimulation, whether it has been stopped or paused, whether the CereStim is waiting for an external trigger, or whether the CereStim is writing a sequence or has been given an invalid sequence. For ease of use, primarily in debugging, the CereLAB API method call for reading the status of the CereStim includes an optional "verbose" flag to enable the display of human-readable output.

3.4 Additional Functionality for Stimulation Routines

On top of a wrapper for the native functions provided by the original C++ CereStim API, CereLAB are higher-level functions for the automation of common or routine tasks. These functions cover a variety of tasks, ranging from simple programs for safety testing before experiments and delivering repetitive single pulses to more complex experimental protocols such as delivering theta burst stimulation. The primary advantage to using a custom-developed stimulation API is that it allows for these common tasks to be included directly into the API itself, rather than having every user develop

their own unique code for the same task. This sharing saves work and standardizes protocols across users for easier comparisons.

Before delivering trains of stimulation at the desired amplitude, it is often necessary to first test a few trains at a lower amplitude, checking to be sure that the patient cannot discern any side effects and that the stimulation does not itself evoke any epileptiform activity or afterdischarges (So and Alwaki, 2018). The CereLAB API contains a function called safetytest to semi-automate this process and to speed up the process by reducing the time necessary for set-up and control. For a specified electrode pair, the safetytest function will stimulate at the given frequency and amplitude five times in a row, with a wait period in between to check the recordings and check-in with the patient. If multiple amplitudes are given, the function will iterate through them in the order given.

The bulk of the results presented in this thesis were collected through the use of three functions in the CereLAB API: Amplitudes, networktest, and singlepulses. The Amplitudes function delivers single pulses at an interstimulus interval with a uniform distribution between 2500 and 3000 milliseconds. These single pulses are delivered at varying amplitudes between 500 and 10,000 microamperes in a block-random order, allowing for the data from the lower amplitude blocks to remain useful even if the experiment was terminated in a higher amplitude block. The networktest function delivers single pulses to a set of stimulation pairs in a random permuted sequence for the specified number of trials. Single pulses are delivered individually at 3 second intervals. The singlepulses function delivers single pulses to one pair of electrodes at an interstimulus interval with a uniform random distribution between 2500 and 3000 milliseconds at 7000 microamperes with alternating polarity for each trial. All three of these functions include automatic logfile generation for reconstructing the sequence of stimuli in data analysis.

Finally, the CereLAB API also includes scripts and functions for experiments not covered in this thesis. The pairedtrainpulse script delivers single pulses of stimulation at a random interval after a train of random frequency. Parameters for the script can be modified in the top section of the local file. The thetaburst function allows for automatic delivery of stimulation trains that approximate theta bursts. For a given amplitude and electrode pair, six trains of 200 Hz stimulation, each lasting 50 ms, are delivered with a train frequency of approximately 6 Hz.

3.5 Documentation

While some experiments have been designed directly into the API, the CereLAB API is primarily intended to allow users to write their own stimulation code. To that end, the CereLAB API has been fully documented with corresponding help text for use in the MATLAB environment. Documentation includes not only high-level functions but low-level BStimulator class methods. Users can call BStimulator methods help by using the construct BStimulator.method or BStimulator/method. Help text provides users with a summary of the method or function purpose, a description of every input and output, including format, and often includes examples of use cases for illustration. Examples of help text documentation can be seen in Figure 3-3.

3.6 Applications

In addition to the experiments presented in subsequent chapters of this thesis, the CereLAB API has been used for a number of other applications by others. Since MATLAB is a common language for designing experiments, particularly with the development and use of Psychtoolbox (Brainard, 1997; Pelli, 1997; Kleiner *et al.*, 2007), the CereLAB API allows for stimulation to be directly integrated into MATLAB code for psychophysical and cognitive tasks. In addition, the API can be combined with real-time Simulink processes to enable closed-loop stimulation (Sarma *et al.*, 2016).

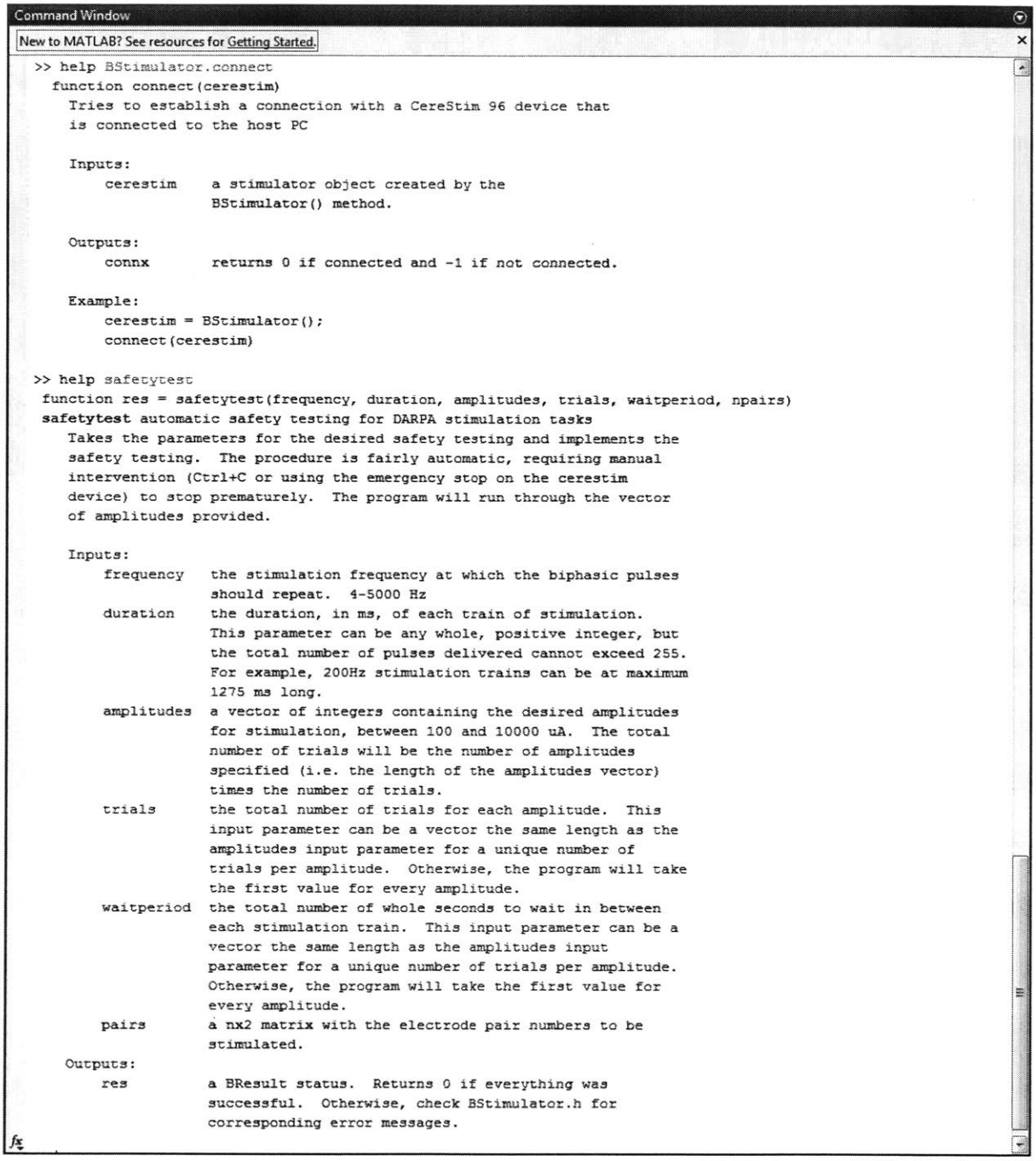

Figure 3-3: CereLAB documentation. Users can call the CereLAB documentation within the MATLAB environment using intuitive MATLAB-style commands. The documented help information includes an overview of the function's purpose, a detailed description of any inputs or outputs, and an example use case.

3.6.1 Open-loop stimulation

One of the main and most common use cases of the CereLAB API is to develop open-loop experiments for electrical stimulation. One example of an open-loop stimulation protocol is the

routine safety testing performed before task-based stimulation to ensure that the desired stimulation parameters – such as amplitude and location – do not provoke any afterdischarges, epileptiform activity, or other side effects. This protocol is described above in section 3.4 and is carried out under the supervision of a trained epileptologist who can monitor the recordings during stimulation.

While the work in this thesis has primarily centered on the properties of the response to single pulses, other work carried out by Ishita Basu and Angelique Paulk, has used CereLAB to focus on the response of the brain to trains of electrical stimulation of varying amplitudes and frequencies (Basu, Robertson, *et al.*, 2018). In addition to the MATLAB API, I was able to program a custom C++ executable for delivering trains of electrical stimulation at a given amplitude (see Figure 3-4). This program, referred to as the Matrix program because it explores the frequency and amplitude matrix of the stimulation parameter space, delivers trains of stimulation across a specified electrode pair and amplitude at 10, 20, 40, 80, 100, 160, and 200 Hz in a block random design (Basu, Robertson, *et al.*, 2018). Higher stimulation amplitudes are more likely (though still unlikely) to cause unwanted side effects, which would typically result in aborting the experiment. By implementing the Matrix program with a

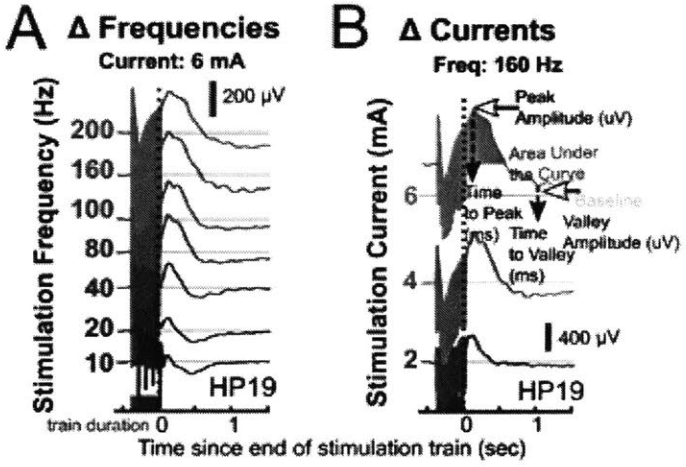

Figure 3-4: custom-built C++ executables delivered trains of stimulation at different amplitudes and frequencies to explore how the response varies with these parameters. Large stimulation artifacts can be seen in the signal during the train; the train duration is indicated by the grey rectangle on the x-axes. **A**: an example from one patient showing how the response to stimulation varies with train frequency. All stimulation in this example was carried out at 6 mA. Each stimulation frequency is represented by a different color from blue (10 Hz) to pink (200 Hz). **B**: an example from one patient showing how the response to stimulation varies with train amplitude. All stimulation in this example was carried out at 160 Hz. Each stimulation amplitude is represented by a different color from red (2 mA) to yellow (6 mA). Stimulation responses are measured here by peak amplitude, time to peak, area under the curve, valley amplitude, and time to valley. **Reproduced with permission from Basu et al. 2018.**

constant amplitude, the researcher is able to slowly increase amplitude at each iteration and ensure that experimental data at lower amplitudes will be collected even if the program must be stopped at higher amplitudes. The Matrix program delivers trains of stimulation at 8 second intervals with 500 ms of random jitter, with a single pulse interspersed between each train. This long interval between trains allows the neurophysiological signals to recover to baseline. The recorded evoked potentials in a subset of stimulation frequencies have been used to fit a neural mass model to simulate responses at other stimulation frequencies (Basu, Crocker, *et al.*, 2018).

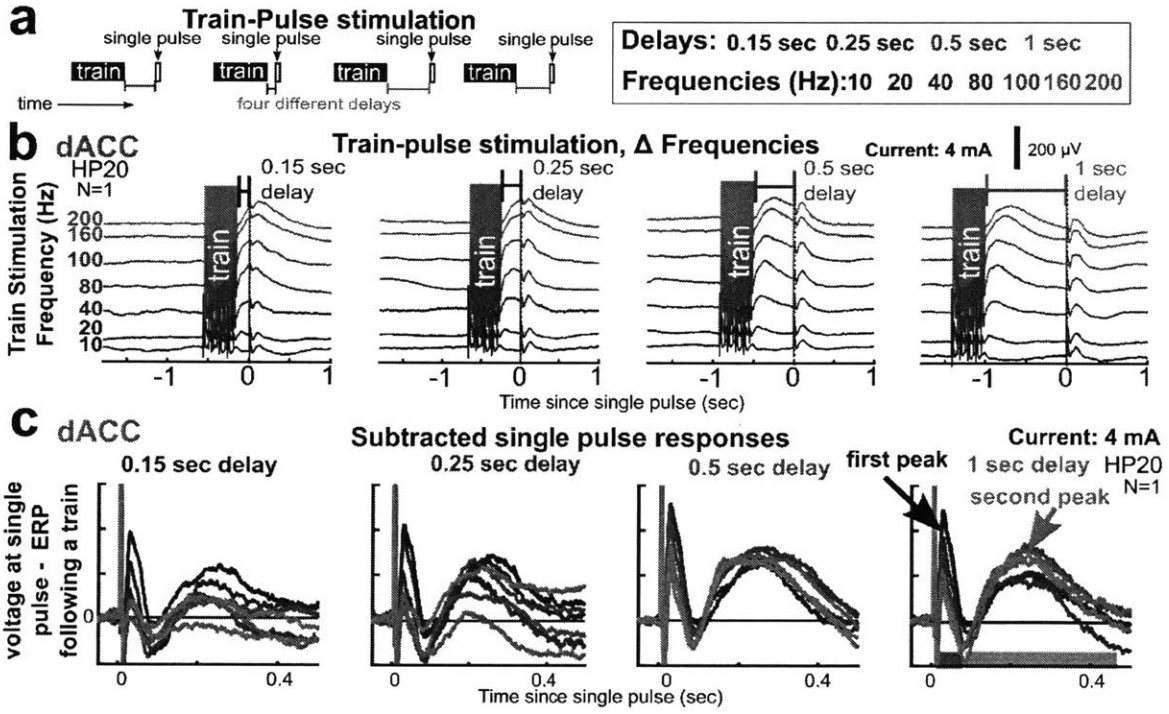

Figure 3-5: the CereLAB API can create stimulation routines such as paired train-pulse. **a**: an overview of the train-pulse experimental paradigm. Trains of stimulation at frequencies from 10 to 200 Hz are delivered, followed by one of four delays from 0.15 to 1 s and then a single pulse of stimulation. **b**: examples from one patient showing the delivery of both trains and single pulses at every possible frequency and delay combination. The single pulse response varies with both frequency and delay. **c**: the single pulse responses from b are overlayed on one another, highlighting the differences across frequencies and delays. **Reproduced with permission by Angelique Paulk.**

In addition to looking at the neurophysiological response to different frequencies and amplitudes of stimulation, changes in neural dynamics can be measured by delivering a single pulse of electrical

stimulation after the train at some delay interval. Paired pulse paradigms have been used for decades as a way to gauge facilitation, potentiation, and depression in a wide variety of contexts(Curtis and Eccles, 1960; Rothwell, 1999). For this investigation carried out by Angelique Paulk, I created a CereLAB script to deliver trains of pulses and delayed single pulses in a block-random order with a specified amplitude and location (see Figure 3-5). This experiment expands on the previous Matrix program by investigating the response of the brain to trains of electric stimulation more closely.

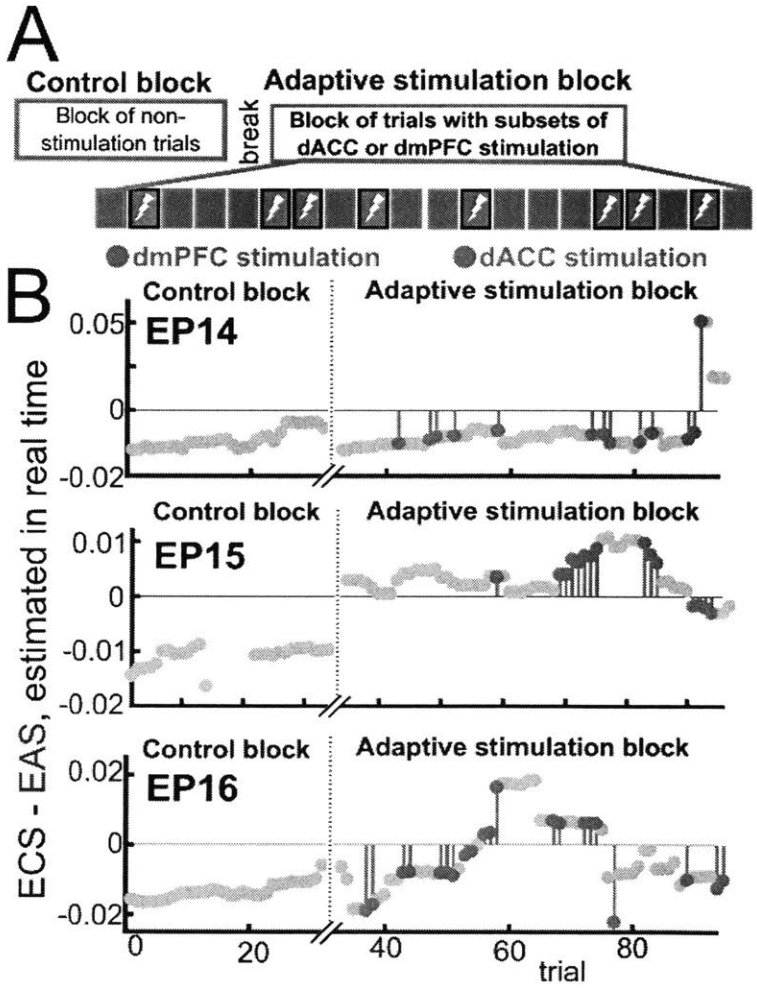

Figure 3-6: the CereLAB API can be used for adaptive real-time stimulation based on performance in a cognitive task. A: an overview of the experimental protocol. First, a control block of task trials without stimulation is implemented to establish a behavioral baseline. After a break, the same task is repeated with adaptive stimulation of either the dorsomedial prefrontal cortex (dmPFC) or the dorsal anterior cingulate cortex (dACC) in some of the trials. B: examples from three participants showing the effects of adaptive stimulation on performance of the task. **Reproduced with permission from Paulk et al. 2018.**

3.6.2 Closed-loop stimulation to behavior

In addition to open-loop routines and scripts, the CereLAB API can be used in conjunction with task-creating toolboxes like Psychtoolbox to integrate stimulation into a cognitive or psychophysical task. This integration has been accomplished already by two investigators – Alik Widge and Angelique Paulk – in two tasks: the Multi-Source Interference

Task and the Emotional Conflict Regulation (ECR) task (Paulk *et al.*, 2018). In particular, the ECR task has been programmed to adaptively select stimulation parameters (in this case, stimulation location) in real-time based on the behavioral performance of the patient in the task (see Figure 3-6) (Paulk *et al.*, 2018).

3.6.3 Closed-loop Stimulation to neurophysiology

Finally, the CereLAB API has been used to deliver closed-loop stimulation in response to neurophysiological activity. Together with Anish Sarma and Rina Zelmann, we have developed a modular, closed-loop system for intracranial stimulation. This system can collect data from intracranial electrodes, process the data using a wide variety of potential signal processing and state estimation techniques, and deliver stimulation based on this processing and estimation. The real-time processing is accomplished with real-time software on the Simulink Real-Time operating system (Mathworks, Natick, MA) on the "Decider". Stimulation parameters can be controlled using a graphical user interface (GUI) at the host computer. The latency of this system has been measured at 5 ms (Sarma *et al.*, 2016).

This system has since been extended by Rina Zelmann to handle real-time changes in stimulation parameters based on ongoing neurophysiological changes. For example, closed-loop changes in stimulation electrodes can be configured such that if a specified parameter falls below a certain threshold, one pair of channels is stimulated, but if the parameter rises above a threshold, then another pair of channels is stimulated. This closed-loop multisite stimulation paradigm has been coded into the host GUI using the CereLAB API, including two higher-level functions called initializeCereStim and changeChannelStimulationCereStim. The first function, initializeCereStim, connects to the CereStim and establishes the parameters for future stimulation, such as frequency, duration, amplitude, and channels of interest. It then loads these parameters into the CereStim to

be stimulated upon receipt of an analog trigger stimulus. The second function, changeChannelStimulationCereStim, keeps the original stimulation parameters but changes the specified stimulation electrode pair, again loading these parameters into the CereStim to be triggered as neurophysiological features are detected.

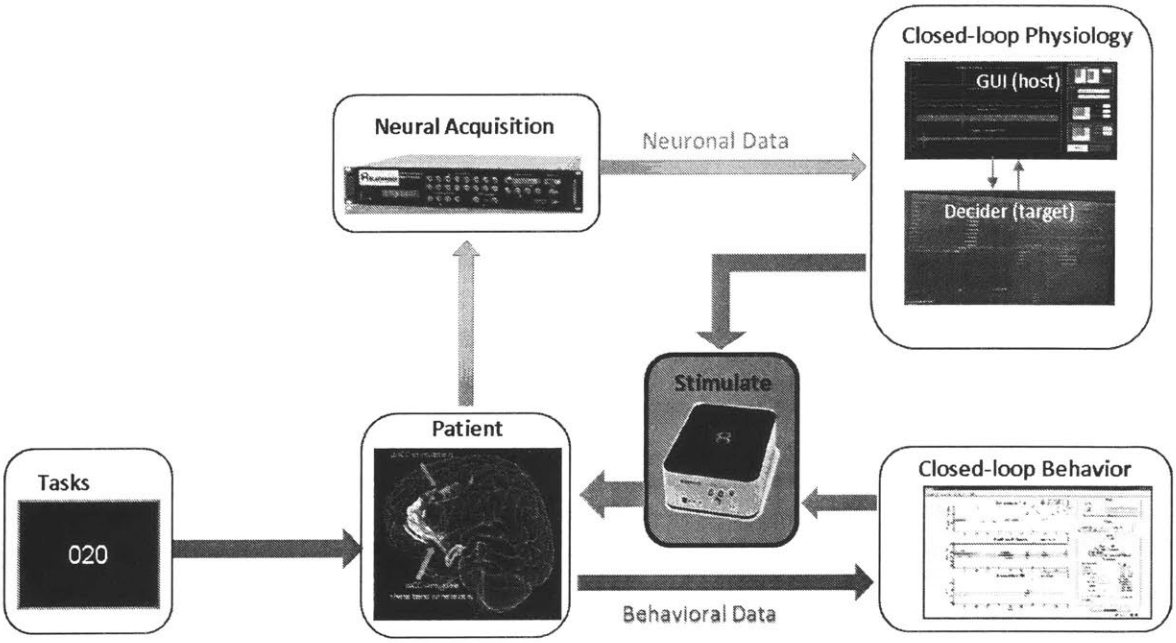

Figure 3-7: an overview of the closed-loop stimulation paradigms. Neural data is acquired from the patient through the neural signal processors and then sent to the Decider to be analyzed for closed-loop physiology (**yellow**). The detection parameters can be modified with the host GUI. Once the specified neurophysiological feature has been detected, this information is sent to the CereStim, along with any relevant stimulation parameters, to initiate stimulation (**orange**). This paradigm can be used on its own or alongside a cognitive or psychophysical task. Any tasks are presented through a separate computer; information about task performance is then sent to a separate computer for closed-loop analysis of behavior (**blue**). Parameters in the closed-loop behavior can also be used to trigger stimulation (**orange**). The CereLAB API is used to send instructions from the closed-loop physiology or closed-loop behavior computers to the CereStim. **Reproduced with permission by Rina Zelmann.**

3.7 Conclusion

In order to facilitate stimulation with the BlackRock CereStim device, I wrote a custom MATLAB API called CereLAB to interface with the original BlackRock C++ API. The CereLAB API uses a MEX interface to convert between MATLAB class objects and C++ pointers to objects, and it comes with higher-order stimulation routines for common and repetitive tasks as well as full MATLAB-friendly

documentation. In addition to the experiments in the proceeding chapters, the CereLAB API has been used for a wide variety of experiments from other scientists in the past few years, including attempts to map out the brain's response to a wide variety of parameters and using stimulation in conjunction with cognitive tasks for open-loop and closed-loop stimulation. The CereLAB API has successfully allowed scientists who are familiar with MATLAB but not C++ to easily utilize the CereStim device to implement their own stimulation experiments.

4 Neurophysiological Responses to Single Pulse Electrical Stimulation in the Human Brain

4.1 Introduction

As discussed above, brain stimulation is an important tool in the clinical mapping of brain areas (Mueller and Morris, 1993; Trébuchon and Chauvel, 2016), in the clinical treatment of movement disorders (Larson, 2014; Mahlknecht, Limousin and Foltynie, 2015), and as a clinical treatment for many other neurological and psychiatric illnesses (Oluigbo, Salma and Rezai, 2012; Laxton, Lipsman and Lozano, 2013; Barrett, 2017). Electrical stimulation of the brain acts primarily on the axons of neurons near the stimulation site (Histed, Bonin and Reid, 2009), though the response of any individual neuron to stimulation is variable(Bosch *et al.*, 2011) and determined by a variety of factors (Brocker and Grill, 2013). These factors increase the difficulty of predicting the effects of direct electrical stimulation, which arise from a complex combination of events within a large volume of brain tissue (Borchers *et al.*, 2011), even in the case of a single pulse of electrical stimulation.

Recent investigations of single pulse electrical stimulation (SPES) have focused on mapping the cortex with the resulting cortico-cortical evoked potentials (CCEPs) (Kunieda *et al.*, 2015). These responses can be recorded both local to the stimulation site and at a portion of cortical sites some distance away and are used to infer connectivity between cortical brain regions (Matsumoto, Nair, Lapresto, *et al.*, 2004). Particularly in humans where tract-tracing studies are rare (Schmahmann and Pandya, 2007), CCEPs present an invaluable opportunity to explore brain connectivity in many regions, including the motor system and frontal lobe (Matsumoto, Nair, LaPresto, *et al.*, 2004; Lacruz *et al.*, 2007).

The 'direct cortical response' to SPES has been primarily characterized by a CCEP with two peaks, labelled most recently as "N1" and "N2" (Adrian, 1936; Purpura *et al.*, 1957; Matsumoto, Nair, Lapresto, *et al.*, 2004). The timing of the first peak has been measured from 6 to 40 milliseconds, and the second peak from 40 to 200 milliseconds (Wilson *et al.*, 1990; Matsuzaki, Juhász and Asano, 2013). The late response, N2, is known to have a wider spatial distribution than N1 (Matsumoto, Nair, LaPresto, *et al.*, 2004; Entz *et al.*, 2014). Laminar and single-unit recordings suggest that N1 is characterized by an increase in firing, whereas N2 is characterized by an initial volley of inhibition (Creutzfeldt, Watanabe and Lux, 1966; Alarcón *et al.*, 2012; Keller, Honey, Mégevand, *et al.*, 2014). In addition to the evoked response, it has been shown that SPES increases high frequency activity (> 80 Hz) during N1 and decreases it during N2 (Kobayashi *et al.*, 2015), and slow wave activity (>4 Hz) increases and is enhanced if the stimulation is delivered during non-REM sleep (Pigorini *et al.*, 2015). Still, the characteristics and mechanisms of these evoked responses remain poorly understood.

To further explore the properties of CCEPs, we analyzed the responses to SPES from 15 human patients with clinically implanted electrodes. We characterize the time course, variability, and distribution of CCEPs in both the time and frequency domain. Focusing on the two characteristic peaks of the CCEP (N1 and N2), we show that the response to SPES can last up to one second, much longer than previously reported, and N2, but not N1, peak timing is later as a function of distance to the stimulation site.

4.2 Methods

4.2.1 Data Collection

I present the data from 15 participants (7 women, 8 men, ages: 19-57) – patients with intractable epilepsy who had implanted invasive depth electrodes (162 – 242 contacts per patient, average number: 211) in both hemispheres as part of their clinical course in preparation for resective brain

surgery. Depth electrodes (Ad-tech Medical, Racine WI, USA, or PMT, Chanhassen, MN, USA) had diameters of 0.8–1.0 mm and consisted of 8-16 platinum/iridium-contacts 1-2.4 mm long. The placement of electrodes was determined by clinical need, with most electrodes in the frontal or temporal lobe. All experiments were conducted in the last 2-3 days of their hospital stay, after clinical decision making and restarting of antiepileptic medications but before resection. All participants gave informed consent to the research protocol, which was approved by the Partners Healthcare Institutional Review Board.

Data were recorded using Blackrock Neural Signal Processors at 2000 samples per second (BlackRock Microsystems Inc., Salt Lake City, Utah). Signals were not filtered to avoid ringing artifacts caused by low-pass filters with sharp transitions. All data were rereferenced using a bipolar scheme before further analysis. Any channels with a high level of background noise (determined visually) were excluded from analysis. Channel locations were determined by coregistering pre-surgery MRI to post-surgery CT(Dykstra *et al.*, 2012; Yang *et al.*, 2012). Reported distances between channels are calculated as the Euclidean distance between the mean locations of each electrode pair.

4.2.2 Stimulation Delivery

SPES was delivered using the Blackrock CereStim (BlackRock Microsystems Inc., Salt Lake City, Utah). Each pulse of stimulation was biphasic and bipolar (between adjacent channels), with a square pulse-width of 90 us and an inter-pulse interval of 53 us. Stimulation pulses were delivered at a total of 33 electrode pairs where little to no epileptiform activity was recorded and distant from the clinically-determined seizure onset zone. Of these sites, 17 were located in the left hemisphere and 16 were located in the right hemisphere; 15 sites are located in the anterior cingulate cortex (4 rostral, 11 dorsal), 13 sites are located in the frontal lobe (2 in the superior frontal gyrus, 5 in the middle frontal gyrus, 5 in orbitofrontal cortex, and 1 in the cingulate sulcus), 4 in the temporal lobe

(2 in the middle temporal gyrus, 1 in the inferior temporal gyrus, and 1 in the amygdala) and 1 in the corpus callosum. One to five sites were stimulated per patient (range: 1-5, average 3). Stimulation was delivered at an amplitude of 6 or 7 mA. Single pulses were delivered at uniformly random intervals between 2.5 and 3.5 seconds, sometimes interspersed with other stimulation, and at least 20 trials were conducted for each site (range: 20-368, average number of trials: 109).

When testing how the CCEP changes in response to varying stimulation amplitudes, single pulses were delivered from 0.5 mA to 10 mA in 0.5 mA increments. Pulses were delivered in 3 blocks, from 0.5 to 3.5 mA, from 4 to 7.5 mA, and from 8 to 10 mA. Each block consists of 10 trials, and for each trial, all stimulation amplitudes within that block are delivered in a shuffled order. This pseudo-random order was chosen because it is possible, though unlikely, for the patient to experience adverse effects from higher stimulation amplitudes. Splitting the amplitudes into segments allows for the experiment to be terminated at higher amplitudes without abandoning the entire experiment.

4.2.3 CCEP time-domain analysis

CCEPs were extracted from the data by averaging the 2 seconds of voltage data before to 2 seconds after the digital trigger signaling stimulation by the CereStim. Similar to previous studies(Keller *et al.*, 2011; Entz *et al.*, 2014), CCEP amplitude was measured using peak amplitude of the rectified average signal after stimulation in the first 5-100 ms, demeaned and normalized by the standard deviation of the signal 5-100 ms (baseline) before stimulation to account for variation between electrodes. CCEP amplitude was calculated as the largest absolute deviation from baseline in the standardized signal between 2.5 and 50 ms (N1) or 50 and 200 ms (N2) after the stimulus delivery. CCEP timing for each peak was calculated as the timing of the same largest absolute deviation from

baseline (Figure 1A,1B). CCEP variability was calculated as the mean standard deviation across trials in each time period, divided by the mean standard deviation across trials at baseline.

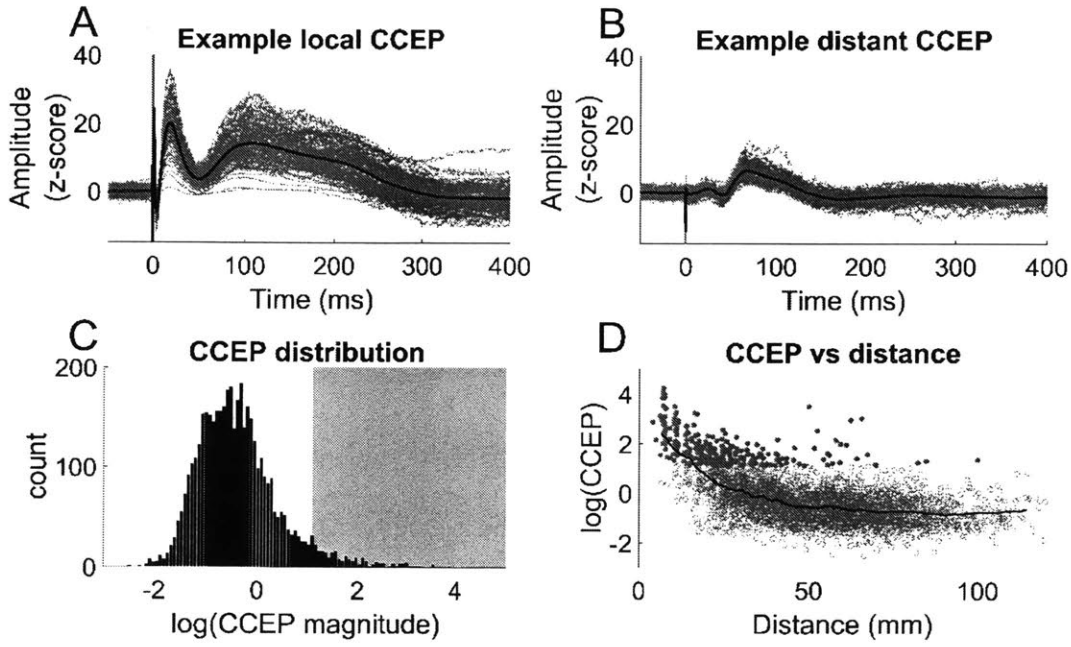

Figure 4-1: Representative local and distant CCEP examples, and CCEP magnitude distribution, including as a function of distance. A representative CCEP response in a local (A) and distant (B) channel in one participant, including individual trials (light grey lines) and the average across trials (solid black). The stimulation artifact can also be seen at t = 0. The log- distribution of all maximum absolute magnitudes, across all channels including channels with no response, is shown in black (C). The light grey region shows the channels that cross the threshold of greater than 3 standard deviations above baseline, considered a CCEP. The likelihood of getting a CCEP decreases with distance, though not monotonically (D). All responses are plotted with open circles, and above-threshold CCEPs are plotted with closed circles. The bold black line represents the average response as a function of distance.

When CCEP amplitudes are binarized into positive and negative responses, a threshold of 3 standard deviations above the baseline mean was chosen(Entz *et al.*, 2014) (Figure 1C). Unless otherwise specified, data were analyzed using the nearest pair of electrodes to the stimulation pair (but not including either anode or cathode) that recorded an evoked response, averaging 6.9 +/- 0.95 mm away from the stimulation site (Figure 1D).

4.2.4 CCEP frequency-domain analysis

To evaluate the average power increase for each trial, we first demeaned and detrended the trials, and then used the multi-taper spectral estimation method with half second windows starting 5 ms after stimulation and advancing in 10ms steps. This spectral data was normalized by the power spectrum up to 5ms preceding stimulation, and then these normalized spectra were averaged for each recording channel. To evaluate the average phase synchrony, the intertrial phase coherence was calculated with EEGLAB (Delorme and Makeig, 2004) for frequencies from 3:100 with 3 cycles each. Results from each site were collected and averaged across patients.

To specifically characterize high gamma activity beyond the high-frequency components of the sharp deflections in the CCEP waveform, we subtracted the average waveform for each site from each trial. Using windows of 20ms, we then estimated the power in the 100-200Hz range using the multi-taper spectral estimation method, with both mean-subtracted and detrended windows.

4.2.5 Significance Calculations

To test the significance between the timing, magnitude, and variance of various groups of CCEPs, two-tailed t-tests were used with p-values reported. For time and time-frequency plots, the number of total tests was very high and the tests for each time point or frequency are not independent. To control for multiple comparisons, a two-staged approach was used. First, a Bonferroni-corrected Type 1 error rate was calculated for each plot in a figure. Next, a cluster-based threshold for significance was calculated using a permutation test. Baseline and post-stimulation values were randomly swapped with 50% probability for 1000 iterations to create a null distribution, and maximum cluster size was recorded at each step. Cluster sizes greater than the Bonferroni-corrected percentile of the null distribution were considered significant.

4.3 Results

4.3.1 Time-domain characteristics

Across 15 patients, SPES was attempted in a total of 33 cortical regions, with significant CCEPs measured in 26 of those attempts. The presence of a significant response to stimulation was defined as a CCEP with an average magnitude at least 3 standard deviations above baseline within the first 2.5-250 ms, which included both the N1 and N2 peaks (Figure 1C).

In the subset of SPES sites that produced a local CCEP, the average magnitude of the CCEP closest to the stimulation electrodes was 25.3 ± 18.0 standard deviations above the mean, with magnitudes ranging from 4.62 to 69.5 standard deviations above the mean. The closest recording site to the stimulation site was on average 6.78 mm (std: 0.935) away. The magnitude of N1 for the closest CCEP to the stimulation site was 24.7 standard deviations above the mean (std: 18.4, min: 4.62, max: 69.5), occurring at 12.9 ms (std: 5.87, min: 2.5, max: 24), whereas for N2 the magnitude was 9.80 standard deviations above the mean (std: 5.70, min: 1.23, max: 23.7), occurring at 127 ms (std: 36.7, min: 59.5, max: 240). During N1, the variability of the signal was 1.59 times higher than baseline (std: 1.53), and during N2, the variability of the signal was 1.71 times higher than baseline (std: 1.56). On a per-channel basis, N1 and N2 magnitudes of the closest CCEP are significantly correlated ($r^2 = 0.25$, $p = 0.0088$).

Within a 3 cm radius of the 26 stimulation sites (16.3% of all recording sites), 27.1% of local recording sites measured a significant CCEP (signals within 3 cm may partially or wholly represent volume-conducted potentials(Shimada *et al.*, 2017)). For these local responses, the average magnitude of the CCEP was 9.60 standard deviations above the mean (std: 10.2, min: 3.03, max: 69.5, Figure 1A). The magnitude of N1 for local recording sites was 9.06 standard deviations above the mean (std: 10.4, min: 0.663, max: 69.5), occurring at 26.7 ms (std: 15.0, min: 2.5, max: 50),

whereas for N2 the magnitude was 4.70 standard deviations above the mean (std: 3.62, min: 0.528, max: 23.7), occurring at 115 ms (std: 54.1, min: 50, max: 248.5) (Figure 2A-B). During N1, the variability of the signal was 1.12 times higher than baseline (std: 0.612), and during N2, the variability of the signal was 1.36 times higher than baseline (std: 0.729) (Figure 2C). On a per-channel basis, N1 and N2 magnitudes of the local CCEPs are significantly correlated ($r^2 = 0.43$, $p = 7.1E-25$).

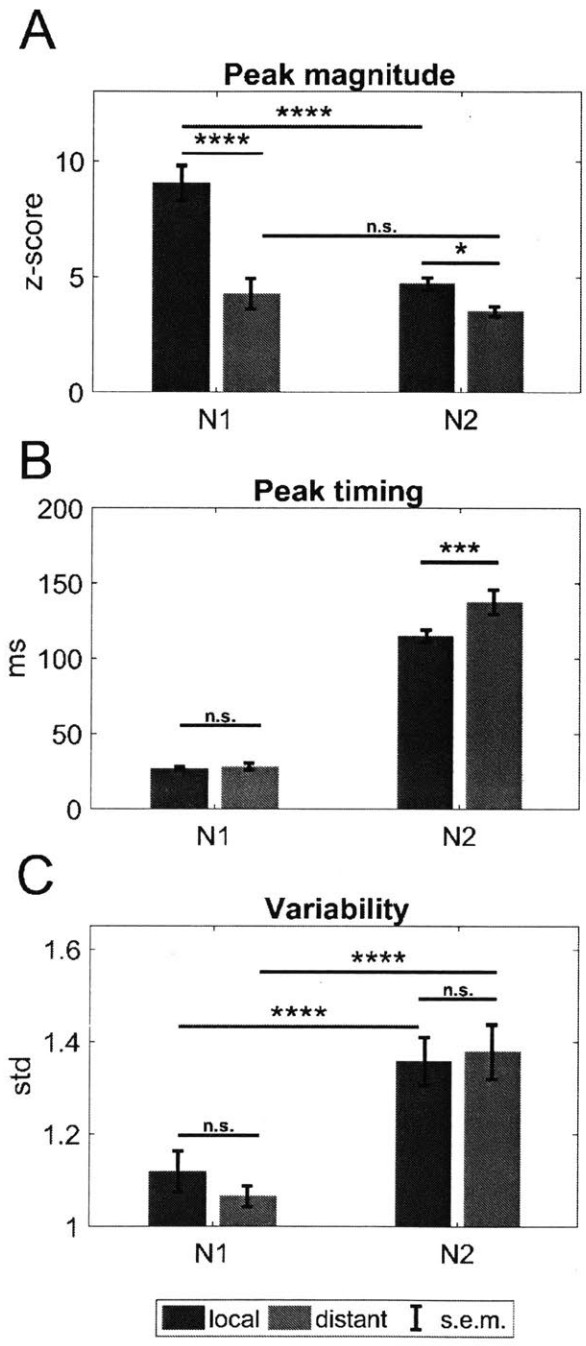

Figure 4-2: N1 vs N2 magnitude, timing, and variability. N2 magnitude is significantly lower than N1 magnitude in local channels (dark grey bars), but there is no significant difference between the peaks in distant channels (light grey bars) (A). Near channels have larger responses overall, in both peaks. There is no significant difference in timing of N1 between local channels and distant channels, but N2 arrives significantly later in distant channels (B). CCEPs generally have an increase in variability of the signal (C). No difference between local channels and distant channels was detected, but N2 showed much higher increase in variability than N1. (s.e.m.: standard error of the mean, n.s.: $p > 0.05$, *: $p < 0.05$, ***: $p < 0.001$, ****: $p < 0.0001$)

For recording sites outside a 3cm radius of the stimulation location (83.7% of all recording sites), only 1.75% of these sites measured a significant CCEP. For these distant responses, the average magnitude of the CCEP was 5.40 standard deviations above the mean (Figure 1B, std: 4.77, min: 3.00, max: 33.5). Unlike in the local CCEPs, for distant responses the magnitude of N1 was often smaller than the magnitude of N2

(Figure 1B). The magnitude of N1 for distant recording sites was 4.26 standard deviations above the mean (std: 5.20, min: 0.255, max: 33.5), occurring at 28.1 ms (std: 16.5, min: 2.5, max: 50), whereas for N2 the magnitude was 3.50 standard deviations above the mean (std: 1.69, min: 0.53, max: 8.68), occurring at 137.6 ms (std: 63.9, min: 50, max: 250; Figure 2A-B). During N1, the variability of the signal was 1.06 times higher than baseline (std: 0.179), and during N2, the variability of the signal was 1.38 times higher than baseline (std: 0.473) (Figure 2C). On a per-channel basis, N1 and N2 magnitudes of the distant CCEPs are not significantly correlated ($r^2 = 0.017$, $p = 0.30$). There was no apparent relationship between the timing of the N1 peak and distance, but N2 peaks in distant electrodes occurred significantly later than in local electrodes (Figure 2B, $p = 0.0061$).

4.3.2 Amplitude response

SPES at varying amplitudes was successfully completed in 3 stimulation sites across 2 patients. In the first participant, the amplitude of both N1 and N2 peaks increases monotonically with increasing stimulus amplitude (Figure 4-3). In both cases, N2 appears to plateau earlier than N1. The smooth monotonic relationship is not seen in the results from the second participant, however. Instead, both peaks appear to increase until about 7 mA of stimulation, and then they abruptly decrease.

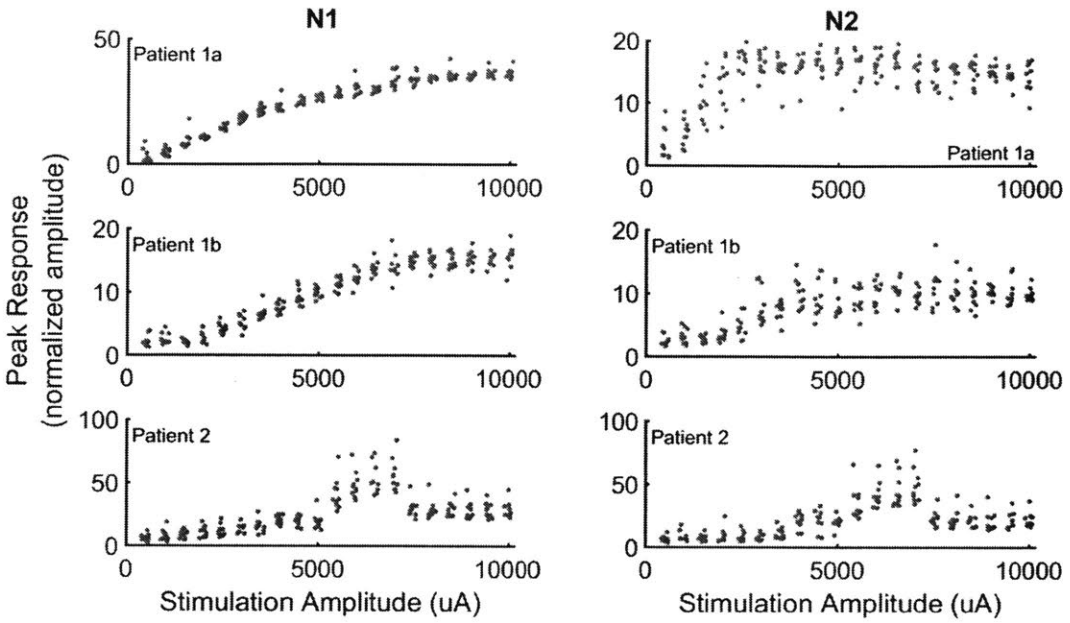

Figure 4-3: the effect of stimulation amplitude on N1 and N2 magnitude in 2 patients. Each row represents a stimulation site, and each column represents either N1 or N2. The peak response increases with increasing stimulation amplitude, but this relationship is not always monotonic.

Taking a closer look at these odd results reveals how the peak-amplitude relationship may be more complicated (Figure 4-4). As the stimulation amplitude increases, the evoked waveform becomes increasingly polyphasic, with a tertiary peak emerging after N1 and N2 around 700 ms. Meanwhile, as the trough between N1 and N2 deepens, N1 and N2 become less prominent. This shape of the CCEP seems to stabilize starting at 8.5 mA. Further data would be needed to determine whether this kind of complex relationship with stimulation amplitude is common.

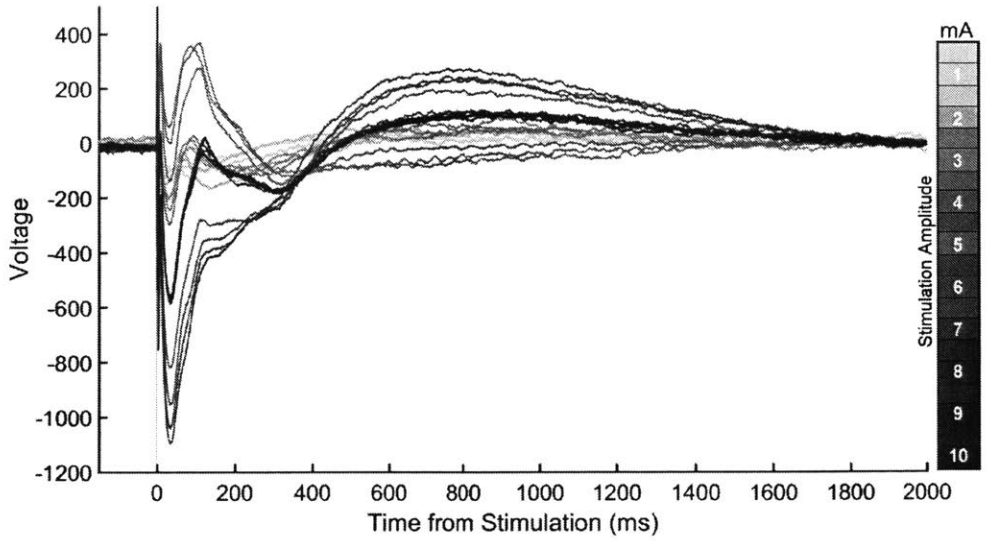

Figure 4-4: One example of CCEPs at varying stimulation amplitudes. Single pulse stimulation was delivered at amplitudes from 0.5 to 10 mA in steps of 0.5 mA in a block-random order. Each waveform represents the average of 10 trials and is plotted with unnormalized voltage units. The stimulation artifact can be seen at time 0.

4.3.3 Time-frequency characteristics

CCEPs exhibit a broadband increase in spectral power in the 1-30 Hz range and a shorter increase in intertrial phase coherence (Figures 3C, 3E). In the time domain, the average CCEP deviates significantly from baseline for 1006 ms in the closest channels (Figures 3A-B). In the frequency domain, the increase in LFP power in these lower frequencies is significant for up to 950 ms (Figure 3D), and the phase synchronization across trials in the same frequency range is significantly higher than baseline for up to 486 ms (Figure 3F). These results show that the measurable response to SPES can last for at least 1 second, far outlasting the N1 and N2 peaks in average CCEP waveform. While using previously reported analysis methods did show high gamma activity after stimulation,

we found that detrending the analysis windows completely removed any spectral content in the high gamma range beyond the first few milliseconds post-stimulation (data not shown).

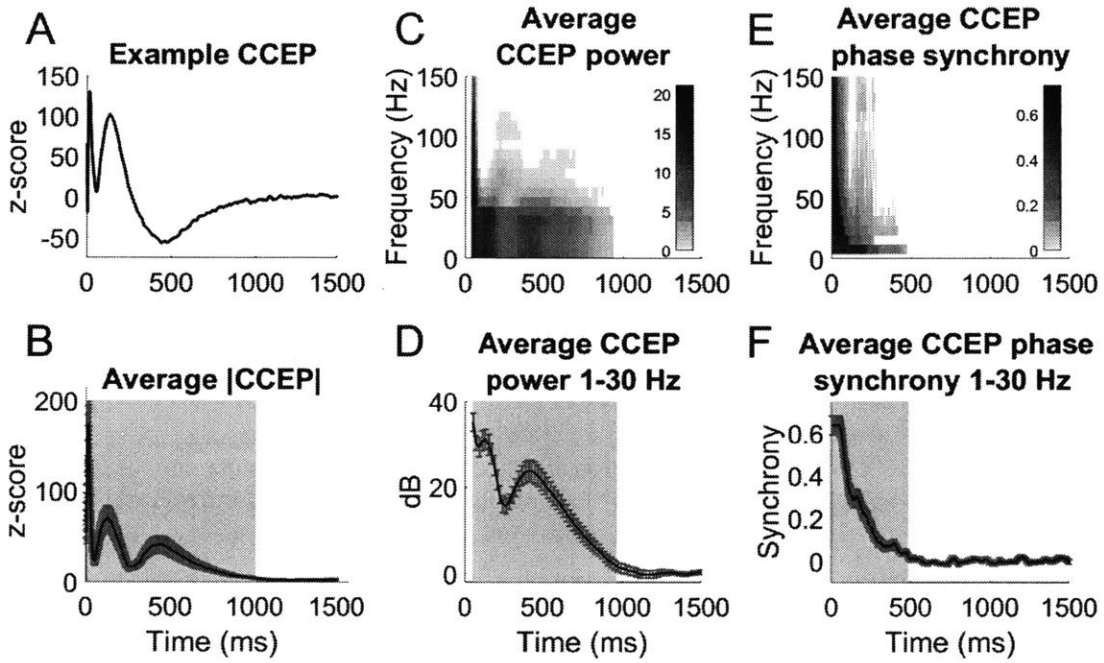

Figure 4-5: The power and phase spectra of the nearest CCEP. A representative CCEP, averaged across trials, on a longer time scale (A). The average absolute value of the CCEP for all participants (B) is significantly higher than baseline for up to 1006 ms. The light grey background indicates the significant time period (corrected for multiple comparisons), and the dark grey error bars represent the standard error of the mean. CCEPs involve an initial broad-band increase in power, followed by a sustained increase in the lower frequencies (C). White areas of the image are non-significant compared to baseline. The increase in power from baseline in the lower frequencies lasts 950 ms (D). Increases in inter-trial phase coherence are much shorter in duration (E). In the lower frequencies, inter-trial phase coherence is significantly higher than baseline for up to 486 ms (F).

The sustained increase in low-frequency power is not just present in channels close to the stimulation site, but in fact can be seen in distant channels that respond to stimulation. This increase in power can be seen for up to 910 ms in near sites and up to 930 ms in far sites (Figure 4A-B). On the other hand, inter-trial phase coherence is much shorter, lasting up to 454.4 ms in near sites and 415.5 ms in far sites (Figure 4C-D). These effects are very similar in duration to the effects measured in the nearest channels to the stimulation site, indicating that these properties do not change with distance.

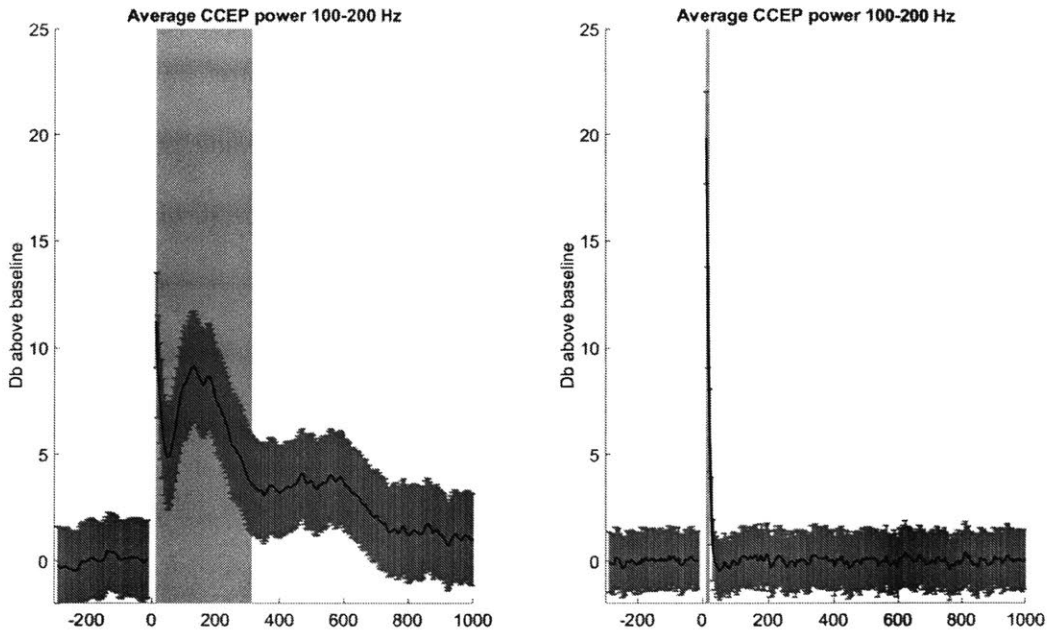

Figure 4-6: High gamma activity measured in the nearest CCEPs without (left) or with (right) detrend correction. Detrend correction eliminates all high gamma activity beyond the first few milliseconds.

4.4 Discussion

The characteristics of CCEPs were systematically explored to better understand the response of the brain to SPES. The two peaks of the evoked response, N1 and N2, differed in their spatial distributions of timing and magnitude and in their total variability. In both time and time-frequency, the response to SPES lasted for approximately one second – many orders of magnitude longer than the stimulus itself.

The differences between N1 and N2 must reflect underlying differences in physiological mechanisms and generation, with N1 being less variable, less dependent on distance for peak timing, and more dependent on distance for magnitude than N2. While the mechanisms of CCEP generation have yet to be elucidated, several mechanisms for each phase of the response have been proposed. It has been suggested than N1 could be a polysynaptic excitatory response mediated by either small, slow fibers with direct cortico-cortical activation or indirect cortico-subcortico-cortical pathways

(Matsumoto, Nair, Lapresto, *et al.*, 2004). The large drop-off with distance could suggest the former, while the lack of timing change with distance could suggest the latter. In contrast, N2 may be generated by a longer-lasting inhibitory response(Keller, Honey, Mégevand, *et al.*, 2014). Since N2 has a larger spatial distribution and varies less in magnitude by distance, it could be that N2 responses are generated from a wider pool of indirect pathways(Matsumoto, Nair, LaPresto, *et al.*, 2004).

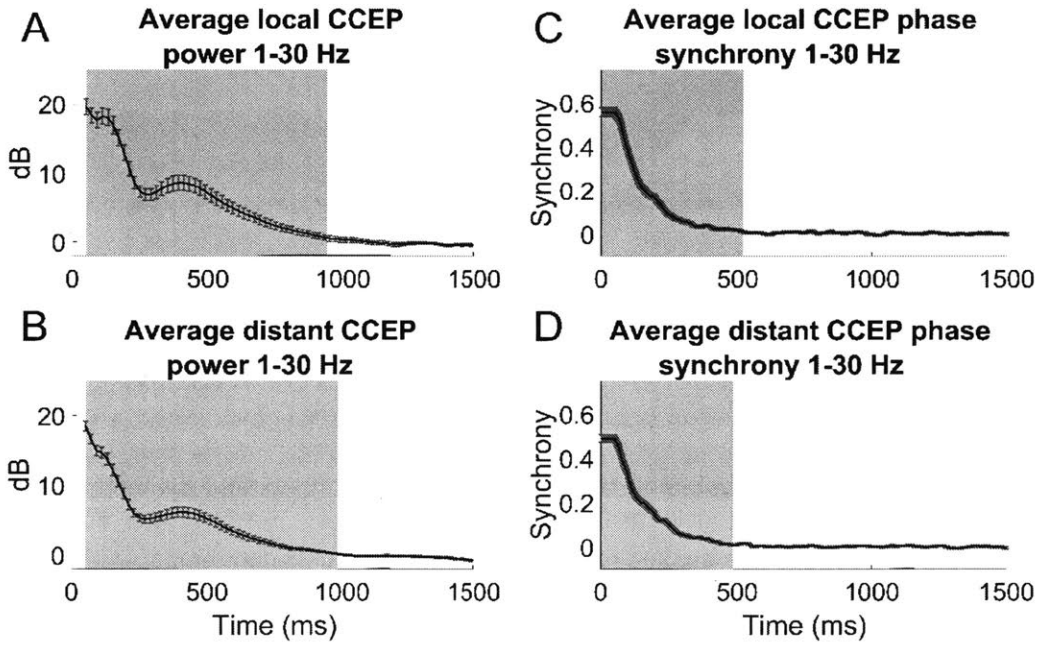

Figure 4-7: As in Figure 4-3, average CCEP power and phase synchrony over time after SPES. The light grey background indicates the significant time period (corrected for multiple comparisons), and the dark grey error bars represent the standard error of the mean. In both local (**A**) and distant (**B**) channels, CCEPs involve a sustained increase in the lower frequencies, lasting nearly 1 second. Inter-trial phase coherence, however, lasts only about half a second in both local (**C**) and distant (**D**) channels.

Beyond these two previously-identified peaks, the CCEP response has a surprisingly long duration compared to visual inspection of the easily identifiable average waveform. Intertrial phase coherence degrades much faster after a pulse of electrical stimulation than low-frequency power, suggesting that averaging across trials – a common technique – may reduce phase-uncoupled signals via destructive interference. Furthermore, studies of CCEPs stimulating at intervals of 1 second may not allow the signal enough time to recover to baseline in between trials. Whatever the mechanism

of CCEP generation, the long duration of the response indicates a strong recruitment of neural circuitry can be induced from a biphasic electrical stimulus of only 250 μs.

Compared to other CCEP studies, our stimulation protocol delivers substantially less charge per pulse, and our recording method has a different spatial sampling than typical surface electrocorticography. Perhaps due to these differences, the likelihood of connectivity here is much lower than previously reported(Entz *et al.*, 2014). Despite concerns about volume conduction(Shimada *et al.*, 2017), only about 25% of local channels and 2% of distant channels recorded an above-threshold response to SPES. Even in "local" channels, the likelihood of a response increased markedly with proximity to the stimulation site, and 3 cm may not be the ideal boundary for distinguishing local from distant responses. Still, the pattern of responses resembles a small-world network, where the majority of connections are local with only a small number of long-distance connections(Bassett and Bullmore, 2017).

In order to better understand the biophysical properties of CCEPs, the characteristics of these responses in both time and frequency domains were systematically explored. We show that the CCEP can last up to one second, indicating a surprisingly long-lasting response of the brain to even very short electrical stimuli. Further, the two phases of the CCEP have distinct properties, likely indicating different mechanisms of generation. This study elucidates important characteristics of CCEPs for mapping protocols and further CCEP studies.

5 Cortico-Cortical Evoked Potentials Resemble Structural Connectivity

5.1 Introduction

The connectivity and structure of brain regions is an important aspect of understanding brain function and pathology. Evoked potentials elicited by single pulse electrical stimulation have been used to map pathways in the central nervous system of humans for decades, with increasing scientific use starting with the coining of cortico-cortical evoked potentials (CCEPs)(Wilson *et al.*, 1990; Matsumoto, Nair, Lapresto, *et al.*, 2004). CCEPs have been used as a tool to estimate the connectivity of cortical areas in important systems of the human brain, including the limbic system (Wilson *et al.*, 1990; Kubota *et al.*, 2013), auditory system(Brugge *et al.*, 2003), language system(Matsumoto, Nair, LaPresto, *et al.*, 2004; Conner *et al.*, 2011; Yamao *et al.*, 2014; Araki *et al.*, 2015), and sensorimotor cortex(Matsumoto *et al.*, 2007; Enatsu *et al.*, 2013). Dynamic changes in cortical connectivity and excitability during sleep have been mapped via CCEP networks (Usami *et al.*, 2015), and CCEP mapping has been used to show possible reorganization of networks in pathological cortex (Enatsu *et al.*, 2012, 2013; Matsumoto, Kunieda and Nair, 2017).

The generation mechanisms of CCEPs are not fully understood, but some characteristics of CCEP networks have been elucidated. CCEPs are not symmetric (Entz *et al.*, 2014; Keller, Honey, Entz, *et al.*, 2014) and can therefore be used to create directed network graphs. Networks derived from CCEP methodology may be stable across days of measurement (Entz *et al.*, 2014), and in the visual cortex, this method provides results consistent with already known network structure (Matsuzaki, Juhász and Asano, 2013). Comparable to other brain network estimates, CCEP networks exhibit small-world topology (Keller, Honey, Entz, *et al.*, 2014). These properties indicate that CCEPs may be an appropriate tool for estimating brain networks. Indeed, CCEP networks correlate with other estimates of brain connectivity, such as resting state high gamma electrocorticography (ECoG)

(Keller, Honey, Entz, *et al.*, 2014) and resting state functional magnetic resonance imaging (fMRI) (Keller *et al.*, 2011).

Typically, brain network estimates are categorized into three distinct types: functional, effective, and structural (Friston, 2011). Functional connectivity identifies channels or brain regions with correlated activity, and includes methods such as correlation, cross-correlation, and magnitude-squared coherence(Bowyer, 2016). While these measures often exhibit large fluctuations on small timescales, they can be used to estimate stable networks over time (Bullock *et al.*, 1995; Chu *et al.*, 2012). While long-range connections can be found during tasks, these three functional connectivity metrics tend to drop off very quickly with distance(Bullock *et al.*, 1995; Muller *et al.*, 2016). Distance has a larger effect on coherence in the higher frequencies (Srinath and Ray, 2014).

Effective connectivity identifies whether channels or brain regions may have causal influence on another, and includes methods such as weighted phase lag index and Granger causality(Friston, 2011). Weighted phase lag index is a measure of connectivity based on the imaginary coherence of two channels, which weights the lag (or lead) of a particular pair of channels by the magnitude of the lag (or lead) (Vinck *et al.*, 2011). By using the imaginary coherence, weighted phase lag index is thought to be robust to spurious connections due to volume conduction (Vinck *et al.*, 2011). Granger causality is a directed measure of connectivity that estimates how much additional benefit a second channel provides in predicting the time series of the first channel, above the autoregressive predictive power of the first channel itself (Wiener, 1956; Granger, 1969; Bressler and Seth, 2011). Compared to functional connectivity, effective connectivity measures often seek to produce the simplest possible explanatory network for the underlying data (Barnett and Seth, 2014).

Structural connectivity estimates whether there is an anatomical connection between brain regions. While tracer studies using dissections are the gold standard for determining structural connectivity,

these methods are impractical for use in scientific and clinical settings involving human participants. Diffusion tensor imaging (DTI) allows for estimates of structural connectivity by measuring the anisotropy of water molecules, allowing for a partial reconstruction of the white matter tracts in the brain(Basser *et al.*, 2000). Though DTI has its limitations – e.g. a bias towards large, short, straight tracts – it has proved a useful tool for a wide variety of connectivity investigations(Jones, 2010). Diffusion tractography has been shown to correlate with CCEP networks in the language system(Conner *et al.*, 2011).

It has been hypothesized that CCEP networks represent functional or effective connectivity (Matsumoto, Nair, LaPresto, *et al.*, 2004; Oya *et al.*, 2017; Trebaul *et al.*, 2018). However, a measure of effective connectivity would require CCEPs to be generated in a causal, directed manner. It is unclear whether CCEPs represent orthodromic or antidromic activation of cortico-cortical pathways(Kunieda *et al.*, 2015). Without a clear physiological understanding of CCEP generation, the relationship of CCEP networks to theoretical frameworks remains an open question. Here, we explore the similarities between CCEP connectivity estimates and common electrocorticographic and imaging estimates of functional, effective, and structural connectivity.

5.2 Methods

5.2.1 Data Collection

Neurophysiological data was recorded from 11 patients (6 females and 5 males) of ages ranging from 19 to 57 (mean 36.9, std 12.5) undergoing invasive monitoring for intractable epilepsy using bilateral intracranial depth electrodes. Depth electrodes (Ad-tech Medical, Racine WI, USA, or PMT, Chanhassen, MN, USA) had diameters of 0.8–1.0 mm and consisted of 8-16 platinum/iridium-contacts 1-2.4 mm long. The placement of these electrodes was determined solely by clinical

criteria, with most electrodes in the frontal or temporal lobe. All patients provided informed consent to participate in any experiments, which were approved by MGH IRB and MIT COUHES.

Voltage data from implanted electrodes were recorded at a sampling rate of 2000 Hz using a custom-built BlackRock recording system. In addition to these electrophysiological recordings, each patient underwent a T1-weighted structural magnetic resonance imaging (MRI) scan which was coregistered to the post-operative computed tomography (CT) scan (Dykstra *et al.*, 2012; Yang *et al.*, 2012). Distance between channels is defined as the Euclidean distance between the average locations for each bipolar electrode pair.

5.2.2 Stimulation

To evoke CCEPs, biphasic bipolar single pulses of stimulation were applied across pairs of adjacent electrodes with a 90us pulse width at 6 or 7 mA. These pulses were delivered by the BlackRock CereStim stimulator at 3 second intervals with +/- 500 ms random jitter with uniform distribution and at an amplitude below the threshold for afterdischarges or for any perceptual or behavior effects reported by the patients. In one participants, these single pulses were delivered interspersed between other trains of stimulation. The number of trials ranged from 20 to 337 (mean 47), and stimulation occurred in one to nine sites per participant. The stimulation sites were not in the seizure onset zone or early seizure spread areas for any patient, and all stimulation experiments were performed while the patients were awake, after the patients resumed antiepileptic medication, and were under medical supervision.

To estimate CCEPs, the following procedure was followed. Recordings were first analyzed using custom software in MATLAB. The data were re-referenced using a bipolar reference scheme between neighboring electrodes then divided into 2 second epochs time-locked to the delivery of the stimulus, including one second pre- and one second post-stimulation. Any per-stimulus data

within 3 ms of the stimulation pulse were excluded from analysis. All channels and trials were visually inspected for artifacts, and any channels or trials with large artifacts were excluded from analysis. CCEP responses were averaged across trials and then quantified per bipolar recording by taking the maximum absolute amplitude of the average evoked potential normalized by the standard deviation at baseline (Keller *et al.*, 2011). Stimulation sites were only included in analysis if CCEPs greater than 3 standard deviations above baseline could be measured, and when CCEP are binarized into positive and negative responses, a threshold of 6 standard deviations above the mean was chosen (Keller *et al.*, 2011; Entz *et al.*, 2014).

5.2.3 Functional Connectivity Calculations

For functional connectivity estimates, 5 minutes of recordings while the participant was awake before or after single pulse stimulation sessions were used. These data were re-referenced with the same bipolar reference scheme, then bandpass filtered from 1-150 Hz and notch filtered from 58-62 Hz and 118-122 Hz (Butterworth 3rd order, forward and reverse). The recordings were then split contiguously into 1 second epochs. As above, channels and trials identified by visual inspection as having large artifacts were excluded from further analysis.

Correlation and cross-correlation measures were used as estimates of functional connectivity in the time domain. For each 1 second epoch, the correlation and maximum cross-correlation with lags between +/- 250 ms were calculated between the stimulation electrode pairs and all other electrode pairs. The 5% thresholds for each channel pair was determined by independently shuffling epochs (with replacement) 10,000 times, then choosing the values at the 2.5th and 97.5th percentile. Then the final network is determined as the percentage of times each correlation or cross-correlation rises above the 5% threshold, yielding values between 0 and 1. For more details, see (Kramer *et al.*, 2011; Chu *et al.*, 2012).

Similarly, magnitude-squared coherence was used as an estimate of functional connectivity in the frequency domain. For each 1 second epoch, magnitude-squared coherence was calculated for each frequency from 1 to 150 Hz between stimulation electrode pairs and all other electrode pairs. Again, for each epoch, a 5% threshold was calculated using a bootstrap method, and the final network for each frequency is the percentage of times each MS-coherence estimate rises above the 5% threshold, yielding values between 0 and 1.

5.2.4 Effective Connectivity Calculations

For effective connectivity estimates, the same 5 minutes of recording was used with the same bipolar reference scheme as for functional connectivity. For pairwise Granger causality estimates, these recordings were split contiguously into 1 second epochs and then decimated from 2000Hz to 250 Hz in order to reduce computational time. Pairwise Granger causality was estimated using the multivariate Granger causality toolbox with a model order of 10 between every recording channel and the stimulation channel for each stimulation site(Barnett and Seth, 2014). Weighted phase lag indices were calculated from 4 to 50 Hz with the FieldTrip toolbox using 2 second contiguous epochs in order to capture lower frequency networks (Oostenveld *et al.*, 2011; Vinck *et al.*, 2011).

5.2.5 Structural Connectivity Calculations

Diffusion tensor imaging was acquired heterogeneously across 8 participants, with b-values of 700 (1 participant), 1000 (3 participants), and 2000 (4 participants) and number of directions ranging from 28 to 74. Structural connectivity between two regions was determined using the FDT toolbox (Behrens *et al.*, 2003, 2007). First, we used bedpostx to locally model the diffusion parameters. The average coordinates of the bipolar electrode pairs from the structural imaging were transformed into diffusion-space using the transformation from the coregistration of the structural MRI and the diffusion MRI with FLIRT (Jenkinson and Smith, 2001; Jenkinson *et al.*, 2002; Greve and Fischl, 2009).

These transformed coordinates were then used to generate binary masks of spheres of 1 centimeter radius centered on each channel. For each stimulation site, probtrackx2 was then used to calculate the number of tracts from the seed mask to the target mask, with the target mask as both a waypoint and a termination mask. This process was repeated for the stimulation mask as seed mask and target recording mask as target mask (generating tracts from the stimulation channel to the target recording channel) and for the stimulation mask as target mask and the target recording mask as seed mask (generating tracts from the target recording channel to the stimulation channel). The number of tracts was then normalized by the total mask volume in order to generate a value for structural connectivity.

5.2.6 Network Comparisons

Every set of connectivity estimates generated for each stimulation site can be represented as a row in the total weighted adjacency matrix of the complete connectivity matrix across channels for each participant. Since participants had an unequal number of stimulation sites, we computed the similarity of connectivity estimates for each row (i.e. each stimulation site). To compare CCEP networks to other network estimates, we calculated the correlation between the two vectors. When controlling for distance, we used a partial correlation with the reciprocal of distance squared as the controlling variable. Unless otherwise noted, all significance calculations are uncorrected t-tests of the Fisher-transformed correlation coefficients – two-sided when comparing two methods, or one-sided when comparing to zero. Confidence intervals were determined using bootstrap-resampling over 1000 iterations.

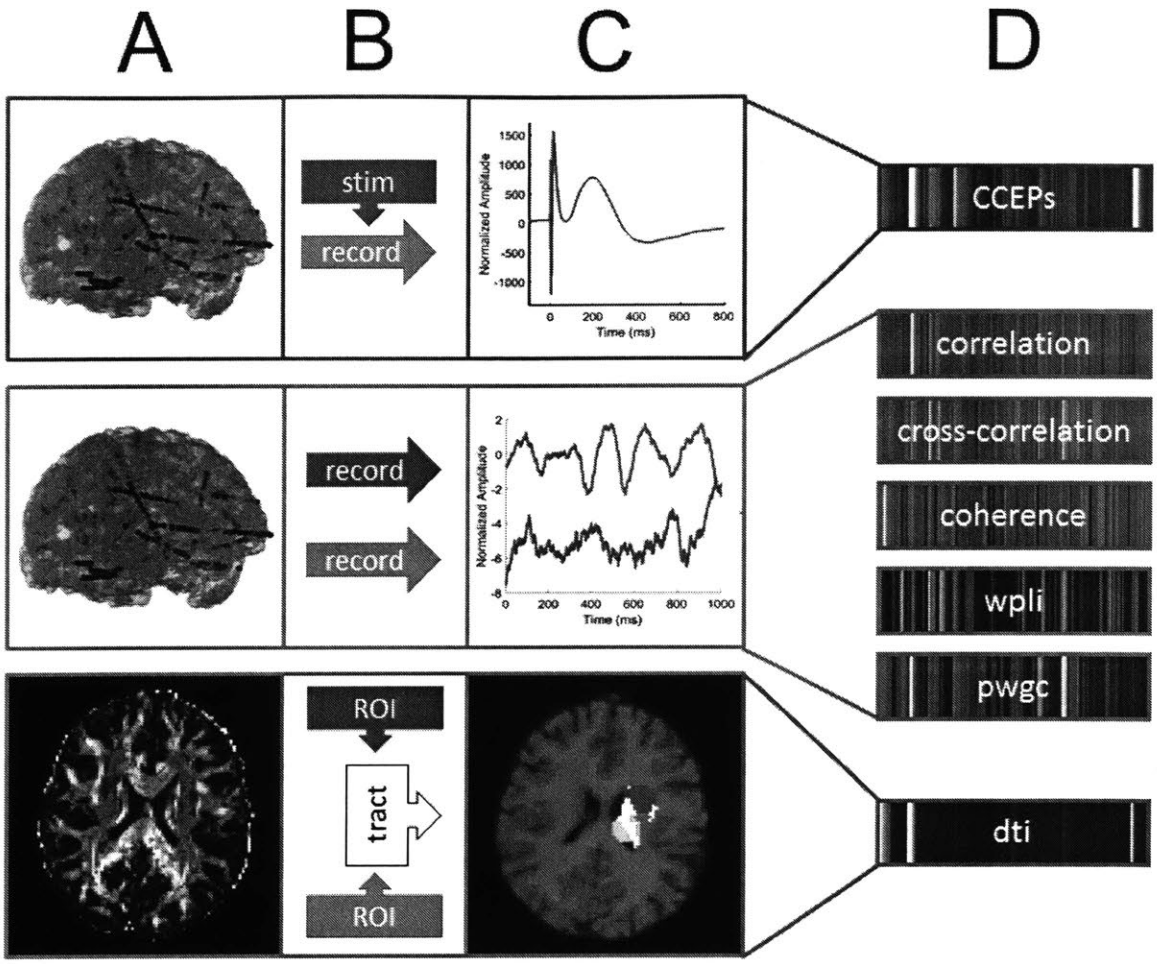

Figure 5-1: an overview of how networks are computed and compared. **A**: reconstruction in one representative participant of data collection by stimulating one channel and recording the others (**red panel**), recording neurophysiological signals at rest in all channels (**yellow panel**), or collecting diffusion tensor imaging (**blue panel**). In the first two panels of column A, channel locations are shown in the 3-D reconstruction of the pial surface from structural MRI, with the stimulation channel marked in red and one of the recording channels marked in green. **B**: schematic representations of the three data collection methods. For CCEP networks, one channel is stimulated and the others are recorded. For functional and effective networks, all channels are recorded. For structural networks, the channel locations are used to create regions of interest (ROIs) for both seed and target masks; tractography is then computed between pairs of ROIs. **C**: representative data samples for each type of data collection method. An example CCEP is shown in the red panel. Resting state electrophysiology is shown in both the stimulation channel (**red**) and a non-stimulation channel (**green**) before the stimulation experiment in the yellow panel. In the blue panel, the ROI created from the stimulation channel location (**red**) and a non-stimulation channel (**green**) is shown overlayed on the structural MRI. The tract between the two ROIs is highlighted in white. **D**: example networks, defined as a vector of pairwise calculations between the stimulation channel or ROI and all other channels or ROIs. Similarity scores are then calculated as the correlation between a given method vector and the CCEP vector. Method labels: pairwise Granger causality (pwgc), weighted phase-lag index (wpli) and diffusion tensor imaging (dti).

5.3 Results

5.3.1 Functional Connectivity

Correlation-derived connectivity patterns share substantial similarities to stimulation-derived connectivity patterns. Across 53 stimulation sites, correlation networks corresponded to stimulation networks with an average similarity score of 0.4978 ± 0.2393 std (Figure 2A). This relationship is reflected in the underlying data; channels with an above-threshold response to stimulation (CCEP-positive) had an average absolute correlation of 0.1976 ± 0.1842 std to the stimulation channel at rest, compared to 0.0370 ± 0.0453 std in channels with no response to stimulation (CCEP-negative) (Figure 2B). The relatively high variance of correlation among stimulation-responsive channels suggests that correlation is not a sensitive measure of predicting CCEPs, but the large difference between CCEP-positive and CCEP-negative channels suggests that correlation is reasonably specific.

Compared to correlation, cross-correlation-derived connectivity patterns are significantly less similar to stimulation-derived connectivity patterns ($p = 1.5061e-08$). Across 53 stimulation sites, cross-correlation networks corresponded to stimulation networks with an average similarity score of 0.2794 ± 0.2152 std (Figure 2A). CCEP-positive channels had a normalized cross-correlation of 0.3411 ± 0.0688 std to the stimulation channel at rest, compared to 0.3000 ± 0.0412 std in channels with no response to stimulation (Figure 2B). While cross-correlation was on average higher in CCEP-positive channels compared to correlation, and with more sensitivity, cross-correlation networks still performed worse than correlation networks as a measure of predicting CCEPs. This drop in performance is caused by the relatively high cross-correlation values between CCEP-negative channels and the stimulation channel, yielding overall less specificity.

The similarity between magnitude-squared-coherence-derived networks and stimulation-derived networks was computed over a range of frequencies, with the best agreement occurring at

approximately 8 Hz (Figure 2C). At this frequency, coherence networks corresponded to stimulation networks with an average similarity score of 0.3981 ± 0.2524 std (Figure 2C), which is significantly better than cross-correlation and worse than correlation ($p = 1.3946e-04$ and 1.2330e-0.5, respectively). Across all frequencies, the lower bound of the uncorrected 95% confidence interval for network similarity is above zero up to 100 Hz (the highest tested). Similar to correlation, CCEP-positive channels show a larger coherence with the stimulation channel than CCEP-negative channels, though with higher variance (Figure 2D).

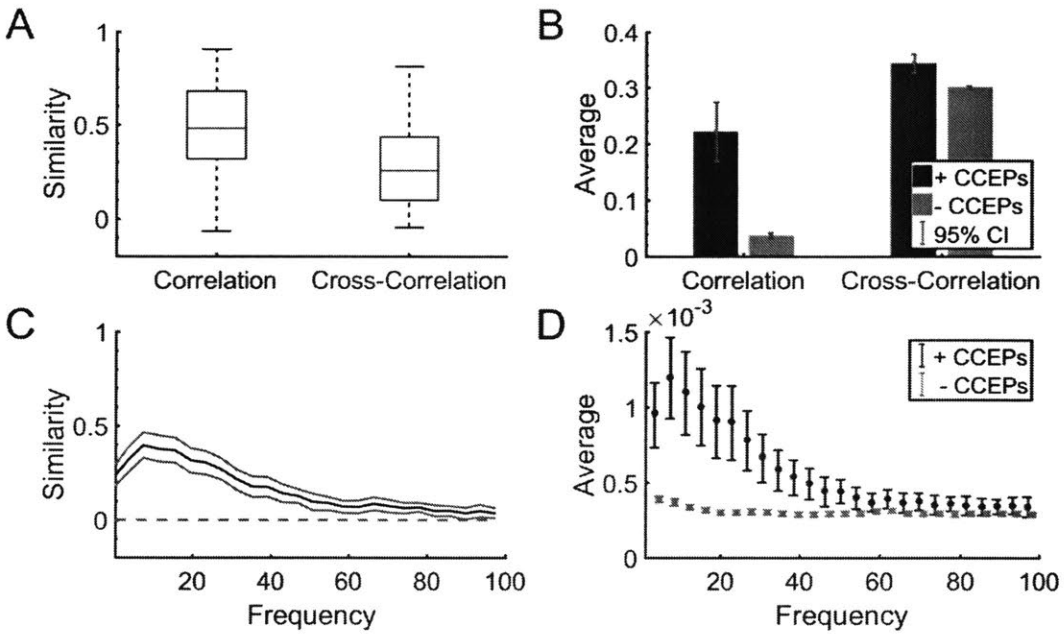

Figure 5-2: functional connectivity networks show similarity to stimulation-evoked networks. **A**: boxplots showing the similarity scores between correlation or cross-correlation networks and CCEPs across 34 for different stimulation sites. The red lines represent the median value, and the top and bottom segments of the blue box represent the 75th and 25th percentile respectively. The whiskers represent the extrema of the data. **B**: the average correlation and normalized cross-correlation values for all channels with (+, blue) or without (-, green) an above threshold CCEP. The presence of a CCEP is defined as any average evoked potential that reaches an absolute value at least 6 standard deviations above baseline mean. Uncorrected confidence intervals (blue error bars) were determined by naive bootstrap resampling. **C**: the mean (black) similarity across the 34 stimulation sites for magnitude-squared coherence networks and CCEP networks at each frequency, and the uncorrected 95% confidence intervals at each frequency (grey) determined by naïve bootstrap resampling. **D**: the average unnormalized magnitude-squared coherence for all channels with (+, blue) or without (-, green) an above threshold CCEP, with the same threshold as in B. Uncorrected confidence intervals (blue error bars) were determined by naive bootstrap resampling. Magnitude-squared coherence has different units than correlation, so the scales are not directly comparable. Rather, the important information is the difference between the + and – groups.

5.3.2 Effective Connectivity

Pairwise Granger causality is a directed measure of connectivity, yielding estimates of connectivity from the stimulation channel to the target recording channel and the other way around. Across 53 stimulation sites, pairwise Granger causality networks from the stimulation channel corresponded to stimulation networks with an average similarity score of 0.3810 ± 0.2688, while pairwise Granger causality networks from the target recording channel corresponded to stimulation networks with an average similarity score of 0.3418 ± 0.2773 std (Figure 3A). No significant difference was found between the two groups ($p = 0.3907$). CCEP-positive channels had higher resting state Granger causality values with the stimulation channel at resting state (0.0137 ± 0.0188 std from the stimulation channel, and 0.0171 ± 0.0198 std from the target recording channel) than CCEP-negative channels (0.0050 ± 0.0121 std from the stimulation channel, and 0.0061 ± 0.0140 std from the target recording channel) (Figure 3B). Overall, these similarities are significantly smaller than functional correlation similarities ($p = 8.0417e\text{-}4$ and $4.0787e\text{-}04$).

The similarity between weighted-phase-lag-index-derived networks and stimulation-derived networks was computed over a range of frequencies, with the best agreement occurring at 8 Hz (Figure 3C). While the lower bound of the uncorrected 95% is higher than zero at all frequencies tested, overall the agreement between weighted phase lag index connectivity and CCEP connectivity is very poor, and the highest similarity score is 0.1038 ± 0.1497 std. Examining the individual values, the average weighted phase lag indices of CCEP-positive channels are higher than CCEP-negative channels, particularly in the 1-10 Hz and 25-35Hz ranges, but the variability is also very high, leading to poor sensitivity (Figure 3D).

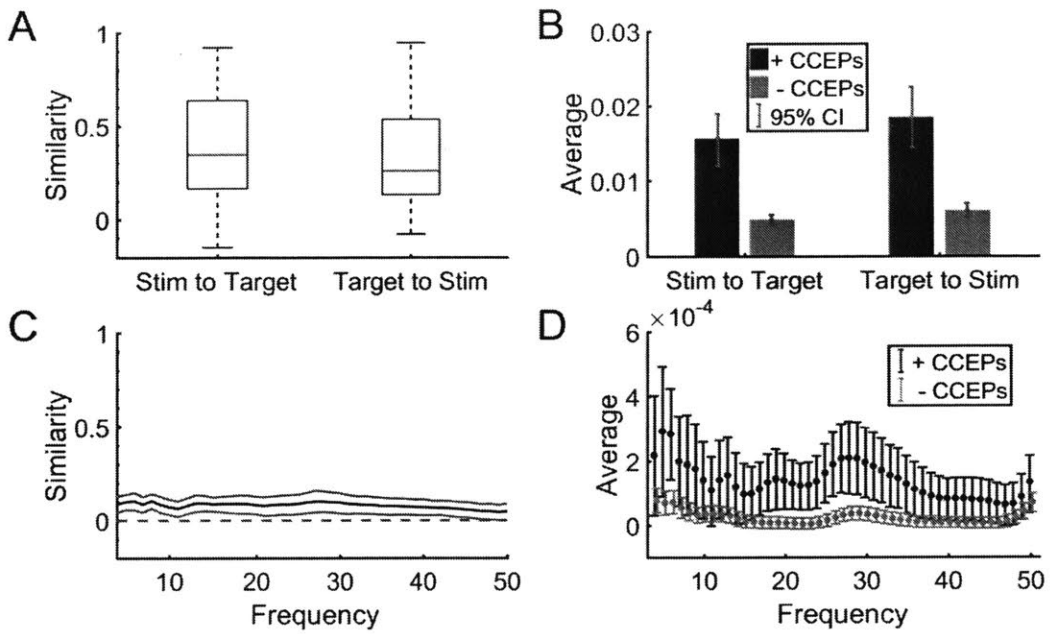

Figure 5-3: effective connectivity shows less similarity to stimulation-evoked networks. **A**: boxplots showing the similarity scores between pairwise Granger causality networks in both directions and CCEPs across 34 for different stimulation sites. Pairwise Granger causality is a directed measure of connectivity, so calculations from the stimulation site to the target channel and from the target channel to the stimulation site are both represented. The red lines represent the median value, and the top and bottom segments of the blue box represent the 75th and 25th percentile respectively. The whiskers represent the extrema of the data. **B**: the average unnormalized pairwise Granger causality values for all channels with (+, blue) or without (-, green) an above threshold CCEP. The presence of a CCEP is defined as any average evoked potential that reaches an absolute value at least 6 standard deviations above baseline mean. Uncorrected confidence intervals (blue error bars) were determined by naive bootstrap resampling. Every measure of connectivity has its own scale, so absolute values are not as important as the difference between the two groups. **C**: the mean (black) similarity across the 34 stimulation sites for weighted phase lag index networks and CCEP networks at each frequency, and the uncorrected 95% confidence intervals at each frequency (grey) determined by naïve bootstrap resampling. **D**: the average weighted phase lag index for all channels with (+, blue) or without (-, green) an above threshold CCEP, with the same threshold as in B. Uncorrected confidence intervals (blue error bars) were determined by naive bootstrap resampling. Every measure of connectivity has its own scale, so absolute values are not as important as the difference between the two groups.

5.3.3 Structural Connectivity

Diffusion tensor imaging was conducted in a subset of our participants, for a total of 34 stimulation sites. Like Granger causality, probabilistic tractography is also a directed measure of connectivity. Across 34 stimulation sites, diffusion-derived networks in both directions had the highest similarity to stimulation-derived networks, with tractography networks from the stimulation channel to the

target channel averaging a similarity score of 0.6799 ± 0.2116 std and tractography networks from the target recording channel to the stimulation channel averaging a similarity score of 0.6741 ± 0.2287 std (Figure 4A). There is no statistically significant difference between the two groups (p = 0.5131), both groups are significantly more similar to CCEP networks than correlation networks (paired t-test using the subset of participants with diffusion tensor imaging, p = 3.4445e-09 and p = 3.5650e-08, respectively). CCEP-positive channels had an average normalized tract percentage of 0.4111 ± 0.2930 std from the stimulation channel to the target recording channel and 0.3992 ± 0.3083 std from the target recording channel to the stimulation channel, compared to 0.0192 ± 0.0720 std and 0.0167 ± 0.0691 in CCEP-negative channels (Figure 4B).

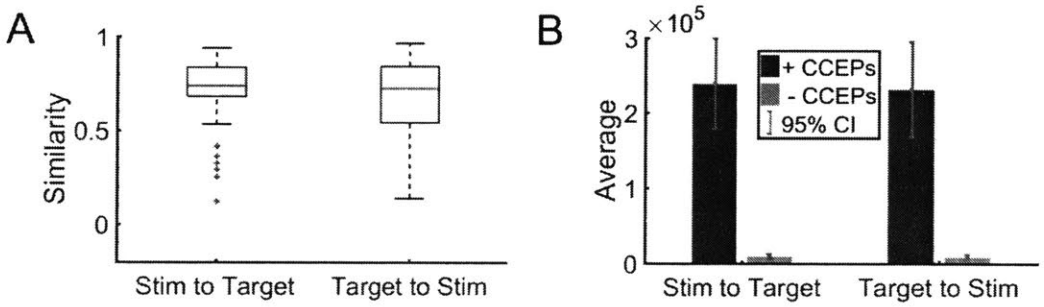

Figure 5-4: structural connectivity shows high similarity to stimulation-evoked networks. **A**: boxplots showing the similarity scores diffusion tensor imaging networks in both directions and CCEPs across 34 for different stimulation sites. Diffusion tensor imaging is a directed measure of connectivity, so calculations from the stimulation site to the target channel and from the target channel to the stimulation site are both represented. The red lines represent the median value, and the top and bottom segments of the blue box represent the 75th and 25th percentile respectively. The whiskers represent the extrema of the data. **B**: the average unnormalized diffusion tensor imaging for all channels with (+, blue) or without (-, green) an above threshold CCEP. The presence of a CCEP is defined as any average evoked potential that reaches an absolute value at least 6 standard deviations above baseline mean. Uncorrected confidence intervals (blue error bars) were determined by naive bootstrap resampling. Every measure of connectivity has its own scale, so absolute values are not as important as the difference between the two groups.

5.3.4 Controlling for Distance

All of these estimates of connectivity share a common cofounding factor – distance from the target recording channel to the stimulation channel. Correcting for distance using a partial correlation substantially lowers the similarity between networks across the board (see Figure 5). Still, all

connectivity estimates except weighted phase lag indices maintain a significant similarity to stimulation networks even when we corrected for distance. While uncorrected network similarity showed DTI as significantly more similar to stimulation networks than correlation, corrected similarity measures between these two methods are no longer significantly different ($p = 0.2980$ for tractography from the stimulation channel and $p = 0.1872$ for tractography to the stimulation channel).

Though the similarity scores decreased when correcting for distance, distance does not have a homogenous effect across connectivity metrics. Splitting the channels into local (within 3cm of the stimulation site) and distant (further than 3cm from the stimulation site) reveals that functional and effective connectivity estimates preferentially predict local channels, while structural connectivity metrics show no difference between local and distant channels (Figure 6). The method with the highest similarity to the local channel CCEPs was correlation, and the method with the highest similarity to the distant channel CCEPs was DTI from the stimulation site to the target site. Breaking the functional connectivity down into its frequency components with magnitude-square coherence, the high beta and gamma frequency bands were not significantly similar to distant channel CCEPs, with mean values close to zero.

Figure 5-5: network measures used in this paper share distance as a confounding factor. (Figure follows on next page). A-D show the relationship between a few selected measures and the Euclidian distance between the stimulation channel and the target channel. **A**: A scatter plot of the normalized absolute peak in the 250 ms post-stimulation (CCEP) at the target channel and distance from the stimulation channel. **B**: A scatter plot of the correlation of the target channel and the stimulation channel and distance between those channels. **C**: A scatter plot of mean normalized magnitude coherence in the 8-12 Hz range between the target and the stimulation channels and distance between those channels. **D**: A scatter plot of the normalized diffusion tensor imaging strength and the Euclidean distance between the target and stimulation channels. **E-G**: the average similarity between CCEP networks and the indicated connectivity measure with (dark purple) or without (light orange) distance correction across 34 stimulation sites. Error bars indicate the standard error of the mean. Method labels: distance (dist), correlation (corr), cross-correlation (xcorr), pairwise Granger causality (pwgc), and diffusion tensor imaging (dti). Frequency bands: 1-4 Hz (delta), 4-8 Hz (theta), 8-12 Hz (alpha), 15-20 Hz (beta1), 20-30 Hz (beta2), 30-50 Hz (gamma).

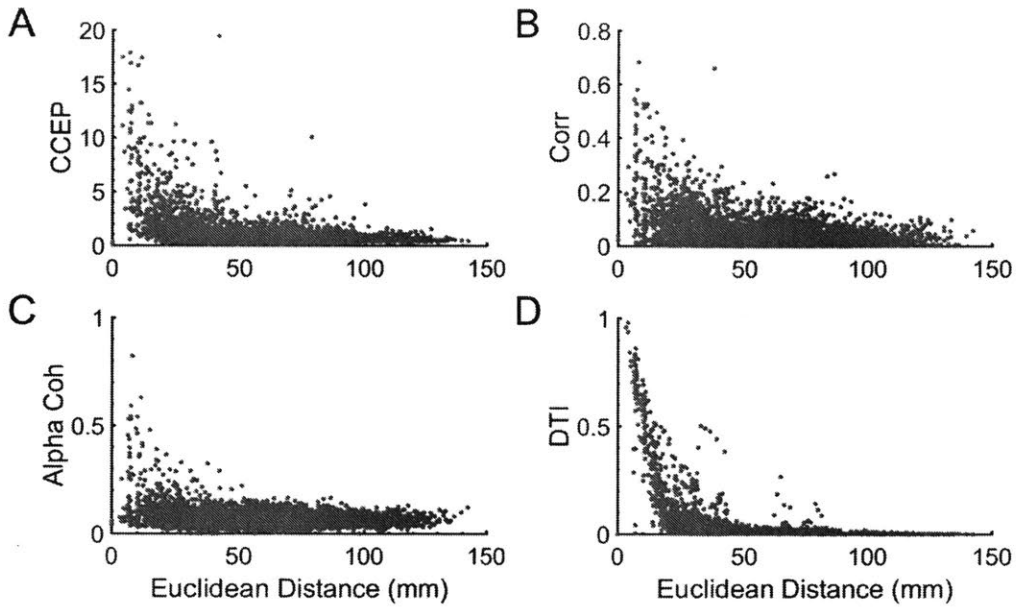
A
CCEP
B
Corr
C
Alpha Coh
D
DTI
Euclidean Distance (mm)
Euclidean Distance (mm)

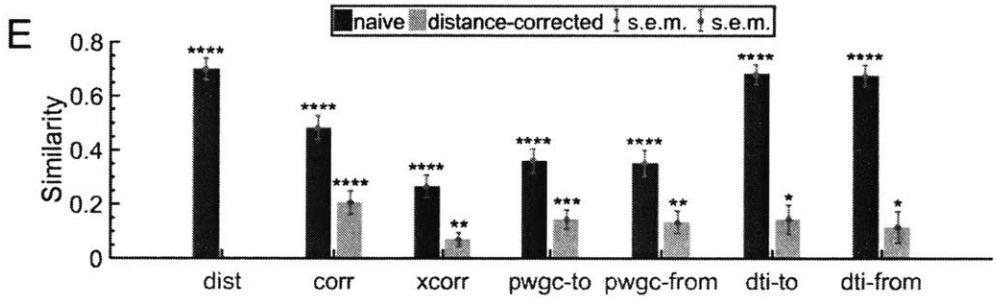
E
naive
distance-corrected
s.e.m.
s.e.m.
Similarity
dist
corr
xcorr
pwgc-to
pwgc-from
dti-to
dti-from

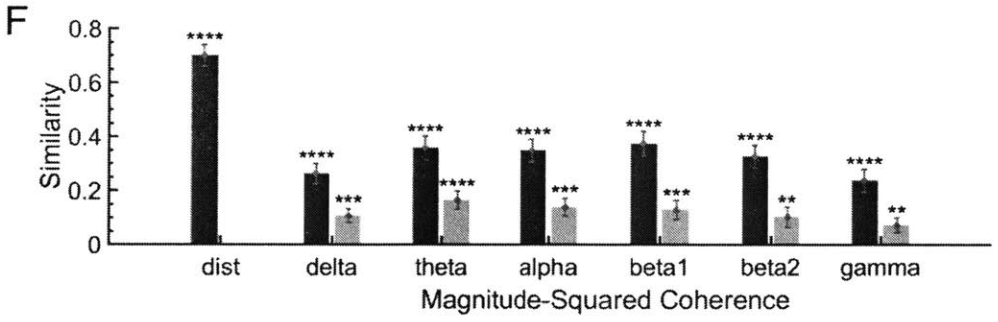
F
Similarity
dist
delta
theta
alpha
beta1
beta2
gamma
Magnitude-Squared Coherence

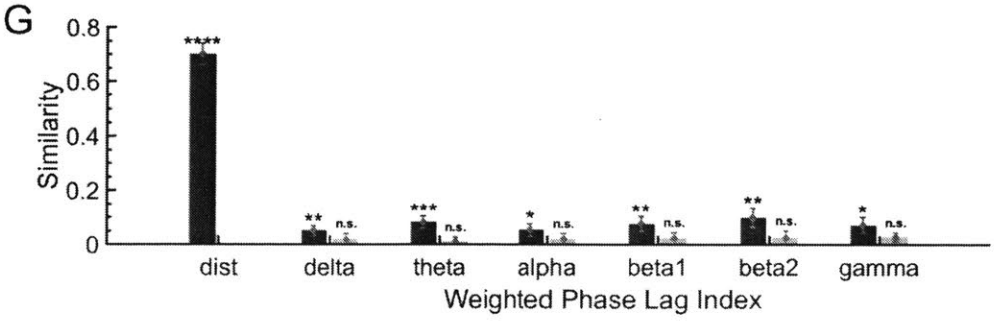
G
Similarity
n.s.
dist
delta
theta
alpha
beta1
beta2
gamma
Weighted Phase Lag Index

Figure 5-6: network similarity for local and distant channels separately. **A-B**: the mean distance-corrected similarity between CCEP networks and the indicated connectivity measure across 34 stimulation sites when channels are split by distance to the stimulation site into two groups: local (dark blue) or distant (orange). Local channels are within 3cm of the stimulation channel, as measured by Euclidean distance, and distant channels are outside that radius. Error bars indicate the standard error of the mean. Method labels: distance (dist), correlation (corr), cross-correlation (xcorr), pairwise Granger causality (pwgc), and diffusion tensor imaging (dti). Frequency bands: 1-4 Hz (delta), 4-8 Hz (theta), 8-12 Hz (alpha), 15-20 Hz (beta1), 20-30 Hz (beta2), 30-50 Hz (gamma).

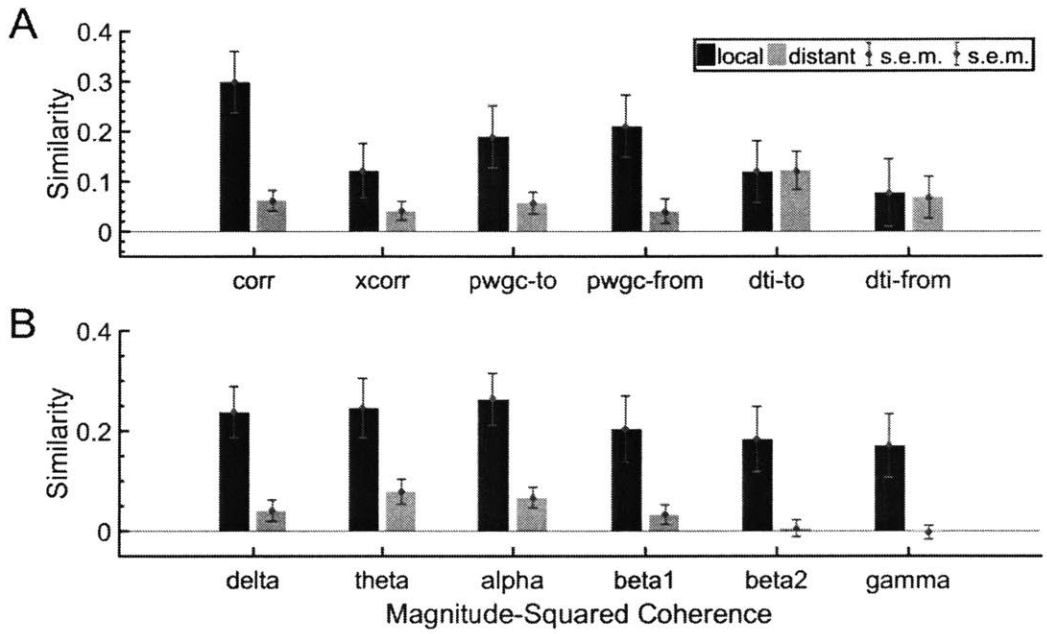

5.3.5 Differences between N1 and N2 networks

5.4 Discussion

In order to explore CCEP networks, we systematically compared these networks to other common estimates of connectivity. Of the connectivity estimates chosen, naïve comparisons show that structural connectivity derived through diffusion tractography are the most similar to stimulation-induced connectivity. However, controlling for distance abolishes the advantage of structural connectivity above functional and effective estimation methods. By segmenting channels into two groups – local and distant – we show that, even controlling for distance, structural connectivity maintains a unique similarity to distant CCEP distributions.

Uncorrected functional connectivity metrics showed a reasonable similarity to stimulation-derived connectivity. Of this group, cross-correlation showed the least similarity to CCEPs, even though cross-correlation has been shown to produce stable networks in EEG over time(Kramer *et al.*, 2011). Unlike the assumption of simultaneity under correlation, cross-correlation has a more plausible biophysical assumption that to connected regions may lag each other in activity. However, the inclusion of a variable lag within a relatively large window increases the noise of the estimation by raising the floor of possible values, and our results show that cross-correlation finds many connections between channels that do not respond to stimulation. Magnitude-squared coherence showed the highest similarity in spatial distribution to CCEPs in the 10-20 Hz range, consistent with the notion that lower frequency oscillations are more spatially distributed and more dependent on white matter connections than high frequency oscillations (Crone, 1998; Miller *et al.*, 2007; Hawasli *et al.*, 2016).

Despite categorization of stimulation as a measure of effective connectivity, the effective connectivity measures chosen here were overall less similar to stimulation networks than functional and structural connectivity measures. Weighted phase lag index fared particularly poorly, though both measures tended to underidentify channels that would be responsive to stimulation. Though Granger causality is a directed measure of connectivity, direction seemed to matter very little in predicting stimulation responses. This lack of difference could be because stimulation may activate white matter tracks in both orthodromic and antidromic directions, or it could be due to the high degree of reciprocal connections between cortical areas (Matsumoto, Nair, LaPresto, *et al.*, 2004; Borchers *et al.*, 2011; Rockland, 2015). Given the incomplete spatial sampling from sEEG recordings, and the speculation that cortico-cortical evoked potentials may include subcortical pathways, hidden sources of brain activity may have limited the accuracy of effective connectivity measures.

In naïve estimates of similarity, connectivity based on diffusion tractography was most similar to connectivity based on CCEPs. DTI is also a directed measure of connectivity, though in practice the directions differ very little from each other because diffusion happens in both orthodromic and antidromic directions along axons. Mechanistically, stimulation is thought to excite primarily axons (Histed, Bonin and Reid, 2009), so its agreement with structural connectivity is perhaps not surprising. Still, it is important to note that both CCEPs and DTI share a common cofounding factor – distance from the stimulation or seed site. Practical limitations of collecting data in a clinical setting resulted in heterogeneous DTI data collection parameters. Though no relationship between these parameters and results were found, a more homogenous data set of higher quality may improve results.

Correcting for distance, the landscape changes dramatically. Weighted phase lag index is the only metric, of the ones we tested, to no longer be significantly similar to CCEP networks after distance correction. Coherence in the gamma band is relatively unaffected by distance corrections, which could be due to its relatively constrained spatial distribution in the first place. While naïve estimates formerly had DTI most similar to stimulation networks, distance correction abolishes this advantage. There is no statistically measurable difference in distance-corrected similarity between DTI, correlation, Granger causality, and coherence in all bands except delta and gamma. These results would seem to indicate that, once corrected for distance, many methods of estimating connectivity perform reasonably similarly in predicting stimulation response.

However, overall comparable distance-corrected similarity scores does not mean that this similarity is homogenously applicable across the entire pool of channels. Segmenting the channels into two groups by distance to the stimulation site reveals that structural connectivity is more robust to distance from the stimulation site, even after correcting for distance. On the other hand, correlation again rises to the top as being most similar to channels closest to the stimulation site.

Structural connectivity may fail to predict local responsive channels because of its poor spatial resolution. Though MRI as a modality has much higher spatial sampling than sEEG, diffusion tractography requires the creation of reasonably large regions of interest as seed and target masks (up to 1 cm in diameter), which limit its utility in estimating connectivity of overlapping ROIs. On the other hand, correlation and coherence, particularly in the higher frequencies, are known to drop off dramatically with distance in the cortex (Muller *et al.*, 2016). Our results affirm that different methods may be more appropriate within specific spatial regimes.

Our results suggest that structural connectivity methods produce very similar networks to those derived by single pulse electrical stimulation. However, this similarity is driven in large part due to the underlying relationship between distance and connectivity in both cases. This relationship is due to a variety of factors, including volume conduction, the cumulative probability of terminating a tract, and the underlying tendency of brain regions to form both physical and functional connectivity with neighboring areas. Still, distance-corrected connectivity is more suited for the purposes of determining which non-invasive methods of connectivity estimation may help predict the effects of stimulation. Taken together, our results indicate many methods may suffice, though functional and effective methods seem particularly well-suited for predicting local effects.

6 Modulation of Cortico-Cortical Evoked Potentials by Brain State

6.1 Introduction

So far we have been considering CCEPs occurring when patients are awake and at rest. Furthermore, we have been operating under the assumption that CCEPs are stationary. Are these assumptions correct?

There is limited evidence to support that the brain's response to stimulation may be affected by large changes in the brain's state. The most researched area so far has been CCEPs recorded during sleep. While previous work has shown that the spatial distribution of CCEP responses does not change between wake and non-rapid-eye-movement (NREM) sleep, individual CCEPs recorded during NREM exhibit a larger response in the slow wave frequencies (<4 Hz) (Pigorini *et al.*, 2015). In addition, studies have found a suppression of activity in the high frequency (> 20 Hz) or high gamma (100-200 Hz) ranges during NREM CCEPs, compared to CCEPs recorded during wake (Pigorini *et al.*, 2015; Usami *et al.*, 2015). Further, NREM CCEPs have been shown to be larger in amplitude than wake CCEPs (Usami *et al.*, 2015), and CCEPs recorded during rapid-eye-movement (REM) sleep seem to indicate a transitory state between sleep and wakefulness (Usami *et al.*, 2017).

Very little research has been done on the impact of anesthesia on CCEPs. Propofol, a common anesthetic, is a gamma-aminobutyric acid A receptor ($GABA_A$) agonist (Trapani *et al.*, 2000; Kotani *et al.*, 2008; Vanlersberghe and Camu, 2008). CCEPs have been recorded while patients were undergoing propofol-induced anesthesia in one study (Yamao *et al.*, 2017). However, in this study, only N1 amplitude is presented and no comparison between awake and anesthetized CCEPs is made.

In addition to large changes in brain state, it is possible that small fluctuations in ongoing oscillatory activity may have an impact on the response of the brain to single pulse electrical stimulation. Two

studies suggest that the effects of brain stimulation are modulated by the phase of frequencies during each pulse for transcranial magnetic stimulation (TMS) (van Elswijk *et al.*, 2010; Dugue, Marque and VanRullen, 2011). In the first, pre-stimulus phase in the motor cortex is shown to modulate post-stimulus motor-evoked potentials(van Elswijk *et al.*, 2010). In the second, alpha (~10Hz) phase in the occipital cortex was shown to modulate the probability that a participant would see a TMS-induced phosphene (Dugue, Marque and VanRullen, 2011). Though these experiments were performed with TMS rather than electrical stimulation, they provide some evidence that the ongoing brain activity may have some impact on the response to stimulation.

Here we explore whether brain state can modulate the CCEP response. First, we look at whether very large changes in brain states can affect the brain's response to stimulation by exploring CCEPs when patients are undergoing anesthesia or sleeping. Second, we see whether CCEPs are affected by the dynamics of ongoing oscillations in brain activity.

6.2 Materials and Methods

6.2.1 Data Collection and Stimulation Delivery

We collected data for sleep and anesthesia in a subset of the 15 participants whose data are used in chapter 4. For sleep, we repeated the same experiments in 1 stimulation site for 3 participants each. Stimulation was delivered in the same manner, in a quiet and dark hospital room in the evening after the patient had been instructed to fall asleep. Sleep was monitored actively with the neurophysiological recordings by a trained clinician, but no sleep staging was performed.

For anesthesia, stimulation experiments were performed with 3 participants in the operating room under active monitoring immediately preceding the surgical explantation of the intracranial electrodes. Stimulation pulses were interleaved with audio stimuli from an audio discrimination task and were delivered every 4 seconds with uniformly distributed jitter of 500 ms. For each pulse,

stimulation was delivered to one of a small set of possible stimulation sites in pseudorandom order. Stimulation started for 5-6 minutes before delivery of propofol and continued for another 5-6 minutes afterwards.

In all cases, data were recorded and stimulation pulses were delivered with the exact system and parameters as described in previous chapters.

6.2.2 CCEP Estimation

As in previous chapters, CCEP magnitudes were estimated as the largest z-normalized absolute value of the signal post-stimulus. However, sleep and anesthesia can both increase the variance of the signal, which would artificially reduce CCEP magnitudes due to the normalization. Therefore, we used the standard deviation of the signal at wake for all normalization in order to ensure that fair comparisons across conditions can be made. Since normalization in this case is primarily to facilitate comparisons between channels, rather than within channels, this method of normalization is appropriate.

6.2.3 Pre-stimulus Power and Phase

Pre-stimulus power and phase were calculated using a metric similar to a previous study by van Elswijk et al. (van Elswijk *et al.*, 2010). For each frequency between 3 and 50 Hz, a window preceding the stimulus of duration three times longer than the period length was chosen, and an FFT was used to calculate the power and phase for each trial. To determine the relationship between pre-stimulus power and post-stimulus response, correlation coefficients were calculated for each frequency between the CCEP amplitude and the LFP power across trials. To determine the relationship between pre-stimulus phase and post-stimulus response, first pre-stimulus phases were grouped into 20 bins based on proximity to 20 equally spaced phases between 0 and 2π. Next, the average CCEP amplitude was calculated for each of these bins, and a best-fit cosine was estimated.

The amplitude of this fitted cosine model is called modulation depth and indicates the strength of the relationship between pre-stimulus phase and post-stimulus response. However, modulation depth cannot be negative and therefore has positive bias as an indicator. To correct for this bias, we shuffled pre-stimulus phases relative to post-stimulus responses and repeated the procedure to calculate the modulation depth under the null hypothesis, and then subtracted this value from the original estimate.

6.2.4 Statistical Significance

To infer the statistical significance of the changes to N1 and N2 amplitude under anesthesia, a two-sided paired t-test of the amplitudes is used and the uncorrected p-values are reported. For the effect of ongoing oscillatory activity on CCEPs, two-sided t-tests indicate that a few individual frequencies produce significant results. However, there are over 100 individual t-tests being computed, so even the null hypothesis could produce a few individual significant results. The results for each frequency are not independent, so to correct for multiple comparisons, a cluster-based approach is used. First, baseline and effect are swapped randomly for each stimulation site. Then, the p-value for each frequency is calculated at the group level. Since frequencies are not independent, the size of the largest group of contiguously significant results is recorded. This process is repeated 1000 times to yield a null hypothesis distribution of cluster sizes, and the 95th percentile of cluster size is used as the threshold for significance.

6.3 Results

6.3.1 CCEPs during sleep

CCEPs were recorded in the same electrode for three different participants both while they were awake and while they were asleep (see Figure 6-1). In the first participant, no significant difference was found between the two peak amplitudes, with N1 normalized amplitude at 21.75 ± 2.45 during

wake and 21.97 ± 1.85 during sleep and N2 normalized amplitude at 15.56 ± 4.11 during wake and 14.88 ± 3.13 during sleep. In the second participant, both N1 and N2 were significantly smaller during sleep than during wake (p = 2.85e-08 and 1.83e-18, respectively). Normalized amplitudes were estimated at 27.38 ± 6.33 during wake and 20.28 ± 12.47 during sleep for N1 and 19.79 ± 2.24 during wake and 11.29 ± 10.13 during sleep for N2. Similarly, in the third participant, both N1 and N2 were significantly smaller during sleep than during wake (p = 5.06e-07 and 1.6892e-26, respectively)[2]. Normalized amplitudes were estimated at 23.08 ± 5.72 during wake and 15.81 ± 4.76 during sleep for N1 and 15.46 ± 5.66 during wake and 5.90 ± 7.84 during sleep for N2.

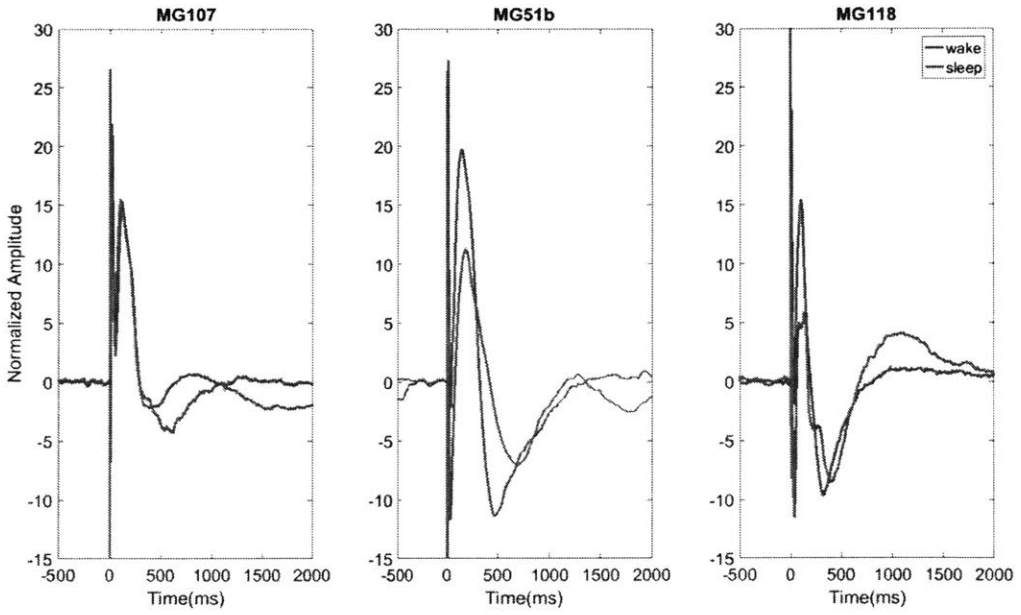

Figure 6-1: CCEPs during sleep and wake for three participants. The blue line represents the mean CCEP while participants were awake, while the orange line represents the mean CCEP while participants were sleeping. The voltage traces have been normalized by the pre-stimulus standard deviation during wake and mean. In two of the three participants, the CCEP is significantly smaller during sleep compared to wake.

Three data points is too few to draw generalizable conclusions about how CCEPs may be changed during sleep. A preliminary power calculation using these three points suggests that more than

[2] For this participant, stimuli were delivered in both bipolar directions, but standard deviations and p-values are reported for the second direction only for ease of comparison.

8000 data points (stimulation sites) would be required for a 90% chance to detect a significant difference in N1 magnitude between sleep and wake, while only 9 stimulation sites would be required to detect a significant difference in N2.

6.3.2 CCEPs during anesthesia

CCEPs were recorded in 12 different sites across 3 participants. Before administration of anesthesia, mean N1 normalized amplitude was 5.48 ± 1.38 and mean N2 normalized amplitude was 3.74 ± 1.30; after administration of anesthesia, mean N1 normalized amplitude was 5.06 ± 1.37 and mean N2 normalized amplitude was 2.56 ± 1.15. Though many of the stimulation sites show a decrease in N1 during anesthesia, the overall effect is very small, and a power calculation suggests that 41 total stimulation sites would be required for a 90% chance to detect a significant difference between the two conditions.

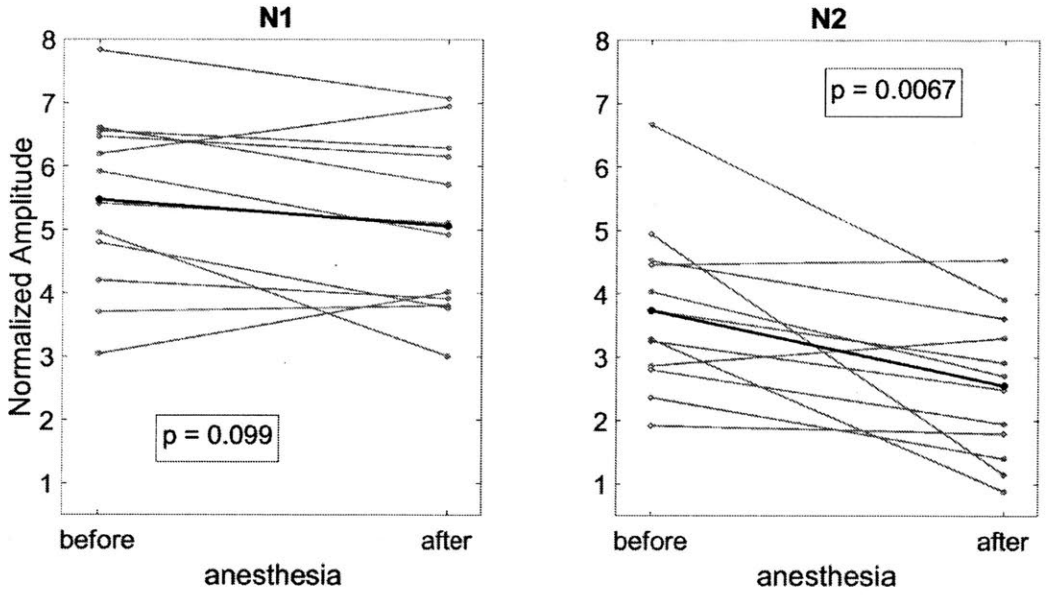

Figure 6-2: N1 and N2 amplitudes before and after administration of anesthesia. Grey bars represent each stimulation site, and the black bars represent the mean across stimulation sites. N2 is significantly smaller after administration of anesthesia, whereas there is no significant change for N1.

6.3.3 Effect of Ongoing Oscillatory Activity on CCEPs

After correcting for multiple comparisons, neither pre-stimulus power nor phase of any frequency has any significant effect on the post-stimulus magnitude of either N1 or N2 in data collected in 26 different sites across 13 patients. Power calculations are difficult to estimate for non-parametric cluster-based multiple comparisons corrected methods, but for the relationship between pre-stimulus power and post-stimulus N2 amplitude, power calculations for individual frequencies suggest that the total number of sites collected needs to be at least 53 – or more than double the current sample size.

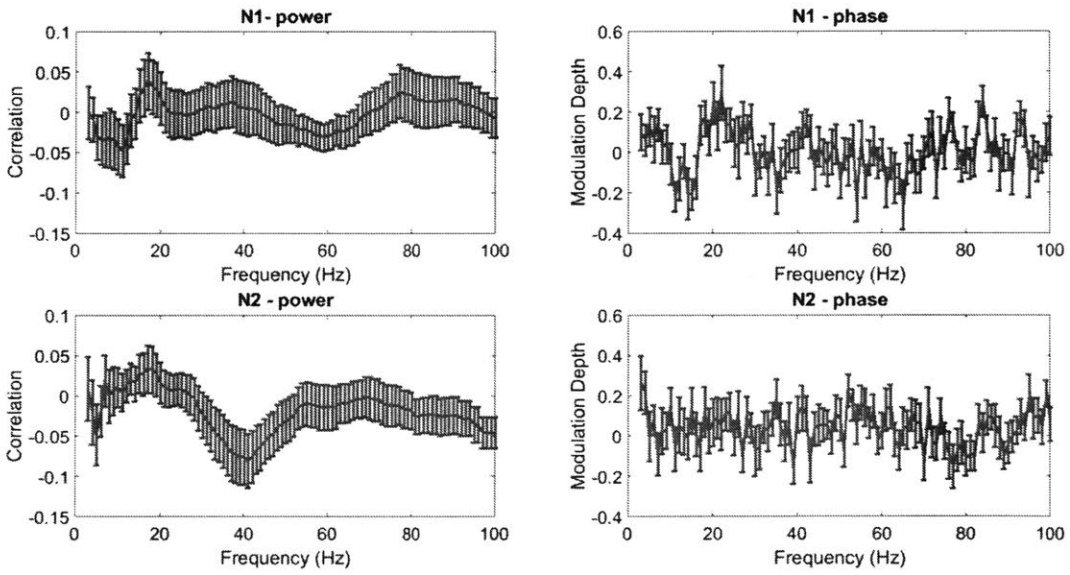

Figure 6-3: Relationship between pre-stimulus power and phase and post-stimulus N1 and N2 response. After a cluster-based correction for multiple comparisons, none of these relationships are significantly different from null.

6.4 Discussion

CCEPs are not static responses to stimulation but dynamically modulated responses that are affected by the state of the brain. In particular, N2 seems to be more affected by brain state than

N1. Anesthesia is in some ways a blunt tool to establish different brain states, and administration of anesthesia yields significant changes in CCEP magnitude. Similarly, sleep involves a very large change to brain dynamics, and though the data here is limited, it suggests that a similar pattern may be found with very few additional replicates. On the other hand, the influence – if any – that the ongoing oscillatory activity has on CCEP magnitude is subtle. The oscillatory activity of the brain at rest is reflecting smaller changes in brain state, compared to sleep or anesthesia, so it is not surprising that this difference in the magnitude of the result would also be small.

Ultimately, the findings here are limited by the weak effect sizes (in the case of ongoing oscillatory power) and a very limited number of participants. Each of these experiments has practical challenges that limit data collection. Sleep experiments must be carried out at night under supervision of a clinician. Anesthesia experiments must be carried out in the operating room with a team of clinicians including an epileptologist and an anesthesiologist. While ongoing oscillatory oscillations can be measured at rest in the epilepsy monitoring unit, the calculations generally require a large number of trials in order to fully capture different brain dynamics, and these experiments can take 15 minutes per stimulation site. Since each stimulation site has a low chance of producing a CCEP (see section 4.3), a successful experimental paradigm could take an hour or more.

Due in part to the low number of participants, the analysis here has treated every stimulation site equally, though the effects could be specific to particular brain regions. Sleep is known to particularly affect higher order association areas of the brain more than primary sensory areas, and oscillatory activity in different frequency bands is thought to play different roles depending on brain region (Michel *et al.*, 1992; Braun *et al.*, 1997; Hofle *et al.*, 1997). With a higher number of replicates, the analysis could be grouped by stimulation or recording channel location.

Still, the limited data collected here yields some interesting comparisons to the current literature. While other studies have found an increase in the CCEP amplitude during NREM sleep (Usami *et al.*, 2015), our preliminary results suggest a decrease – at least in N2. More data needs to be collected, but these results are surprising, and no obvious explanation exists for the contradiction. Previous studies on CCEPs during anesthesia note the presence of CCEPs and focus on N1 exclusively (Yamao *et al.*, 2014, 2017). Our results suggest a reason for this focus on N1 – the N2 peak appears to disappear almost entirely during anesthesia.

Finally, our data fail to reproduce the previous result indicating a relationship between pre-stimulus amplitude and post-stimulus CCEP (Usami *et al.*, 2018). A large reason for this disparity is differences in methodology; while we look for relationships across 26 stimulation sites, Usami et al. found a significant relationship in only 7 of 14 total stimulation sites. Even then, a significant result was only found in a subset of channels; overall, the significant relationship found by Usami et al. occurred in less than 7% of recording sites with significant CCEPs. Furthermore, the authors find only positive effects (i.e. higher alpha yields higher CCEPs) but fail to correct for the fact that higher power in the lower frequencies may simply add larger background oscillations on top of the CCEP, resulting in larger waveforms. The low incidence rate suggests that this relationship – to the extent that it even exists – is a rare phenomenon.

7 Conclusions

7.1 Summary of Results

We studied the neurophysiological response single pulse electrical stimulation in human patients – a precursory key step to better understanding how therapeutic brain stimulation works and to develop more effective treatment going forward. To allow for easy control of the stimulation device by a group of researchers, I first developed the CereLAB API – a MATLAB API and MEX interface for communicating with and programming the BlackRock CereStim device. I then explored the properties of CCEPs in three areas – their basic time-frequency characteristics, their spatial spread and networks, and their modulation by brain states.

The CereLAB API has been used by a handful of researchers across multiple institutions. It employs MEX datatypes to convert C++ pointers into MATLB-friendly class handles using MATLAB's native object-oriented programming capabilities. I used this API to implement the stimulation experiments outlined in chapters 4-6 of this work. The API has also been used to explore how the response changes with varying frequencies and amplitudes, to produce complex combinations of frequency trains and single pulses, and to deliver adaptive stimulation based on a patient's behavior in a task or their ongoing brain activity.

When measured in either the time or the frequency domain, CCEPs deviate significantly from base line for at least almost a second. This duration is two or three orders of magnitude larger than the stimulus itself, and nearly twice as long as previously reported, qualitative estimates. The CCEP is perhaps longer than expected because the increase in phase synchrony after stimulation returns to baseline far quicker than the increase in power in the 1-30 Hz frequency range. In addition, the two peaks of the CCEP demonstrate different characteristics, suggesting that the two peaks have different generating mechanisms. N1 amplitude is less variable than N2 amplitude. Comparing

distant CCEPs to local ones, the amplitude of both peaks decrease with increasing distance, but the decrease of N1 is much greater than the decrease seen in N2. On the other hand, distant N2 peaks occur significantly later than local N2 peaks, while no difference in timing was detected between distant and local N1 peaks.

CCEP networks are very similar to structural networks derived from DTI – moreso than common estimates of functional or effective connectivity. However, the probability of a connection between brain regions is heavily dependent on the distance between the two regions; neural networks are organized such that most connections are local, with a much smaller proportion of long-range connections. All connectivity estimates reflect this underlying structure to some degree, but connectivity estimates are most useful when they provide additional information and can help predict connectivity beyond this distance relationship.

Correcting for distance, CCEP networks were no longer more closely matched to structural connectivity than functional or effective connectivity. Instead, many connectivity estimates performed relatively similarly. On first glance, these results are quite surprising. If sophisticated connectivity estimates such as DTI perform just as well as very simple ones such as correlation, what is the point of ever bothering with computationally and resource-intensive techniques? A closer look gives us the answer. While distance-corrected correlation and DTI do globally align with distance-corrected CCEPs to a similar degree, their predictive power is not spread across all electrodes equally. Rather, DTI is better at predicting long-range connections than short-range, while correlation is better at predicting short-range rather than long-range connections. These differences likely derive from the differences in methodology – DTI has poor spatial resolution, making it ill-suited to distinguish between differences at the local, and therefore spatially smaller, scale, while correlation across electrodes is known to diminish rapidly with distance.

Despite at least one finding to the contrary, CCEPs do not appear to be modulated by ongoing oscillatory activity in the brain – at least in the wake, resting state. If any relationship does exist, it is very subtle and would require a much larger dataset to prove. However, these negative results do not mean that CCEPs are an entirely static phenomenon. Our results indicate that CCEPs are substantially modified after administration of anesthesia, including a reduction or even complete elimination of N2 but not N1.

7.2 Possible Implications

One of the most surprising results of this work was the extremely long relative duration of the evoked potential, compared to the initial stimulus itself. This duration is not immediately obvious in a qualitative assessment of the CCEP, particularly when judged by eye, but it has immediate implications for both experimental design and scientific understanding of brain stimulation. Quite a few CCEP studies report results using experimental protocols with 1 second or less between each stimulus delivery. Our results suggest that this type of experimental design does not allow enough time for the neurophysiological signals to return to baseline. Stimulating an already-perturbed signal could have as yet unknown cumulative effects. Aside from the practicalities, this extended duration of the response demonstrates one of the brain's most striking features – its ability to turn ephemeral inputs into sustained neuronal activity via feed-forward circuitry.

The processing of this circuitry is perhaps best illustrated by the discrete neurological features of the CCEP. Though the CCEP is characterized by an increase in power in the lower frequency bands, it is not an oscillatory feature with a singular generating mechanism. Rather, the two characteristic peaks that comprise the CCEP have unique properties. The idea that N1 and N2 represent distinct neural features is not new – preliminary laminar recordings and paired-pulse experiments have suggested that N1 is generated by excitatory activity primarily in layers 4 and 6, followed by a period

of suppression of activity in layer 4, and that N2 is generated by subsequent "rebound" excitatory activity in more superficial layers of cortex. Our results add evidence to this proposed generating mechanism.

The involvement of the deeper layers of the cortex in CCEP generation aligns well with the evidence that stimulation primarily excites axons. This information is also consistent with the high correspondence between the spatial distribution of CCEPs and connectivity metrics derived from estimates of white matter connectivity through DTI. This high correspondence bolsters the idea that structural connectivity is predictive of the spread of the response to stimulation in the brain. Indeed, many studies already use DTI to model the possible effects of various deep brain stimulation paradigms (Coenen *et al.*, 2012). Brain networks exhibit small-world topology; i.e. most connections in the brain are local, with long-range connections being much rarer. It makes sense, therefore, that any estimate of brain connectivity (including CCEP networks and DTI networks) would exhibit this underlying structure and consequently inherit a strong relationship between connectivity probability and distance. In that case, any estimate of brain connectivity is useful to the extent that it can provide information above the baseline likelihood of connectivity based on distance. By this logic, distance-corrected measurements reveal that functional connectivity metrics are just as predictive as structural connectivity, particularly in determining short-range connections. These results suggest that more accurate models of stimulation effects may be created by incorporating functional connectivity into estimates of the spatial spread of the effects.

If we assume that the similarity between CCEP networks and DTI networks indicates that CCEPs ultimately represent a metric of structural connectivity, it would reasonably follow that over short time periods, CCEPs are essentially time-invariant responses – particularly with respect to functional brain states. Our experiments failed to uncover any strong relationship between the pre-stimulus amplitude or phase of any frequency from 1 to 50 Hz and the post-stimulus evoked potential

amplitude, supporting this assumption. The suggestion that the response to stimulation is time-invariant is an attractive one; time-invariant systems are substantially easier than time-varying systems to model and to dynamically control, which would ease the development of closed-loop therapeutic stimulation. Unfortunately, our results also show a large, fast change in CCEPs following the induction of anesthesia, and possible changes to the CCEP during sleep, meaning that CCEPs are at least susceptible to some short-term dynamics of brain activity. Anesthesia-induced changes in neural activity are hardly likely to be relevant to human patients during the courses of their daily lives, and most brain stimulation therapies target symptoms of diseases that are most prominent during wakefulness. Still, further study is necessary to determine how CCEPs may be modulated with other changes in cortical dynamics, and how well the assumption of time-invariance can approximate the effects of stimulation.

7.3 Next Steps

The work presented here is far from completed. The preliminary evidence we have collected for CCEPs during sleep, during anesthesia, and at varying stimulation amplitudes should be expanded in order to draw quantitative conclusions from the results. The dose-response curve of stimulation is vital to our ability to model the effects of stimulation and may shed further light on distinctions between the characteristics of N1 and N2. Modulations of the CCEP during sleep and anesthesia could give more information on any fluctuations of the brain's response to stimulation – important for predicting closed-loop stimulation effects. An expanded dataset would allow for a fuller exploration of the properties of the CCEP under altered brain states, including network and time-frequency changes.

A closer look at the data I have collected could yield some interesting results as well. Much of the work done in Chapter 4, looking at the properties of the CCEP, was analyzed on a group level.

Looking at these properties per stimulation site could answer a few more questions. First, analyzing the duration of the response on a per-channel basis could give confidence bounds on the duration of the response and allow us to make comparisons between different conditions (such as brain region or distance to the stimulation electrode). Similarly, analyzing the peak timing on a stimulation-site level could enable us to determine the exact nature of the delay – e.g. is the relationship between distance and peak timing linear? – and would also increase the power of our statistical testing to detect differences in N1 peak timing. Our data set is currently too small, but if it were to increase, a breakdown of the results by anatomical properties of the stimulation and recording sites (brain region and proximity to white matter) could add nuance to our conclusions. The field of estimating connectivity between brain regions is rich with diverse methods that were not addressed in this work but could still be interesting to compare to CCEP networks.

Finally, new experiments and new tools would deepen our knowledge of the discoveries laid out in this work. Experimental time is one of the most precious resources for experiments with human patients in a clinical setting. The CereLAB API could be expanded to include a larger variety of debugging features and more high-level functions for common stimulation paradigms. A method of interleaving single pulse stimulation and subsequently recovering the signal for the response to each individual pulse would greatly speed up the collection of CCEP network data and possibly allow for a larger proportion of the network to be sampled. The clinical course of the patient generally determines the placement of electrodes. In the case that these electrodes are placed on sensorimotor cortex, similar analysis techniques could be applied to other evoked potentials, such as motor-evoked potentials from single pulse stimulation. Recordings in subcortical areas could help determine whether CCEPs are truly caused by direct connectivity between cortical areas, or whether they are perhaps mediated by subcortical connections. Multiunit or laminar recordings during CCEPs could uncover the generating mechanisms of CCEP properties.

References

Adrian, E. (1936) 'The spread of activity in the cerebral cortex', *The Journal of Physiology*, 88(2), pp. 127–161.

Alarcón, G., Martinez, J., Kerai, S. V, Lacruz, M. E., Quiroga, R. Q., Selway, R. P., Richardson, M. P., García Seoane, J. J. and Valentín, A. (2012) 'In vivo neuronal firing patterns during human epileptiform discharges replicated by electrical stimulation.', *Clinical Neurophysiology*, 123(9), pp. 1736–44.

Araki, K., Terada, K., Usui, K., Usui, N., Araki, Y., Baba, K., Matsuda, K., Tottori, T. and Inoue, Y. (2015) 'Bidirectional neural connectivity between basal temporal and posterior language areas in humans', *Clinical Neurophysiology*, 126(4), pp. 682–688.

Babb, T. L., Mariani, E., Seidner, K. A., Mutafyan, G., Halgren, E., Wilson, C. L. and Crandall, P. H. (1980) 'A circuit for safe diagnostic electrical stimulation of the human brain', *Neurol Res*, 2(2), pp. 181–197.

Barnett, L. and Seth, A. K. (2014) 'The MVGC multivariate Granger causality toolbox: A new approach to Granger-causal inference', *Journal of Neuroscience Methods*, 223, pp. 50–68.

Barrett, K. (2017) 'Psychiatric neurosurgery in the 21st century: overview and the growth of deep brain stimulation', *BJPsych Bulletin*. Royal College of Psychiatrists, 41(5), pp. 281–286.

Basser, P. J., Pajevic, S., Pierpaoli, C., Duda, J. and Aldroubi, A. (2000) 'In vivo fiber tractography using DT-MRI data', *Magnetic Resonance in Medicine*, 44(4), pp. 625–632.

Bassett, D. S. and Bullmore, E. T. (2017) 'Small-World Brain Networks Revisited', *Neuroscientist*, pp. 499–516.

Basu, I., Crocker, B., Farnes, K., Robertson, M. M., Paulk, A. C., Vallejo, D. I., Dougherty, D. D., Cash, S. S., Eskandar, E. N., Kramer, M. M. and Widge, A. S. (2018) 'A neural mass model to predict electrical stimulation evoked responses in human and non-human primate brain.', *In Review*.

Basu, I., Robertson, M. M., Crocker, B., Peled, N., Farnes, K., Vallejo-Lopez, D. I., Deng, H., Thombs, M., Martinez-Rubio, C., Cheng, J. J., McDonald, E., Dougherty, D. D., Eskandar, E. N., Widge, A. S., Paulk, A. C. and Cash, S. S. (2018) 'Consistent Linear and Non-Linear Responses to Electrical Brain Stimulation Across Individuals and Primate Species', *Submitted for publication*.

Behrens, T. E. J., Woolrich, M. W., Jenkinson, M., Johansen-Berg, H., Nunes, R. G., Clare, S., Matthews, P. M., Brady, J. M. and Smith, S. M. (2003) 'Characterization and propagation of uncertainty in diffusion-weighted MR imaging', *Magnetic Resonance in Medicine*, 50(5), pp. 1077–1088.

Behrens, T. E. J., Berg, H. J., Jbabdi, S., Rushworth, M. F. S. and Woolrich, M. W. (2007) 'Probabilistic diffusion tractography with multiple fibre orientations: What can we gain?', *NeuroImage*, 34(1), pp. 144–155.

Birdno, M. J. and Grill, W. M. (2008) 'Mechanisms of Deep Brain Stimulation in Movement Disorders as Revealed by Changes in Stimulus Frequency', *Neurotherapeutics*, 5(1), pp. 14–25.

Boccard, S. G. J., Pereira, E. A. C. and Aziz, T. Z. (2015) 'Deep brain stimulation for chronic pain', *Journal of Clinical Neuroscience*, 22(10), pp. 1537–1543.

Borchers, S., Himmelbach, M., Logothetis, N. and Karnath, H.-O. (2011) 'Direct electrical stimulation of human cortex — the gold standard for mapping brain functions?', *Nature Reviews Neuroscience*, 13(1), pp. 63–70.

Bosch, C., Degos, B., Deniau, J. M. and Venance, L. (2011) 'Subthalamic nucleus high-frequency stimulation generates a concomitant synaptic excitation-inhibition in substantia nigra pars reticulata', *Journal of Physiology*, 589(17), pp. 4189–4207.

Bowyer, S. M. (2016) 'Coherence a measure of the brain networks: past and present', *Neuropsychiatric Electrophysiology*, 2(1), p. 1.

Brainard, D. H. (1997) 'The Psychophysics Toolbox', *Spatial Vision*, 10(4), pp. 433–436.

Braun, A., Balkin, T. J., Wesenten, N. J., Carson, R. E., Varga, M., Baldwin, P., Selbie, S., Belenky, G. and Herscovitch, P. (1997) 'Regional cerebral blood flow throughout the sleep-wake cycle. An H2(15)O PET study', *Brain*. Oxford University Press, 120(7), pp. 1173–1197.

Brazier, M. a (1964) 'Evoked responses recorded from the depths of the human brain.', *Annals of the New York Academy of Sciences*, 112, pp. 33–59.

Bressler, S. L. and Seth, A. K. (2011) 'Wiener–Granger Causality: A well established methodology', *NeuroImage*. Academic Press, 58(2), pp. 323–329.

Brocker, D. T. and Grill, W. M. (2013) 'Principles of electrical stimulation of neural tissue', in *Handbook of Clinical Neurology*, pp. 3–18.

Brugge, J. F., Volkov, I. O., Garell, P. C., Reale, R. A. and Howard, M. a (2003) 'Functional connections between auditory cortex on Heschl's gyrus and on the lateral superior temporal gyrus in humans.', *Journal of Neurophysiology*, 90(6), pp. 3750–3763.

Bullock, T. H., McClune, M. C., Achimowicz, J. Z., Iragui-Madoz, V. J., Duckrow, R. B. and Spencer, S. S. (1995) 'Temporal fluctuations in coherence of brain waves.', *Proceedings of the National Academy of Sciences*, 92(25), pp. 11568–11572.

Burns, B. D. (1950) 'Some properties of the cat's isolated cerebral cortex.', *The Journal of Physiology*, 111(1–2), pp. 50–68.

Burns, B. D. (1951) 'Some properties of isolated cerebral cortex in the unanesthetized cat.', *The Journal of Physiology*, 112(1–2), pp. 156–75.

Catterall, W. A., Raman, I. M., Robinson, H. P. C., Sejnowski, T. J. and Paulsen, O. (2012) 'The Hodgkin-Huxley Heritage: From Channels to Circuits', *Journal of Neuroscience*. Society for Neuroscience, 32(41), pp. 14064–14073.

Chang, H. T. (1951a) 'Changes in excitability of cerebral cortex following single electric shock applied to cortical surface.', *Journal of Neurophysiology*, 14(2), pp. 95–111.

Chang, H. T. (1951b) 'Dendritic potential of cortical neurons produced by direct electrical stimulation of the cerebral cortex.', *Journal of Neurophysiology*, 14(1), pp. 1–21.

Chaturvedi, A., Luján, J. L. and McIntyre, C. C. (2013) 'Artificial neural network based characterization of the volume of tissue activated during deep brain stimulation.', *Journal of Neural Engineering*, 10(5), p. 056023.

Chu, C. J., Kramer, M. A., Pathmanathan, J., Bianchi, M. T., Westover, M. B., Wizon, L. and Cash, S. S. (2012) 'Emergence of Stable Functional Networks in Long-Term Human Electroencephalography', *Journal of Neuroscience*, 32(8), pp. 2703–2713.

Clay, J. R., Forger, D. B. and Paydarfar, D. (2012) 'Ionic mechanism underlying optimal stimuli for neuronal excitation: role of Na+ channel inactivation.', *PLoS One*, 7(9), p. e45983.

Coenen, V. A., Schlaepfer, T. E., Allert, N. and Mädler, B. (2012) 'Diffusion Tensor Imaging and Neuromodulation. DTI as Key Technology for Deep Brain Stimulation.', *International Review of Neurobiology*, 107, pp. 207–234.

Conner, C. R., Ellmore, T. M., DiSano, M. A., Pieters, T. A., Potter, A. W. and Tandon, N. (2011) 'Anatomic and electro-physiologic connectivity of the language system: A combined DTI-CCEP study', *Computers in Biology and Medicine*, 41(12), pp. 1100–1109.

Cooper, S. E., Kuncel, A. M., Wolgamuth, B. R., Rezai, A. R. and Grill, W. M. (2008) 'A model predicting optimal

parameters for deep brain stimulation in essential tremor', *Journal of Clinical Neurophysiology*, 25(5), pp. 265–273.

Creutzfeldt, O., Ba, G. and Schoen, L. (1956) 'Reaktionen einzelner Neurone des senso-motorischen Cortex nach elektrischen Iteizen', 619, pp. 597–619.

Creutzfeldt, O. D., Watanabe, S. and Lux, H. D. (1966) 'Relation between EEG phenomena and potentials of single cortical cells: I. Evoked responses after thalamic and epicortical stimulation.', *Electroencephalography and Clinical Neurophysiology*, 20(1), pp. 1–18.

Crone, N. (1998) 'Functional mapping of human sensorimotor cortex with electrocorticographic spectral analysis. II. Event-related synchronization in the gamma band', *Brain*, 121(12), pp. 2301–2315.

Curtis, D. R. and Eccles, J. C. (1960) 'Synaptic action during and after repetitive stimulation', *The Journal of Physiology*, 150(2), pp. 374–398.

Curtis, H. (1940a) 'An analysis of cortical potentials mediated by the corpus callosum', *Journal of Neurophysiology*, 3, pp. 414–422.

Curtis, H. (1940b) 'Intercortical connections of corpus callosum as indicated by evoked potentials.', *Journal of Neurophysiology*, 3.

Delgado, J. M., Hamlin, H. and Koskoff, Y. D. (1955) 'Electrical activity after stimulation and electrocoagulation of the human frontal lobe.', *The Yale Journal of Biology and Medicine*, 28(3–4), pp. 233–244.

Delorme, A. and Makeig, S. (2004) 'EEGLAB: An open source toolbox for analysis of single-trial EEG dynamics including independent component analysis', *Journal of Neuroscience Methods*, 134(1), pp. 9–21.

Dugue, L., Marque, P. and VanRullen, R. (2011) 'The Phase of Ongoing Oscillations Mediates the Causal Relation between Brain Excitation and Visual Perception', *Journal of Neuroscience*, 31(33), pp. 11889–11893.

Dykstra, A. R., Chan, A. M., Quinn, B. T., Zepeda, R., Keller, C. J., Cormier, J., Madsen, J. R., Eskandar, E. N. and Cash, S. S. (2012) 'Individualized localization and cortical surface-based registration of intracranial electrodes.', *NeuroImage*, 59(4), pp. 3563–70.

Eccles, J. C. (1951) 'Interpretation of action potentials evoked in the cerebral cortex', *Electroencephalography and Clinical Neurophysiology*, 3, pp. 449–464.

van Elswijk, G., Maij, F., Schoffelen, J.-M., Overeem, S., Stegeman, D. F. and Fries, P. (2010) 'Corticospinal beta-band synchronization entails rhythmic gain modulation.', *The Journal of Neuroscience*, 30(12), pp. 4481–8.

Enatsu, R., Jin, K., Elwan, S., Kubota, Y., Piao, Z., O'Connor, T., Horning, K., Burgess, R. C., Bingaman, W. and Nair, D. R. (2012) 'Correlations between ictal propagation and response to electrical cortical stimulation: A cortico-cortical evoked potential study', *Epilepsy Research*, 101(1–2), pp. 76–87.

Enatsu, R., Kubota, Y., Kakisaka, Y., Bulacio, J., Piao, Z., O'Connor, T., Horning, K., Mosher, J., Burgess, R. C., Bingaman, W. and Nair, D. R. (2013) 'Reorganization of posterior language area in temporal lobe epilepsy: A cortico-cortical evoked potential study', *Epilepsy Research*, 103(1), pp. 73–82.

Entz, L., Tóth, E., Keller, C. J., Bickel, S., Groppe, D. M., Fabó, D., Kozák, L. R., Eross, L., Ulbert, I. and Mehta, A. D. (2014) 'Evoked effective connectivity of the human neocortex', *Human Brain Mapping*, 35(12), pp. 5736–5753.

Fitzgerald, P. B. and Segrave, R. A. (2015) 'Deep brain stimulation in mental health: Review of evidence for clinical efficacy', *Australian and New Zealand Journal of Psychiatry*, pp. 979–993.

Friston, K. J. (2011) 'Functional and Effective Connectivity: A Review', *Brain Connectivity*, 1(1), pp. 13–36.

Göppert-Mayer, M. (1931) 'Über Elementarakte mit zwei Quantensprüngen', *Annalen der Physik*, 401(3), pp.

273–294.

Gordon, B., Lesser, R. P., Rance, N. E., Hart, J., Webber, R., Uematsu, S. and Fisher, R. S. (1990) 'Parameters for direct cortical electrical stimulation in the human: histopathologic confirmation.', *Electroencephalography and Clinical Neurophysiology*, 75(5), pp. 371–7.

Granger, C. W. J. (1969) 'Investigating Causal Relations by Econometric Models and Cross-spectral Methods', *Econometrica*, 37(3), p. 424.

Graupe, D., Basu, I., Tuninetti, D., Vannemreddy, P. and Slavin, K. V (2010) 'Adaptively controlling deep brain stimulation in essential tremor patient via surface electromyography', *Neurological Research*, 32(9), pp. 899–904.

Greve, D. N. and Fischl, B. (2009) 'Accurate and robust brain image alignment using boundary-based registration', *NeuroImage*, 48(1), pp. 63–72.

Hahn, P. J. and McIntyre, C. C. (2010) 'Modeling shifts in the rate and pattern of subthalamopallidal network activity during deep brain stimulation', *Journal of Computational Neuroscience*, 28(3), pp. 425–441.

Hanajima, R., Ashby, P., Lang, A. . E. and Lozano, A. . M. (2002) 'Effects of acute stimulation through contacts placed on the motor cortex for chronic stimulation', *Clinical Neurophysiology*, 113(5), pp. 635–641.

Hawasli, A. H., Kim, D., Ledbetter, N. M., Dahiya, S., Barbour, D. L. and Leuthardt, E. C. (2016) 'Influence of White and Gray Matter Connections on Endogenous Human Cortical Oscillations', *Frontiers in Human Neuroscience*. Frontiers Media SA, 10, p. 330.

Histed, M. H., Bonin, V. and Reid, R. C. (2009) 'Direct Activation of Sparse, Distributed Populations of Cortical Neurons by Electrical Microstimulation', *Neuron*, 63(4), pp. 508–522.

Hodgkin, A. L. and Huxley, A. F. (1952) 'A quantitative description of membrane current and its application to conduction and excitation in nerve', *The Journal of Physiology*, 117(4), pp. 500–544.

Hodgkin, A. L. and Katz, B. (1985) 'The effect of sodium ions on the electrical activity of the giant axon of the squid', *Developmental Brain Research*, 20(1), pp. 97–106.

Hofle, N., Paus, T., Reutens, D., Fiset, P., Gotman, J., Evans, A. C. and Jones, B. E. (1997) 'Regional cerebral blood flow changes as a function of delta and spindle activity during slow wave sleep in humans.', *The Journal of Neuroscience*, 17(12), pp. 4800–8.

Holsheimer, J., Demeulemeester, H., Nuttin, B. and De Sutter, P. (2000) 'Identification of the target neuronal elements in electrical deep brain stimulation', *European Journal of Neuroscience*, 12(12), pp. 4573–4577.

Jankovic, J. and Poewe, W. (2012) 'Therapies in Parkinson's disease', *Current Opinion in Neurology*, pp. 433–447.

Jenkinson, M., Bannister, P., Brady, M. and Smith, S. (2002) 'Improved optimization for the robust and accurate linear registration and motion correction of brain images', *NeuroImage*, 17(2), pp. 825–841.

Jenkinson, M. and Smith, S. (2001) 'A global optimisation method for robust affine registration of brain images', *Medical Image Analysis*, 5(2), pp. 143–156.

Jiménez-Jiménez, D., Abete-Rivas, M., Martín-López, D., Lacruz, M. E., Selway, R. P., Valentín, A. and Alarcón, G. (2015) 'Incidence of functional bi-temporal connections in the human brain in vivo and their relevance to epilepsy surgery', *Cortex*, 5, pp. 0–10.

Jones, D. (2010) 'Challenges and limitations of quantifying brain connectivity in vivo with diffusion MRI', *Imaging Med.*, 2(3), pp. 341–355.

Keller, C. J., Bickel, S., Entz, L., Ulbert, I., Milham, M. P., Kelly, C. and Mehta, A. D. (2011) 'Intrinsic functional

architecture predicts electrically evoked responses in the human brain', *Proceedings of the National Academy of Sciences*, 108(25), pp. 10308–10313.

Keller, C. J., Honey, C. J., Entz, L., Bickel, S., Groppe, D. M., Toth, E., Ulbert, I., Lado, F. A. and Mehta, A. D. (2014) 'Corticocortical evoked potentials reveal projectors and integrators in human brain networks.', *The Journal of Neuroscience*, 34(27), pp. 9152–63.

Keller, C. J., Honey, C. J., Mégevand, P., Entz, L., Ulbert, I. and Mehta, A. D. (2014) 'Mapping human brain networks with cortico-cortical evoked potentials.', *Philosophical transactions of the Royal Society of London. Series B, Biological sciences*, 369(1653).

Kleiner, M., Brainard, D. H., Pelli, D. G., Broussard, C., Wolf, T. and Niehorster, D. (2007) 'What's new in Psychtoolbox-3?', *Perception*, 36, p. S14.

Kobayashi, K., Matsumoto, R., Matsuhashi, M., Usami, K., Shimotake, A., Kunieda, T., Kikuchi, T., Mikuni, N., Miyamoto, S., Fukuyama, H., Takahashi, R. and Ikeda, A. (2015) 'Different Mode of Afferents Determines the Frequency Range of High Frequency Activities in the Human Brain: Direct Electrocorticographic Comparison between Peripheral Nerve and Direct Cortical Stimulation', *Plos One*, 10(6), p. e0130461.

Kotani, Y., Shimazawa, M., Yoshimura, S., Iwama, T. and Hara, H. (2008) 'The experimental and clinical pharmacology of propofol, an anesthetic agent with neuroprotective properties', *CNS Neuroscience and Therapeutics*, pp. 95–106.

Kramer, M. A., Eden, U. T., Lepage, K. Q., Kolaczyk, E. D., Bianchi, M. T. and Cash, S. S. (2011) 'Emergence of Persistent Networks in Long-Term Intracranial EEG Recordings', *Journal of Neuroscience*, 31(44), pp. 15757–15767.

Kubota, Y., Enatsu, R., Gonzalez-Martinez, J., Bulacio, J., Mosher, J., Burgess, R. C. and Nair, D. R. (2013) 'In vivo human hippocampal cingulate connectivity: A corticocortical evoked potentials (CCEPs) study.', *Clinical Neurophysiology*, pp. 1–10.

Kuncel, A. M. and Grill, W. M. (2004) 'Selection of stimulus parameters for deep brain stimulation', *Clinical Neurophysiology*, pp. 2431–2441.

Kunieda, T., Yamao, Y., Kikuchi, T. and Matsumoto, R. (2015) 'New Approach for Exploring Cerebral Functional Connectivity: Review of Cortico-cortical Evoked Potential', *Neurologia medico-chirurgica*, 55(5), pp. 374–382.

Lacruz, M. E., García Seoane, J. J., Valentin, A., Selway, R. and Alarcón, G. (2007) 'Frontal and temporal functional connections of the living human brain.', *The European Journal of Neuroscience*, 26(5), pp. 1357–70.

Lai, H. C. and Jan, L. Y. (2006) 'The distribution and targeting of neuronal voltage-gated ion channels', *Nature Reviews Neuroscience*, pp. 548–562.

Larson, P. S. (2014) 'Deep Brain Stimulation for Movement Disorders', *Neurotherapeutics*, 11(3), pp. 465–474.

Latteri, A., Arena, P. and Mazzone, P. (2011) 'Characterizing deep brain stimulation effects in computationally efficient neural network models', *Nonlinear Biomedical Physics*, pp. 1–14.

Laxton, A. W., Lipsman, N. and Lozano, A. M. (2013) 'Deep brain stimulation for cognitive disorders', *Handbook of Clinical Neurology*, 116, pp. 307–311.

Li, C. L. and Chou, S. N. (1962) 'Cortical intracellular synaptic potentials and direct cortical stimulation.', *Journal of Cellular and Comparative Physiology*, 60, pp. 1–16.

López-Muñoz, F., Boya, J. and Alamo, C. (2006) 'Neuron theory, the cornerstone of neuroscience, on the centenary of the Nobel Prize award to Santiago Ramón y Cajal', *Brain Research Bulletin*, 70(4–6), pp. 391–405.

Mahlknecht, P., Limousin, P. and Foltynie, T. (2015) 'Deep brain stimulation for movement disorders: update

on recent discoveries and outlook on future developments', *Journal of Neurology*, 262(11), pp. 2583–2595.

Manola, L., Holsheimer, J., Veltink, P. and Buitenweg, J. R. (2007) 'Anodal vs cathodal stimulation of motor cortex: a modeling study.', *Clinical Neurophysiology*, 118(2), pp. 464–74.

Marras, C., Beck, J. C., Bower, J. H., Roberts, E., Ritz, B., Ross, G. W., Abbott, R. D., Savica, R., Van Den Eeden, S. K., Willis, A. W. and Tanner, C. (2018) 'Prevalence of Parkinson's disease across North America', *NPJ Parkinson's Disease*, 4(1), p. 21.

MATLAB (2016a) 'handle class', in *MATLAB Documentation*. R2016b edn. Natick, MA: The MathWorks, Inc.

MATLAB (2016b) 'Object-Oriented Programming', in *MATLAB Documentation*. R2016b edn. Natick, MA: The MathWorks, Inc.

Matsumoto, R., Nair, D. R., Lapresto, E., Najm, I., Bingaman, W. and Lüders, H. O. (2004) 'Cortico-cortical evoked potentials', in Lüders, H. O. (ed.) *Deep brain stimulation and epilepsy*. London: Martin Dunitz, pp. 105–111.

Matsumoto, R., Nair, D. R., LaPresto, E., Najm, I., Bingaman, W., Shibasaki, H. and Lüders, H. O. (2004) 'Functional connectivity in the human language system: a cortico-cortical evoked potential study.', *Brain*, 127(Pt 10), pp. 2316–30.

Matsumoto, R., Nair, D. R., LaPresto, E., Bingaman, W., Shibasaki, H. and Lüders, H. O. (2007) 'Functional connectivity in human cortical motor system: a cortico-cortical evoked potential study.', *Brain*, 130(Pt 1), pp. 181–97.

Matsumoto, R., Kunieda, T. and Nair, D. (2017) 'Single pulse electrical stimulation to probe functional and pathological connectivity in epilepsy', *Seizure*, 44, pp. 27–36.

Matsuzaki, N., Juhász, C. and Asano, E. (2013) 'Cortico-cortical evoked potentials and stimulation-elicited gamma activity preferentially propagate from lower- to higher-order visual areas.', *Clinical Neurophysiology*, 124(7), pp. 1290–6.

McCreery, D. and Agnew, W. (1990) 'Charge density and charge per phase as cofactors in neural injury induced by electrical stimulation', *IEEE Transactions on Biomedical Engineering*, 37.

McIntyre, C. C., Grill, W. M., Sherman, D. L. and Thakor, N. V. (2004) 'Cellular Effects of Deep Brain Stimulation: Model-Based Analysis of Activation and Inhibition', *Journal of Neurophysiology*, 91(4), pp. 1457–1469.

McIntyre, C. C. and Grill, W. M. (1999) 'Excitation of central nervous system neurons by nonuniform electric fields.', *Biophysical Journal*, 76(2), pp. 878–88.

McIntyre, C. C. and Grill, W. M. (2002) 'Extracellular Stimulation of Central Neurons: Influence of Stimulus Waveform and Frequency on Neuronal Output', *Journal of Neurophysiology*, 88(4), pp. 1592–1604.

McIntyre, C. C. and Hahn, P. J. (2010) 'Network perspectives on the mechanisms of deep brain stimulation', *Neurobiology of Disease*, 38(3), pp. 329–337.

Michel, C. M., Lehmann, D., Henggeler, B. and Brandeis, D. (1992) 'Localization of the sources of EEG delta, theta, alpha and beta frequency bands using the FFT dipole approximation.', *Electroencephalography and Clinical Neurophysiology*, 82(1), pp. 38–44.

Miller, K. J., Leuthardt, E. C., Schalk, G., Rao, R. P. N., Anderson, N. R., Moran, D. W., Miller, J. W. and Ojemann, J. G. (2007) 'Spectral Changes in Cortical Surface Potentials during Motor Movement', *Journal of Neuroscience*, 27(9), pp. 2424–2432.

Modolo, J., Legros, A., Thomas, A. W. and Beuter, A. (2011) 'Model-driven therapeutic treatment of neurological disorders: reshaping brain rhythms with neuromodulation.', *Interface focus*, 1(1), pp. 61–74.

Morrell, M. J. and Halpern, C. (2016) 'Responsive Direct Brain Stimulation for Epilepsy', *Neurosurgery Clinics of North America*, 27(1), pp. 111–121.

Mueller, W. M. and Morris, G. L. (1993) 'Intraoperative and extraoperative identification of eloquent brain using stimulation mapping.', *Neurosurgery clinics of North America*, 4(2), pp. 217–22.

Muller, L., Hamilton, L. S., Edwards, E., Bouchard, K. E. and Chang, E. F. (2016) 'Spatial resolution dependence on spectral frequency in human speech cortex electrocorticography', *Journal of Neural Engineering*, 13(5), p. 056013.

Nathan, S. S., Sinha, S. R., Gordon, B., Lesser, R. P. and Thakor, N. V. (1993) 'Determination of current density distributions generated by electrical stimulation of the human cerebral cortex', *Electroencephalography and Clinical Neurophysiology*, pp. 183–192.

Nowak, L. G. and Bullier, J. (1998) 'Axons, but not cell bodies, are activated by electrical stimulation in cortical gray matter', *Experimental Brain Research*, 118(4), pp. 477–488.

O'Doherty, J. E., Lebedev, M. A., Hanson, T. L., Fitzsimmons, N. A. and Nicolelis, M. A. L. (2009) 'A brain-machine interface instructed by direct intracortical microstimulation', *Frontiers in Integrative Neuroscience*, 3, p. 20.

Oluigbo, C. O., Salma, A. and Rezai, A. R. (2012) 'Deep Brain Stimulation for Neurological Disorders', *IEEE Reviews in Biomedical Engineering*, 5, pp. 88–99.

Oostenveld, R., Fries, P., Maris, E. and Schoffelen, J. M. (2011) 'FieldTrip: Open source software for advanced analysis of MEG, EEG, and invasive electrophysiological data', *Computational Intelligence and Neuroscience*, 2011, p. 156869.

Oya, H., Howard, M. A., Magnotta, V. A., Kruger, A., Griffiths, T. D., Lemieux, L., Carmichael, D. W., Petkov, C. I., Kawasaki, H., Kovach, C. K., Sutterer, M. J. and Adolphs, R. (2017) 'Mapping effective connectivity in the human brain with concurrent intracranial electrical stimulation and BOLD-fMRI', *Journal of Neuroscience Methods*, 277, pp. 101–112.

Paulk, A. C., Farnes, K., Yousefi, A., Peled, N., Crocker, B., Vallejo-Lopez, D., Belok, G., Zorowitz, S., Afzal, A., Gilmour, A., Nossensen, N., Ellard, K. E., Eden, U. T., Deckersbach, T., Dougherty, D. D., Widge, A. S., Eskandar, E. N. and Cash, S. S. (2018) 'Cingulate stimulation bidirectionally changes emotion regulation during an Emotion Conflict Resolution Task', *Submitted for publication*.

Pelli, D. G. (1997) 'The VideoToolbox software for visual psychophysics: Transforming numbers into movies', *Spatial Vision*, 10(4), pp. 437–442.

Pigorini, A., Sarasso, S., Proserpio, P., Szymanski, C., Arnulfo, G., Casarotto, S., Fecchio, M., Rosanova, M., Mariotti, M., Russo, G. Lo, Palva, M. J., Nobili, L. and Massimini, M. (2015) 'Bistability breaks-off deterministic responses to intracortical stimulation during non-REM sleep', *NeuroImage*, 112, pp. 105–113.

Purpura, D. P., Pool, J. L., Ransohoff, J., Frumin, M. J. and Housepian, E. M. (1957) 'Observations on evoked dendritic potentials of human cortex.', *Electroencephalography and Clinical Neurophysiology*, 9(3), pp. 453–459.

Ranck, J. B. (1975) 'Which elements are excited in electrical stimulation of mammalian central nervous system: a review.', *Brain Research*, 98(3), pp. 417–40.

Ritaccio, A. L., Brunner, P. and Schalk, G. (2018) 'Electrical Stimulation Mapping of the Brain', *Journal of Clinical Neurophysiology*, 35(2), pp. 86–97.

Rockland, K. S. (2015) 'About connections', *Frontiers in Neuroanatomy*. Frontiers, 9, p. 61.

Rosenblueth, A. and Cannon, W. (1941) 'Cortical responses to electrical stimulation', *American Journal Of*

Physiology, 135(1941), pp. 690–739.

Rothwell, J. C. (1999) 'Paired-pulse investigations of short-latency intracortical facilitation using TMS in humans.', *Electroencephalography and clinical neurophysiology. Supplement*, 51, pp. 113–9.

Rutecki, P. A., Grossman, R. G., Armstrong, D. and Irish-Loewen, S. (1989) 'Electrophysiological connections between the hippocampus and entorhinal cortex in patients with complex partial seizures.', *Journal of Neurosurgery*, 70(5), pp. 667–75.

Sarma, A. A., Crocker, B., Cash, S. S. and Truccolo, W. (2016) 'A modular, closed-loop platform for intracranial stimulation in people with neurological disorders', in *2016 38th Annual International Conference of the IEEE Engineering in Medicine and Biology Society (EMBC)*. IEEE, pp. 3139–3142.

Schmahmann, J. D. and Pandya, D. N. (2007) 'Cerebral White Matter — Historical Evolution of Facts and Notions Concerning the Organization of the Fiber Pathways of the Brain', *Journal of the History of the Neurosciences*, 16(3), pp. 237–267.

Shannon, R. V (1992) 'A Model of Save Levels for Electrical Stimulation', *IEEE T Bio-Med Eng*, pp. 424–426.

Shimada, S., Kunii, N., Kawai, K., Matsuo, T., Ishishita, Y., Ibayashi, K. and Saito, N. (2017) 'Impact of volume-conducted potential in interpretation of cortico-cortical evoked potential: Detailed analysis of high-resolution electrocorticography using two mathematical approaches', *Clinical Neurophysiology*, 128(4), pp. 549–557.

Smith, Y., Wichmann, T., Factor, S. A. and DeLong, M. R. (2012) 'Parkinson's Disease Therapeutics: New Developments and Challenges Since the Introduction of Levodopa', *Neuropsychopharmacology*, 37(1), pp. 213–246.

So, E. L. and Alwaki, A. (2018) 'A Guide for Cortical Electrical Stimulation Mapping', *Journal of Clinical Neurophysiology*, 35(2), pp. 98–105.

Spieles-Engemann, A. L., Behbehani, M. M., Collier, T. J., Wohlgenant, S. L., Steece-Collier, K., Paumier, K., Daley, B. F., Gombash, S., Madhavan, L., Mandybur, G. T., Lipton, J. W., Terpstra, B. T. and Sortwell, C. E. (2010) 'Stimulation of the rat subthalamic nucleus is neuroprotective following significant nigral dopamine neuron loss', *Neurobiology of Disease*, 39(1), pp. 105–115.

Sprenger, F. and Poewe, W. (2013) 'Management of Motor and Non-Motor Symptoms in Parkinson's Disease', *CNS Drugs*, 27(4), pp. 259–272.

Srinath, R. and Ray, S. (2014) 'Effect of amplitude correlations on coherence in the local field potential', *Journal of Neurophysiology*, 112(4), pp. 741–751.

Stosiek, C., Garaschuk, O., Holthoff, K. and Konnerth, A. (2003) 'In vivo two-photon calcium imaging of neuronal networks', *Proceedings of the National Academy of Sciences*, 100(12), pp. 7319–7324.

Swann, N. C., Cai, W., Conner, C. R., Pieters, T. a, Claffey, M. P., George, J. S., Aron, A. R. and Tandon, N. (2012) 'Roles for the pre-supplementary motor area and the right inferior frontal gyrus in stopping action: Electrophysiological responses and functional and structural connectivity', *NeuroImage*, 59(3), pp. 2860–2870.

Tehovnik, E. J. and Slocum, W. M. (2013) 'Two-photon imaging and the activation of cortical neurons', *Neuroscience*, 245, pp. 12–25.

Trapani, G., Altomare, C., Liso, G., Sanna, E. and Biggio, G. (2000) 'Propofol in anesthesia. Mechanism of action, structure-activity relationships, and drug delivery.', *Current medicinal chemistry*, 7(2), pp. 249–71.

Trebaul, L. *et al.* (2018) 'Probabilistic functional tractography of the human cortex revisited', *NeuroImage*. Academic Press, 181, pp. 414–429.

Trébuchon, A. and Chauvel, P. (2016) 'Electrical Stimulation for Seizure Induction and Functional Mapping in

Stereoelectroencephalography', *Journal of Clinical Neurophysiology*, 33(6), pp. 511–521.

Tsubokawa, T., Katayama, Y., Yamamoto, T., Hirayama, T. and Koyama, S. (1991) 'Chronic motor cortex stimulation for the treatment of central pain.', *Acta neurochirurgica. Supplementum*, 52, pp. 137–9.

Tsubokawa, T., Katayama, Y., Yamamoto, T., Hirayama, T. and Koyama, S. (1993) 'Chronic motor cortex stimulation in patients with thalamic pain.', *Journal of Neurosurgery*, 78(3), pp. 393–401.

Usami, K., Matsumoto, R., Kobayashi, K., Hitomi, T., Shimotake, A., Kikuchi, T., Matsuhashi, M., Kunieda, T., Mikuni, N., Miyamoto, S., Fukuyama, H., Takahashi, R. and Ikeda, A. (2015) 'Sleep modulates cortical connectivity and excitability in humans: Direct evidence from neural activity induced by single-pulse electrical stimulation', *Human Brain Mapping*, 36(11), pp. 4714–4729.

Usami, K., Matsumoto, R., Kobayashi, K., Hitomi, T., Matsuhashi, M., Shimotake, A., Kikuchi, T., Yoshida, K., Kunieda, T., Mikuni, N., Miyamoto, S., Takahashi, R. and Ikeda, A. (2017) 'Phasic REM Transiently Approaches Wakefulness in the Human Cortex—A Single-Pulse Electrical Stimulation Study', *Sleep*, 40(8).

Usami, K., Milsap, G. W., Korzeniewska, A., Collard, M. J., Wang, Y., Lesser, R. P., Anderson, W. S. and Crone, N. E. (2018) 'Cortical Responses to Input From Distant Areas are Modulated by Local Spontaneous Alpha/Beta Oscillations', *Cerebral Cortex*, (March), pp. 1–11.

Vanlersberghe, C. and Camu, F. (2008) 'Propofol', in *Modern Anesthetics*. Berlin, Heidelberg: Springer Berlin Heidelberg, pp. 227–252.

Vinck, M., Oostenveld, R., van Wingerden, M., Battaglia, F. and Pennartz, C. M. A. (2011) 'An improved index of phase-synchronization for electrophysiological data in the presence of volume-conduction, noise and sample-size bias', *NeuroImage*, 55(4), pp. 1548–1565.

Wagle Shukla, A., Zeilman, P., Fernandez, H., Bajwa, J. A. and Mehanna, R. (2017) 'DBS Programming: An Evolving Approach for Patients with Parkinson's Disease', *Parkinson's Disease*.

Walker, H. C., Watts, R. L., Schrandt, C. J., Huang, H., Guthrie, S. L., Guthrie, B. L. and Montgomery Erwin B, J. (2011) 'Activation of subthalamic neurons by contralateral subthalamic deep brain stimulation in Parkinson disease', *Journal of Neurophysiology*, 105(3), pp. 1112–1121.

Widge, A. S., Malone, D. A. and Dougherty, D. D. (2018) 'Closing the loop on deep brain stimulation for treatment-resistant depression', *Frontiers in Neuroscience*, p. 175.

Wiener, N. (1956) 'The theory of prediction', in Beckenbach, E. (ed.) *Modern Mathematics for Engineers*. New York: McGraw Hill.

Wilson, C. L., Isokawa, M., Babb, T. L. and Crandall, P. H. (1990) 'Functional connections in the human temporal lobe. I. Analysis of limbic system pathways using neuronal responses evoked by electrical stimulation.', *Experimental Brain Research*, 82(2), pp. 279–92.

Wongsarnpigoon, A. and Grill, W. (2010) 'Energy-efficient waveform shapes for neural stimulation revealed with a genetic algorithm', *Journal of Neural Engineering*, 7(4), pp. 1–20.

Woodford, O. (2018) 'Example MATLAB class wrapper for a C++ class'.

Yamao, Y., Matsumoto, R., Kunieda, T., Arakawa, Y., Kobayashi, K., Usami, K., Shibata, S., Kikuchi, T., Sawamoto, N., Mikuni, N., Ikeda, A., Fukuyama, H. and Miyamoto, S. (2014) 'Intraoperative dorsal language network mapping by using single-pulse electrical stimulation', *Human Brain Mapping*, 35(9), pp. 4345–4361.

Yamao, Y., Suzuki, K., Kunieda, T., Matsumoto, R., Arakawa, Y., Nakae, T., Nishida, S., Inano, R., Shibata, S., Shimotake, A., Kikuchi, T., Sawamoto, N., Mikuni, N., Ikeda, A., Fukuyama, H. and Miyamoto, S. (2017) 'Clinical impact of intraoperative CCEP monitoring in evaluating the dorsal language white matter pathway', *Human Brain Mapping*, 38(4), pp. 1977–1991.

Yang, A. I., Wang, X., Doyle, W. K., Halgren, E., Carlson, C., Belcher, T. L., Cash, S. S., Devinsky, O. and Thesen, T. (2012) 'Localization of dense intracranial electrode arrays using magnetic resonance imaging', *NeuroImage*, 63(1), pp. 157–165.

Zack, M. M. and Kobau, R. (2017) 'National and State Estimates of the Numbers of Adults and Children with Active Epilepsy — United States, 2015', *MMWR. Morbidity and Mortality Weekly Report*, 66(31), pp. 821–825.